Inelastic X-Ray Scattering at the APS

E. Ercan Alp
Argonne National Laboratory

NSLS-II Workshops,
Brookhaven Nat. Lab, Upton, NY
February 7-8, 2008

Advanced Photon Source, APS

Inelastic Scattering at the APS (2008)

A SHORT SUMMARY OF CURRENT INELASTIC X-RAY SCATTERING TECHNIQUES

Technique	Source of interaction	Typical resolution	Deetection method	Location at the APS
Momentum-resolved, high energy resolution IXS: HERIX	Collective excitations of atoms, ions, molecules, PHONONS	1-3 meV	Back-scattering, curved and diced crystal analyzer	3-ID 30-ID
Momentum-resolved, medium energy resolution resonant IXS: MERIX	Valence electrons near Fermi level	100-500 meV	Near-back-scattering, curved and diced crystal analyzer	9-ID, 12-ID, 33-ID
Momentum-integrated, nuclear resonant IXS: NRIXS	Collective excitations monitored through a nuclear resonance	0.5-2 meV	Nano-second time resolved detectors monitoring nuclear level decay	3-ID, 16-ID
High resolution Compton scattering: CS	Core and valence electrons	1 eV	Triple Laue crystal analyzer, PSD detector	
Magnetic Compton scattering: MCS	Spin polarized electrons	100 eV	Solid state detector	11-ID
X-ray Raman spectroscopy: XRS	Core electron excitations of low-Z elements	1 eV	Back-scattering curved flat analyzers	13-ID, 16-ID
X-ray emission spectroscopy: XES	X-ray fluorescence by incident photons: photon-in/photon-out	0.5 eV	Back-scattering curved flat analyzers	10-ID
Soft-X-ray IXS : PEEM	x-ray induced photoemission: photon-in/electron-out	5 meV	Electron spectrometer	4-ID

4 stations: A-B-C-D

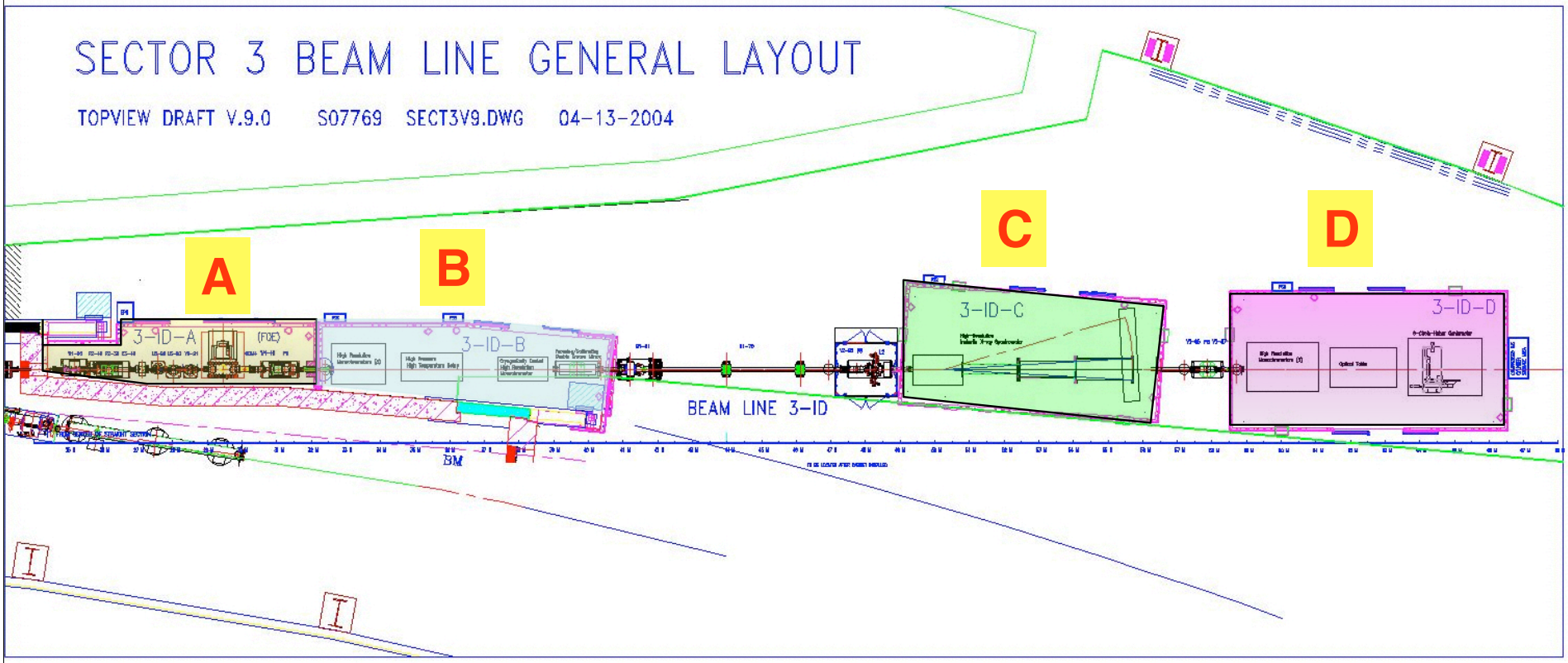

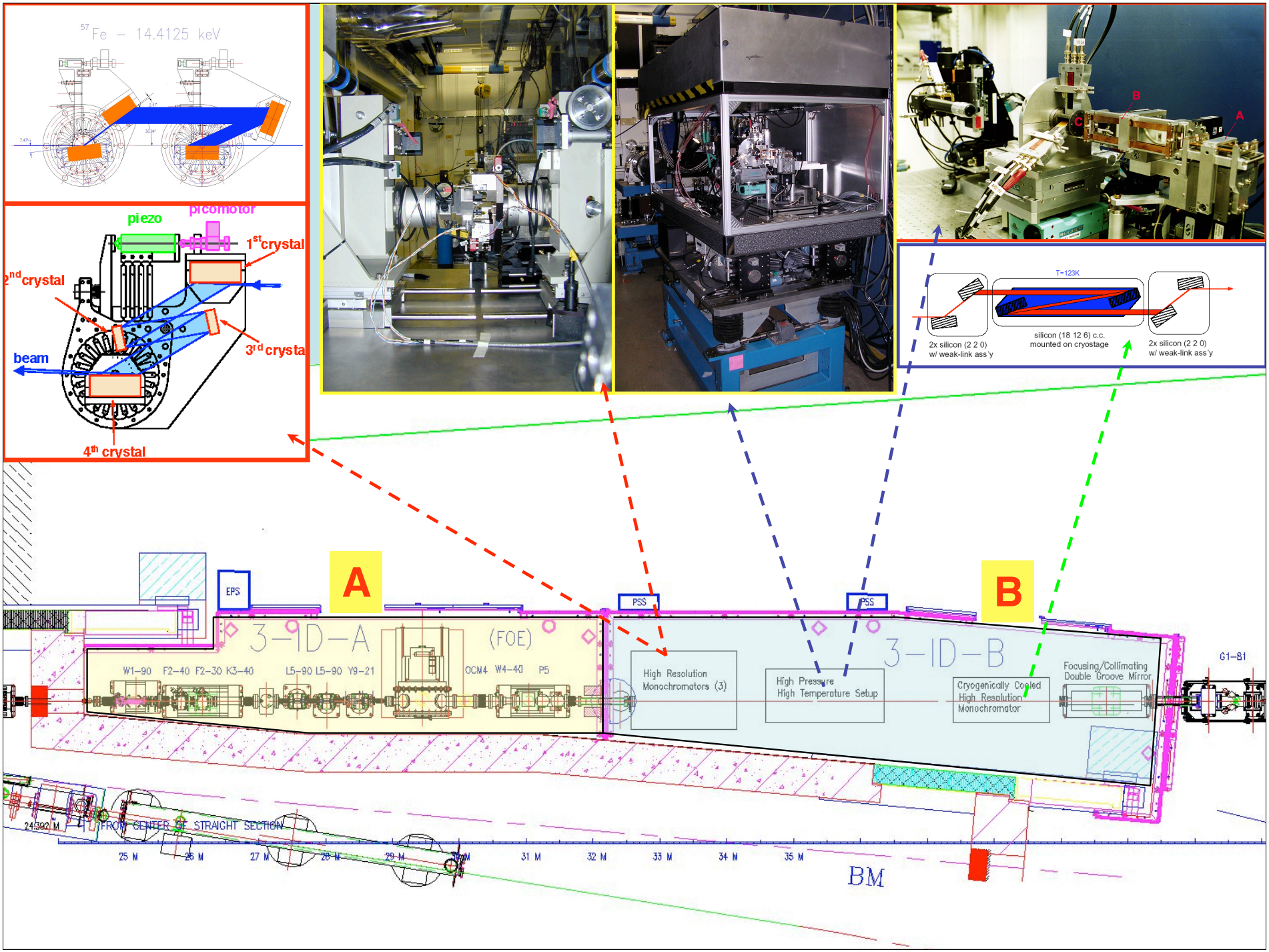
57Fe – 14.4125 keV
piezo
picomotor
1st crystal
2nd crystal
3rd crysta
beam
4th crystal
A
B
C
T=123K
2x silicon (2 2 0)
w/ weak-link ass'y
silicon (18 12 6) c.c.
mounted on cryostage
2x silicon (2 2 0)
w/ weak-link ass'y
EPS
PSS
PSS
3-ID-A
(FOE)
W1-90 F2-40 F2-30 K3-40
L5-90 L5-90 Y9-21
OCM4 W4-40 P5
3-ID-B
High Resolution
Monochromators (3)
High Pressure
High Temperature Setup
Cryogenically Cooled
High Resolution
Monochromator
Focusing/Collimating
Double Groove Mirror
G1-81
24392 M
FROM CENTER OF STRAIGHT SECTION
25 M
26 M
27 M
28 M
29 M
31 M
32 M
33 M
34 M
35 M
BM

Generations of high-resolution monochromators

1992

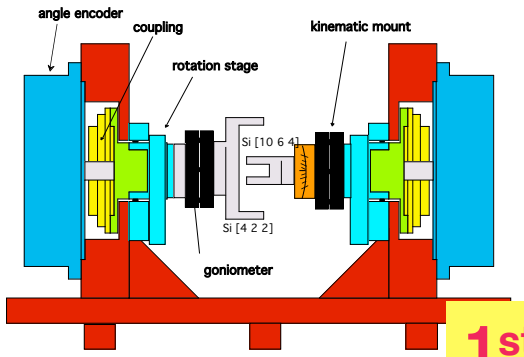

1st

1999

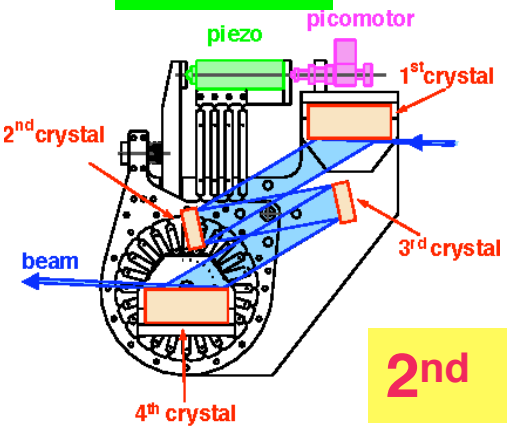

2nd

2002

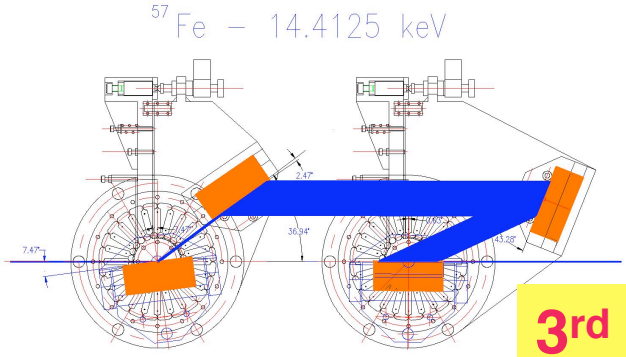

3rd

2004

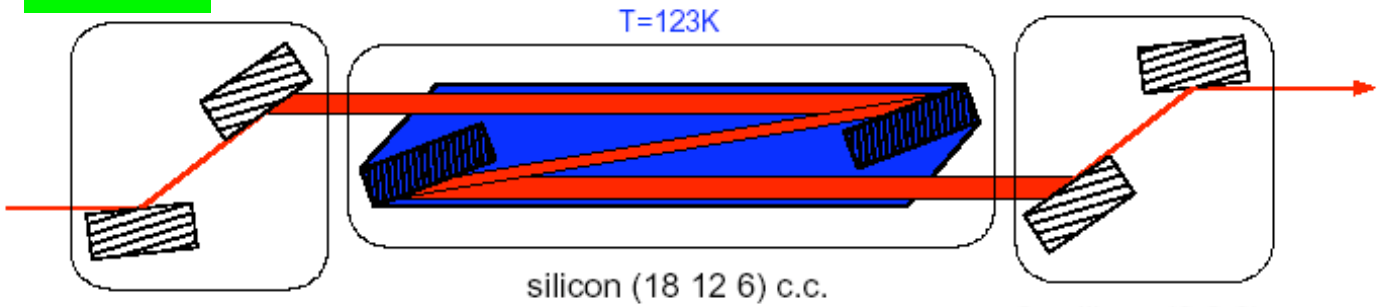

4th

T. Toellner

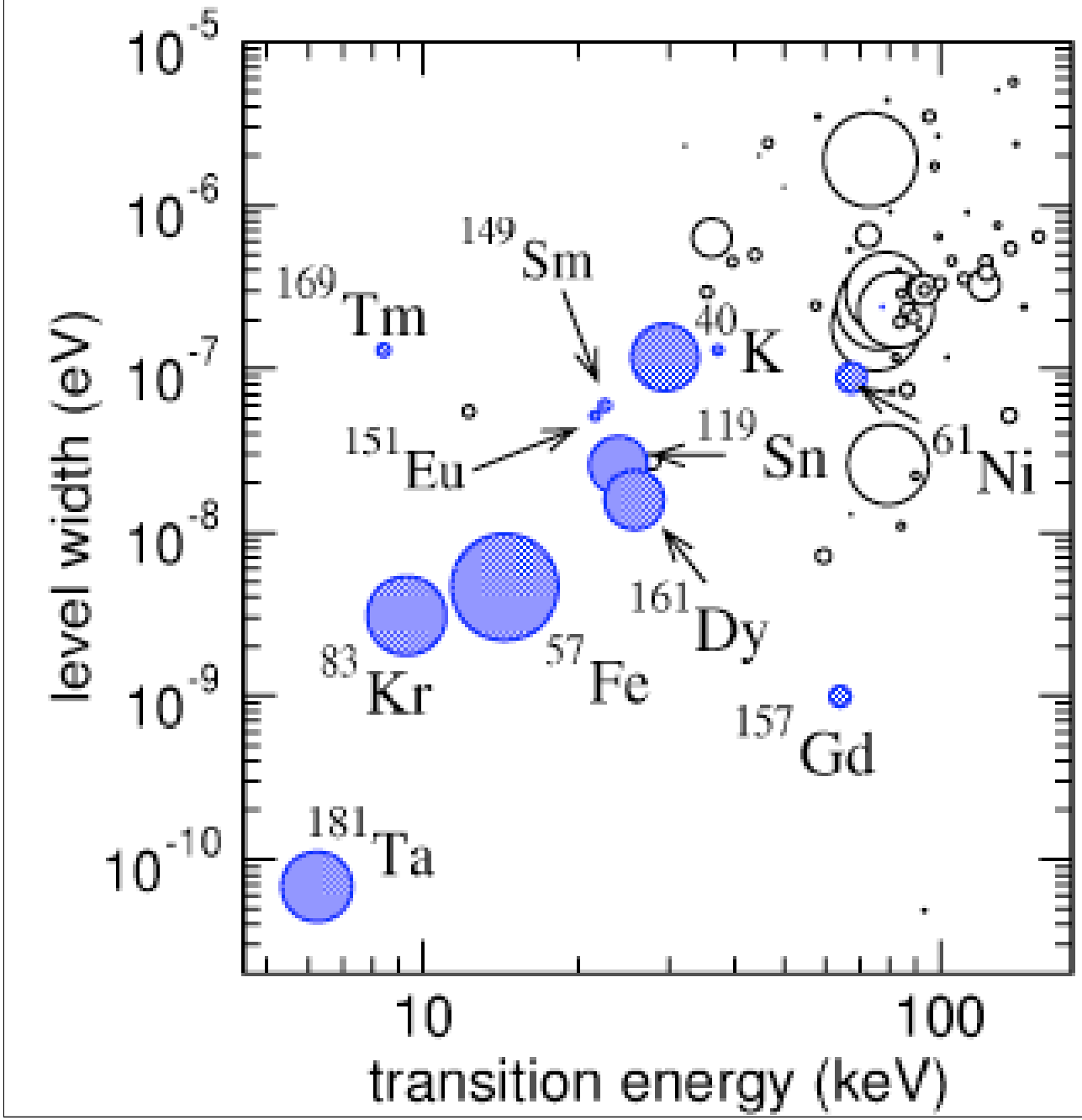
level width (eV)
transition energy (keV)
10
100
10^{-5}
10^{-6}
10^{-7}
10^{-8}
10^{-9}
10^{-10}
^{169}Tm
^{149}Sm
^{40}K
^{151}Eu
^{119}Sn
^{61}Ni
^{161}Dy
^{83}Kr
^{57}Fe
^{157}Gd
^{181}Ta

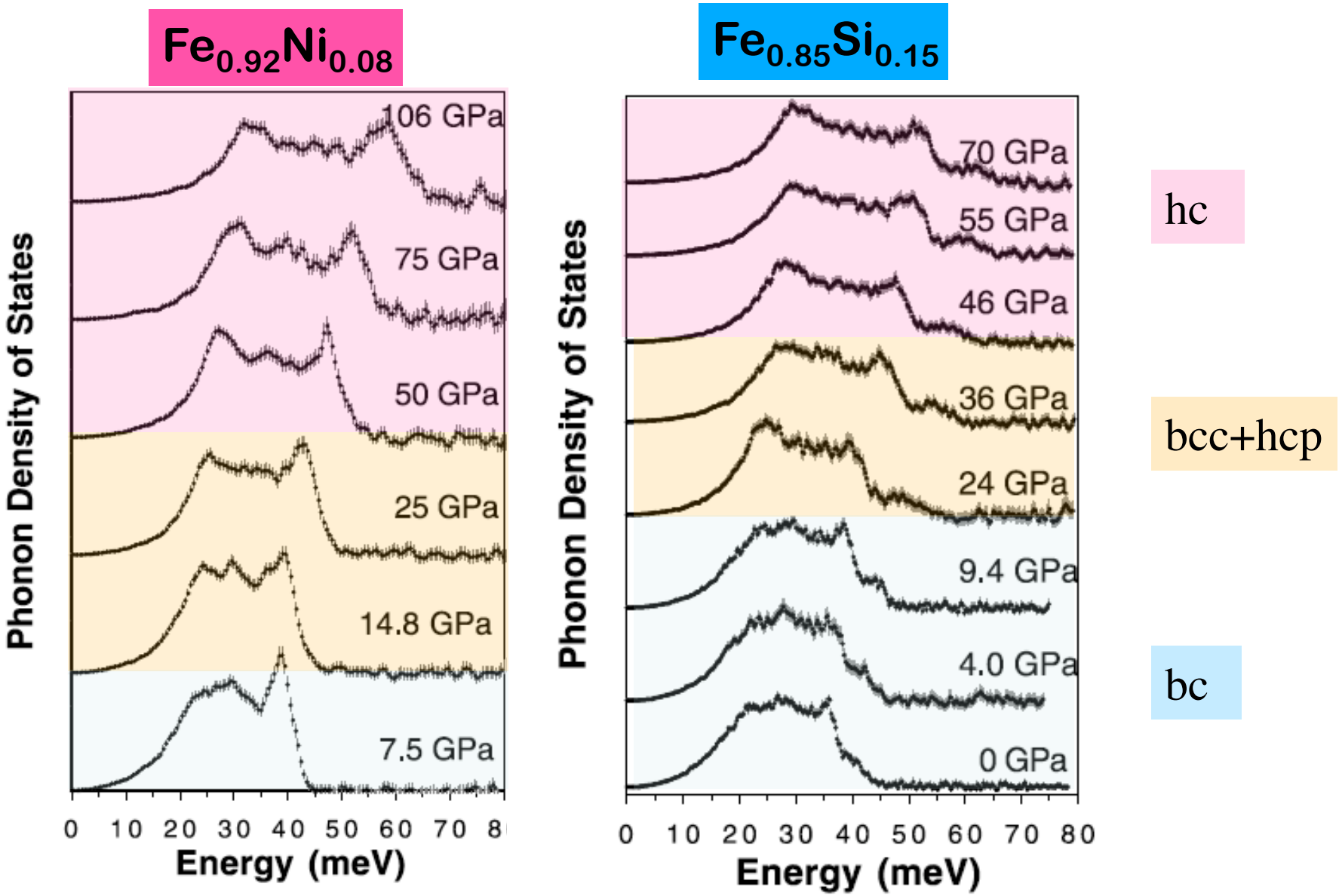

J.F. Lin, et al, Geophys. Res. Lett., 30 (2003) 2112

Speed of sound of Iron at high pressure/temperatures

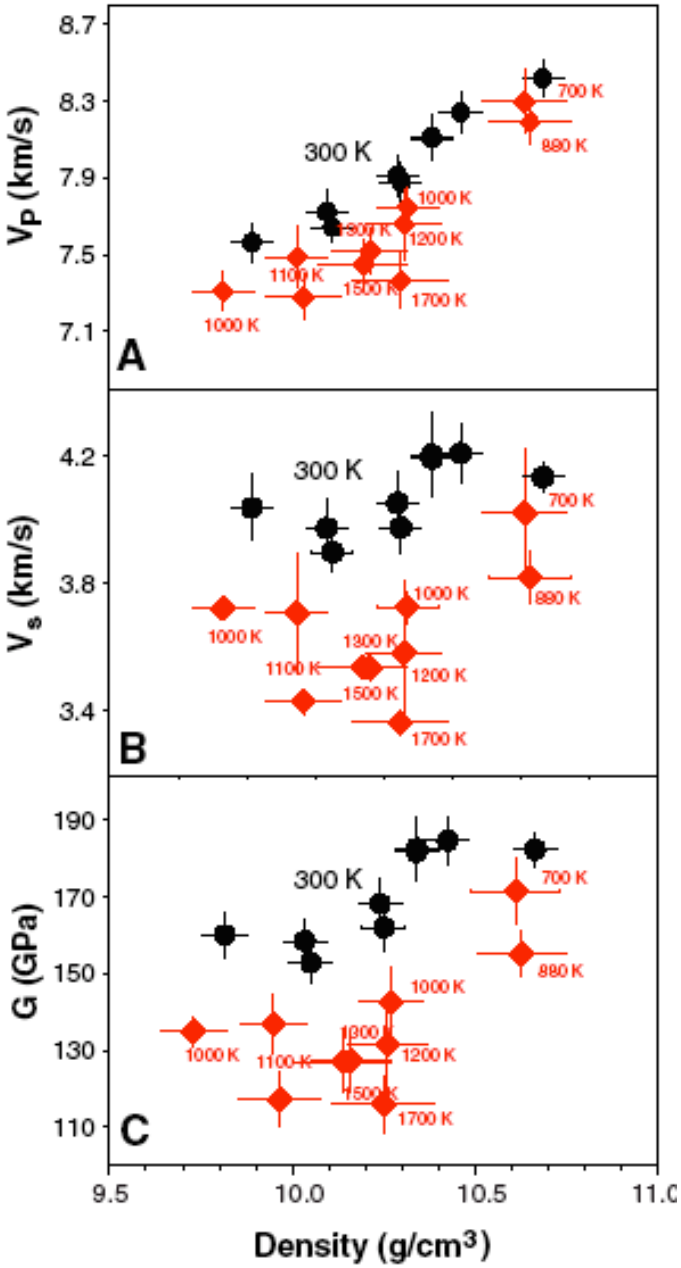

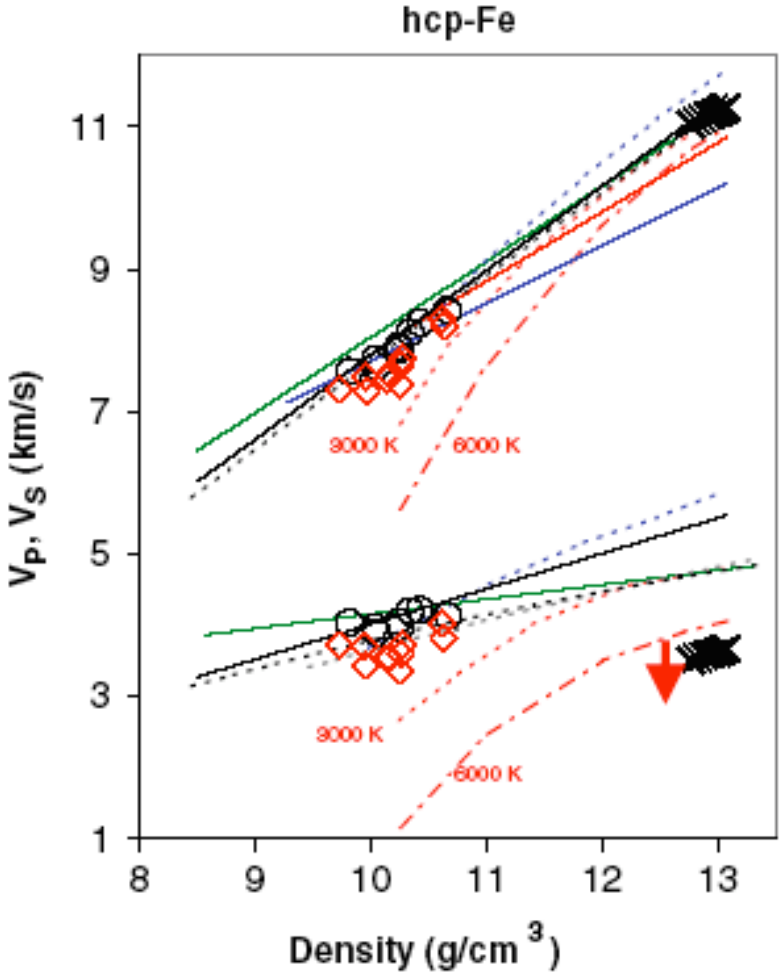

Lin, Sturhahn, Zhao, Shen, Mao, Hemley, Science, 308, (2005) 1892

$EuFe_4Sb_{12}$

Maybe the first sample to be studied partially and completely

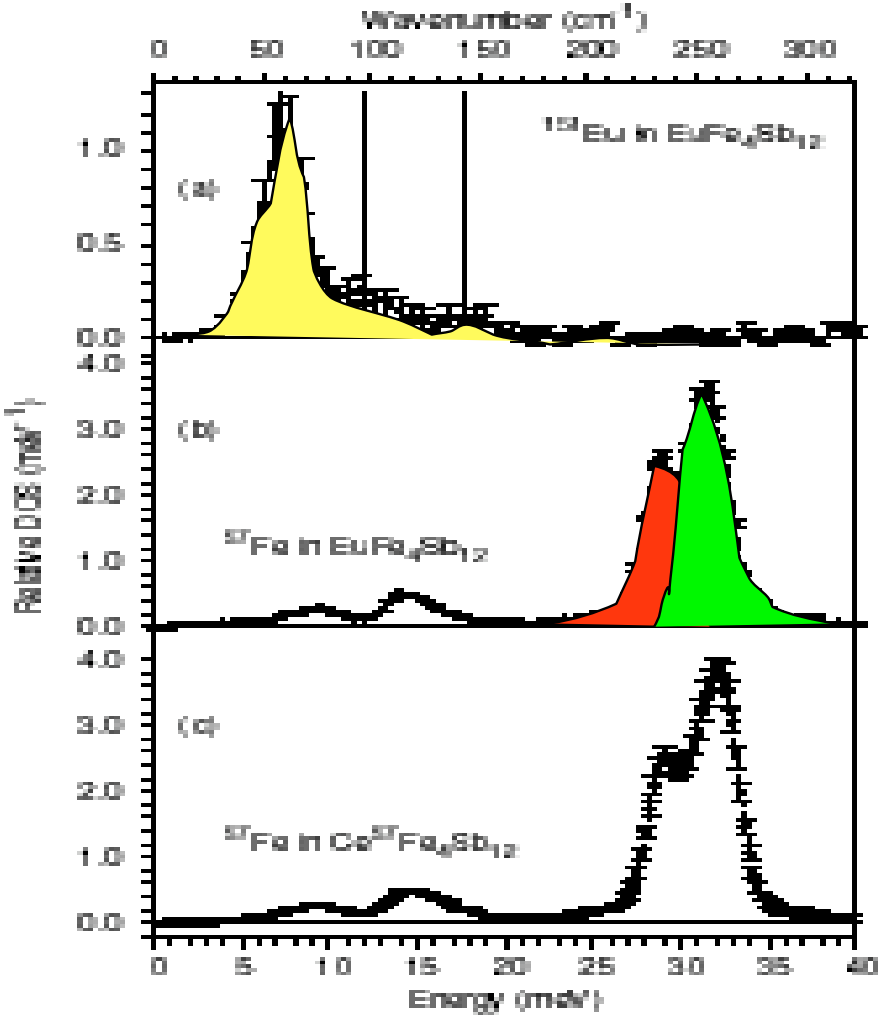

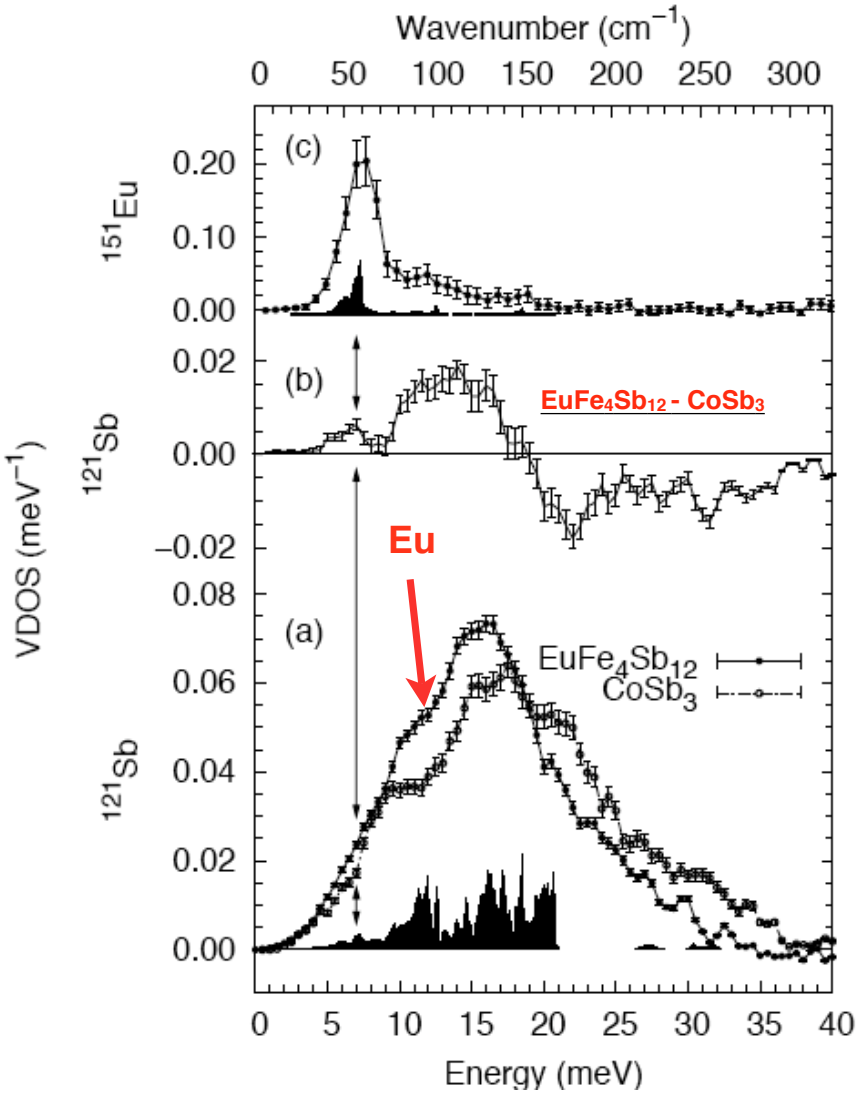

Filled skutterudite: $EuFe_4Sb_{12}$

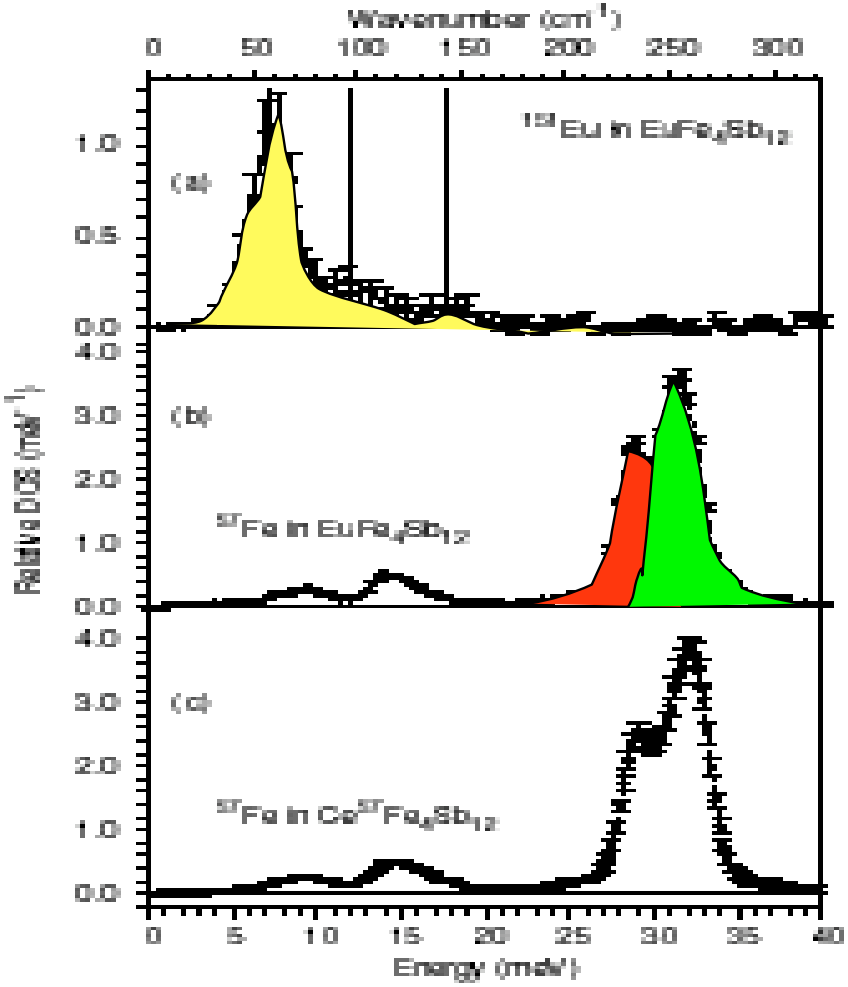

G. Long et al (Phys Rev B, 71 (2005) 140302

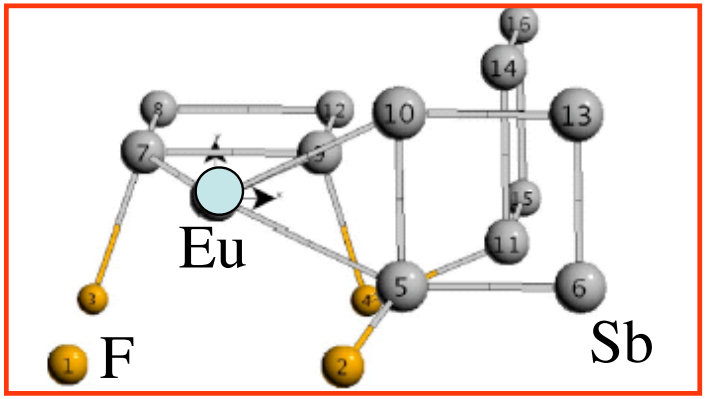

e

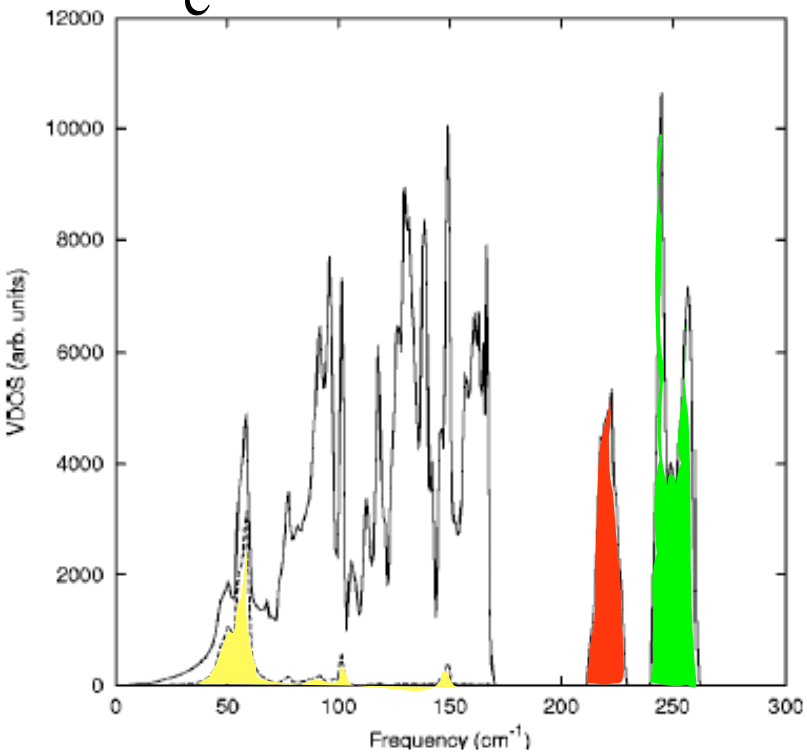

FIG. 4. Calculated vibrational density of states (VDOS): Total VDOS (solid) and La projected VDOS (dashed).

Feldman, et al, Phys Rev B 68 (2003) 94301

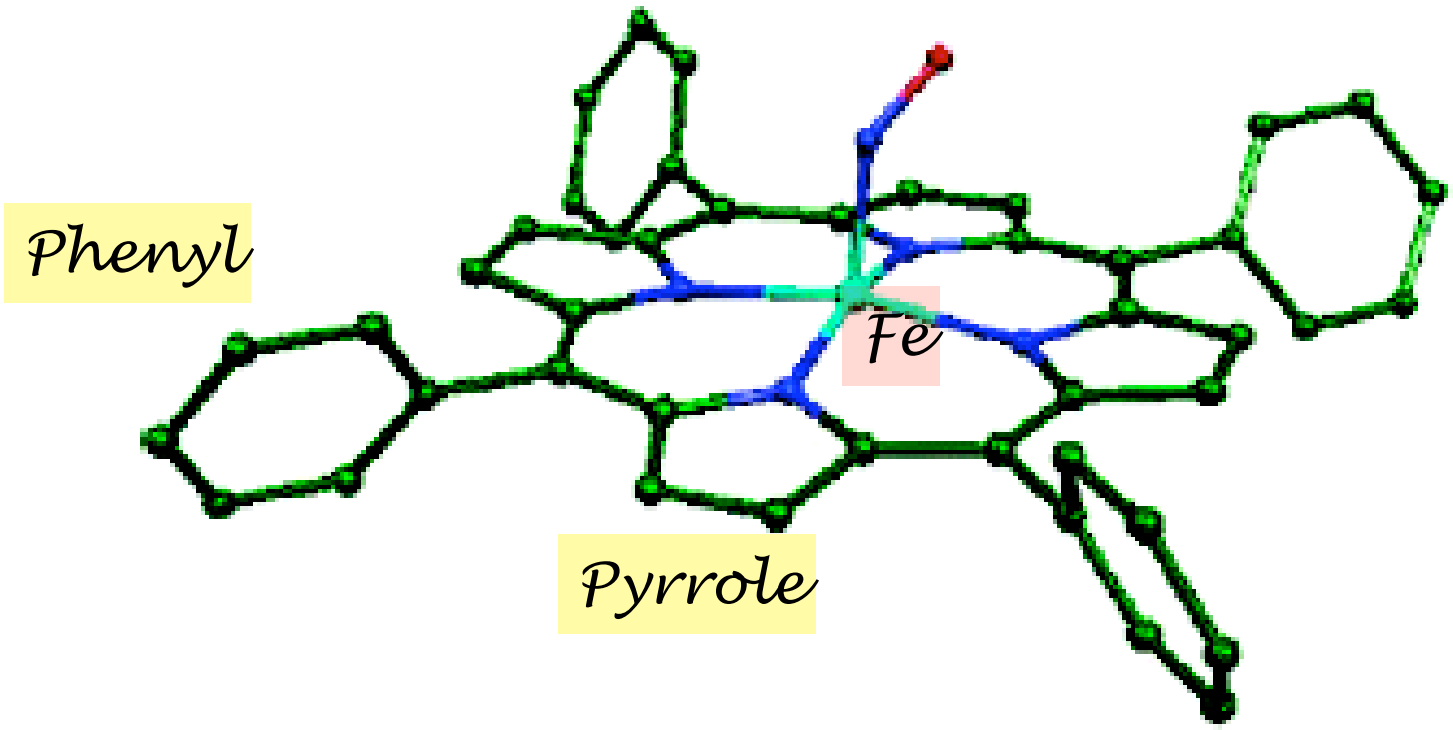

Figure 1. Calculated structure of ferrous nitrosyl tetraphenylporphyrin,

In-plane vibrations of heme Fe have not been identified in Raman spectra due to lack of electric dipole moment in D_{4h} symmetry.

Solvent absorption limit IR studies below 125 meV (1000 cm^{-1}).

Low frequency reactive modes are rarely identified with Raman or IR.

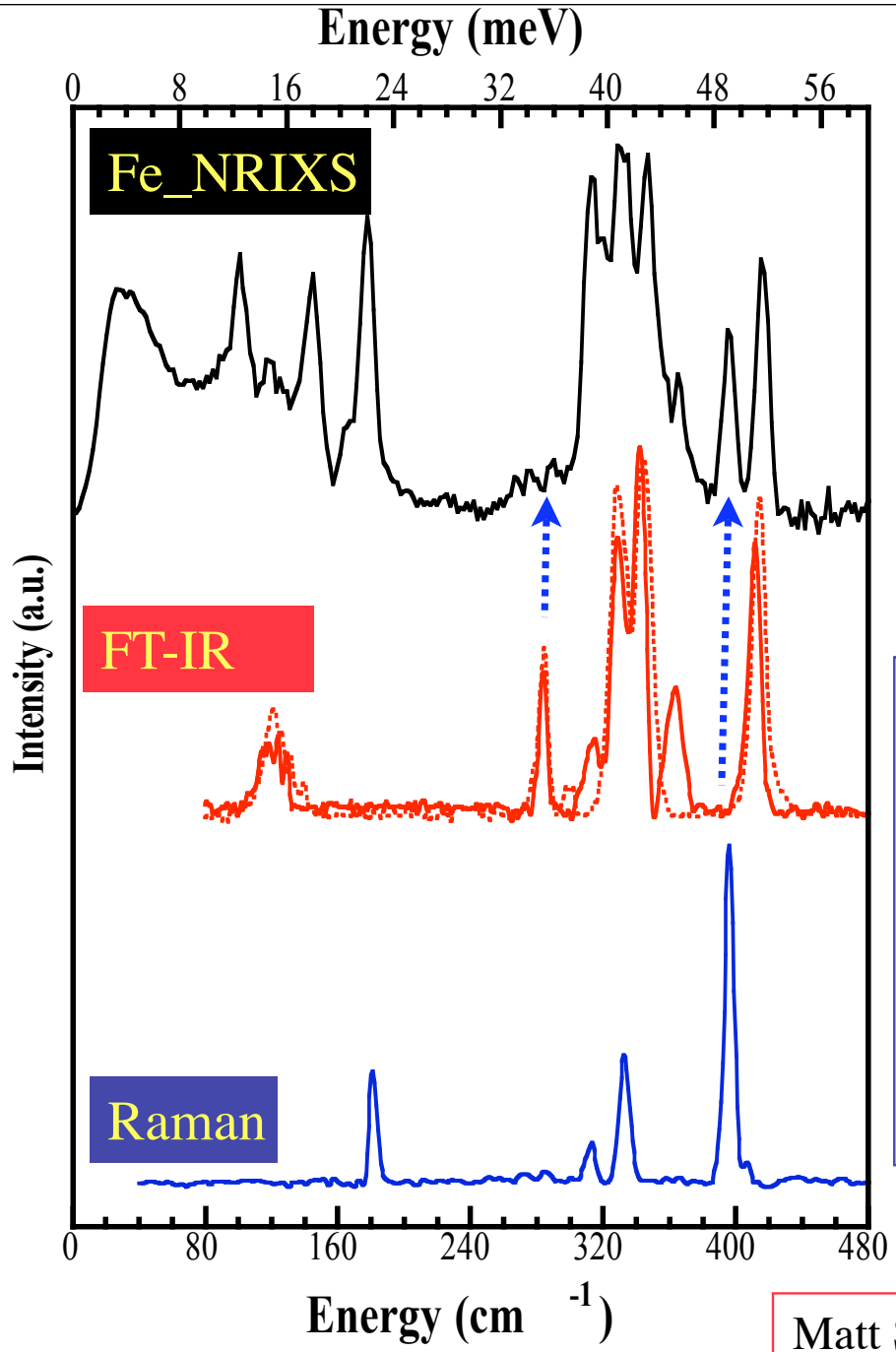

$[NEt_4]_2[Fe_2S_2Cl_4]$.

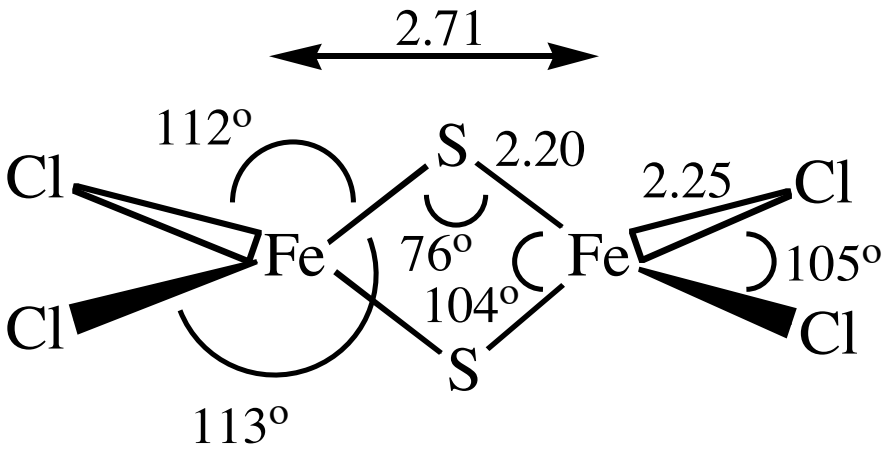

Some unique advantages of NRIXS

- Low frequency motions
2. No selection rule except motion of atoms along x-ray propagation
3. Peak intensity ~ mode participation ~ actual displacement
4. No matrix effects or limitations
5. Element and isotope selective
6. No unpredictable cancellations in scattering terms

Matt Smith, et al, Inorganic Chemistry, 2005, 44,5562

Iron-sulfur cubane compounds

- **Reduced {4Fe4S}$^{+}$ has not been possible to observe with resonant Raman technique, in contrast to oxidized {4Fe4S}$^{2+}$**

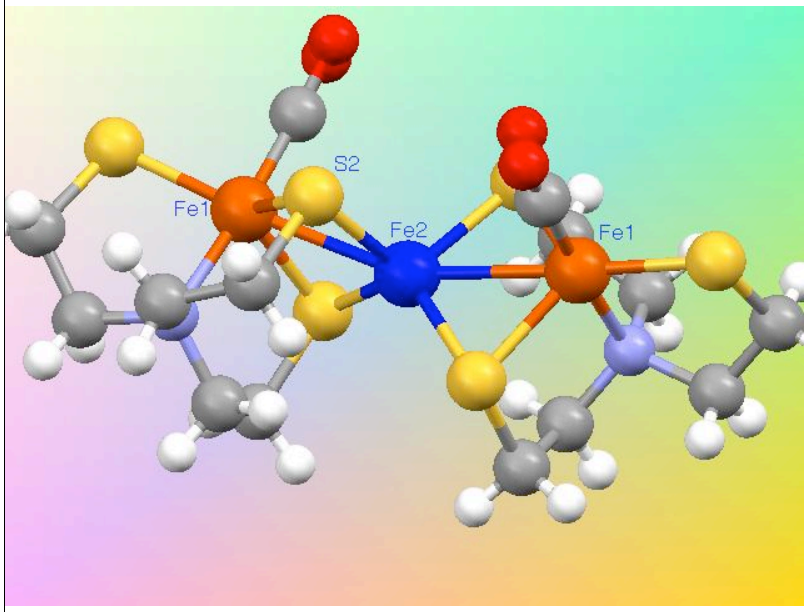

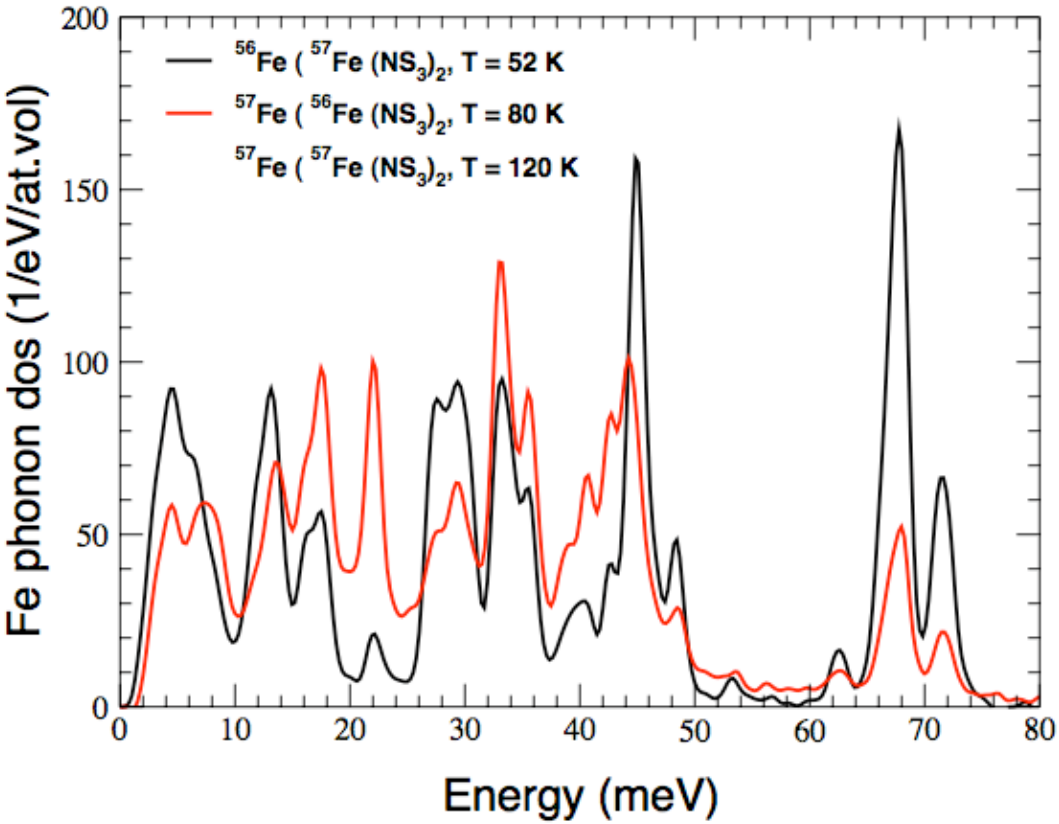

U. Jayasooriya et al, unpublished

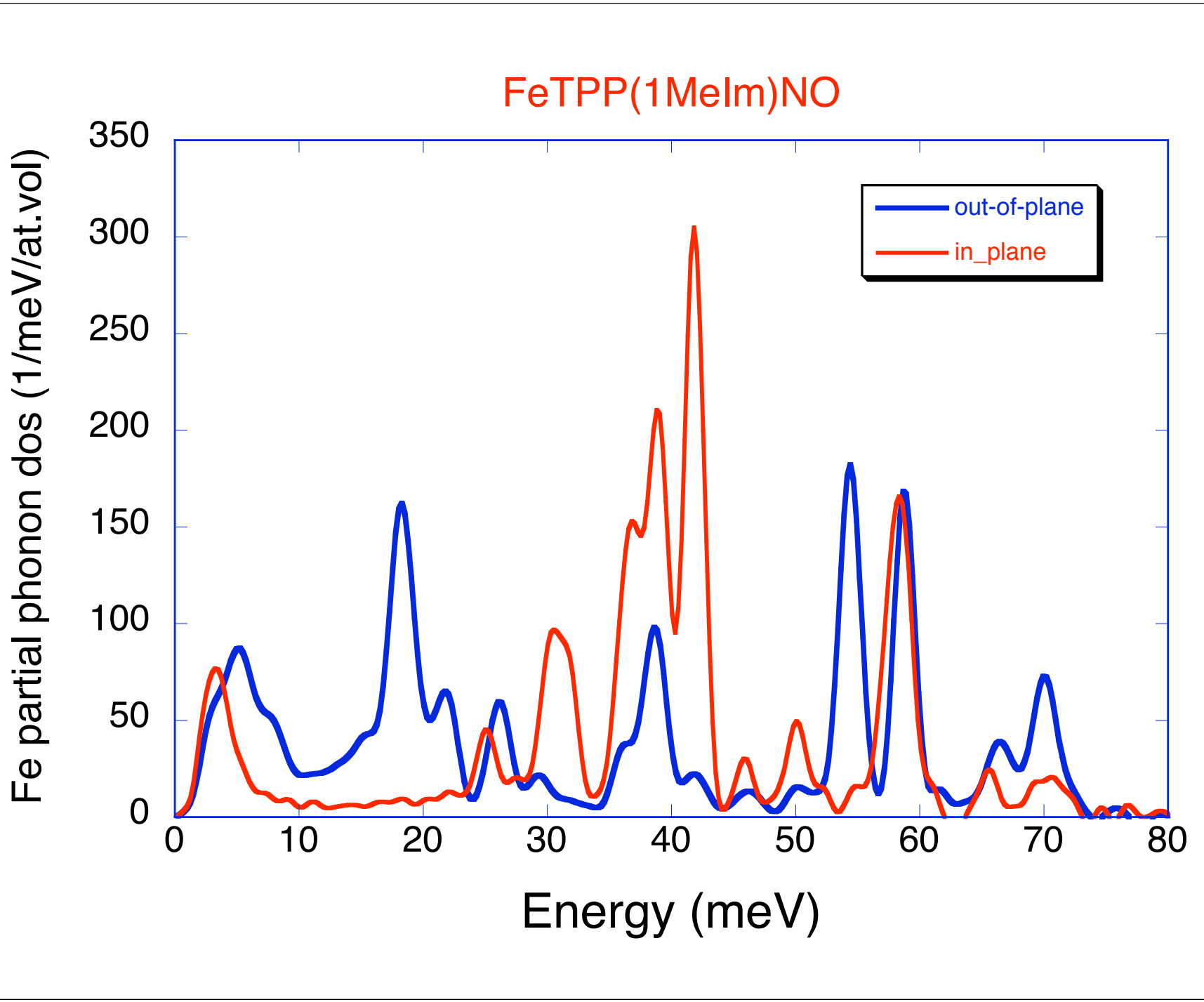
FeTPP(1MeIm)NO
Fe partial phonon dos (1/meV/at.vol)
Energy (meV)
out-of-plane
in_plane
0
50
100
150
200
250
300
350
0
10
20
30
40
50
60
70
80

Record resolution at 23.870 keV
^{119}Sn nuclear resonance
T. Toellner, 2003

$$E/\Delta E = 1.7 \cdot 10^8$$

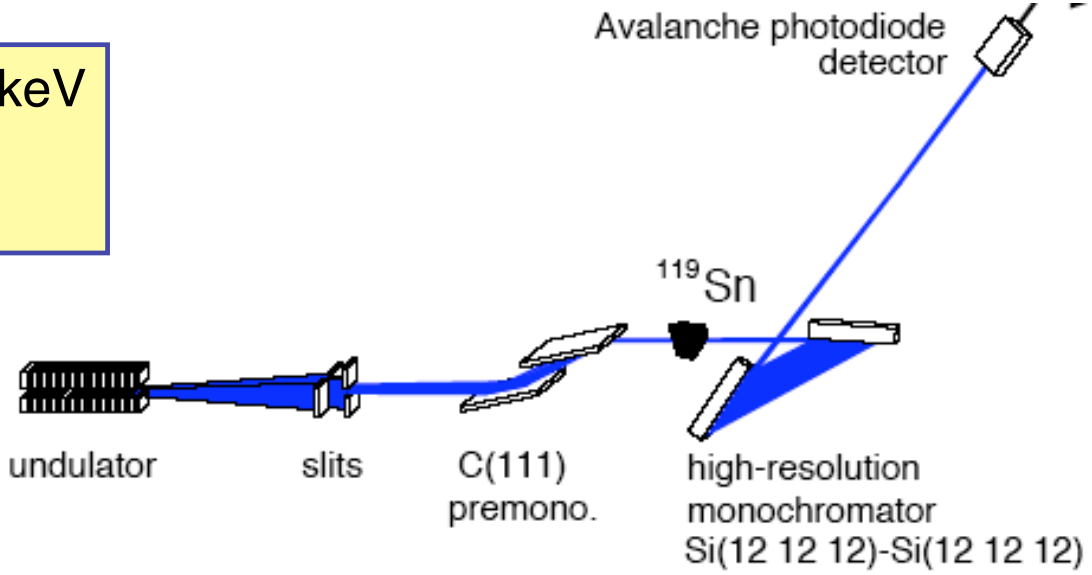

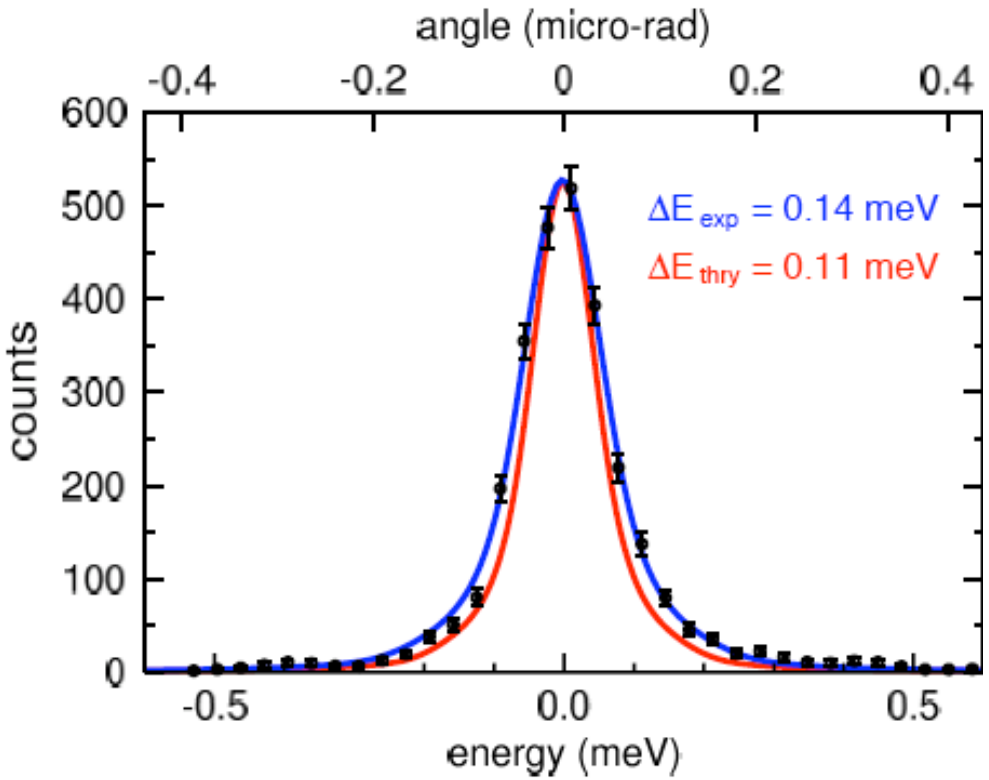

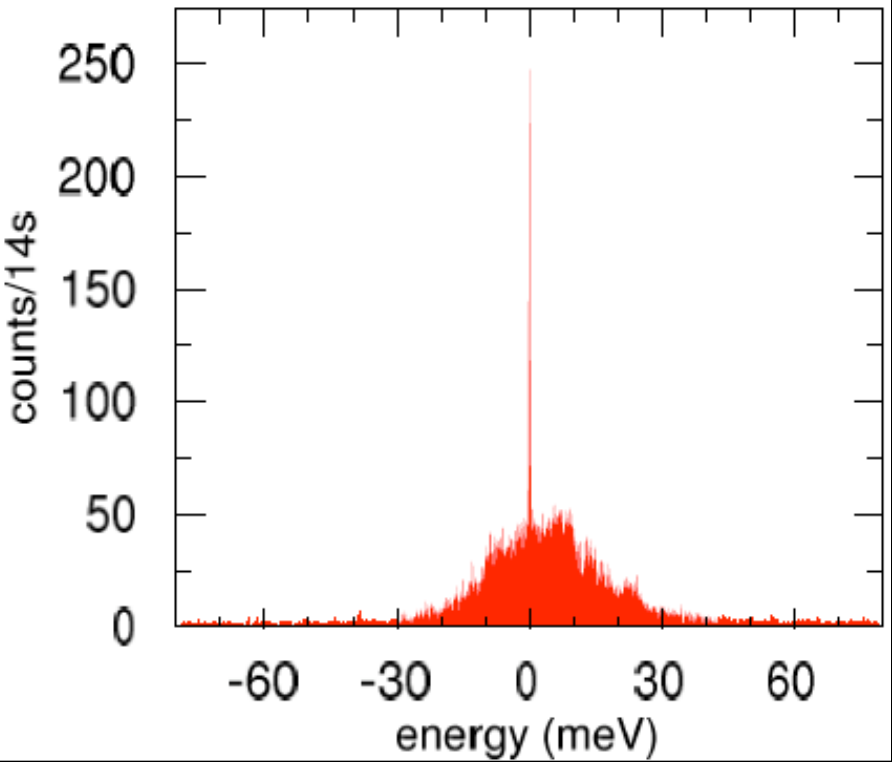

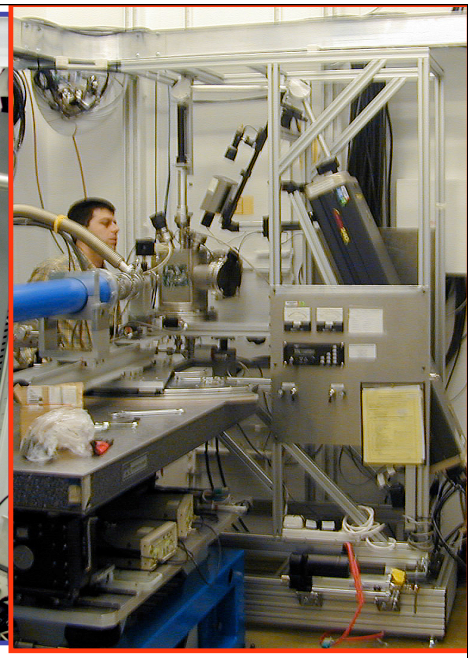

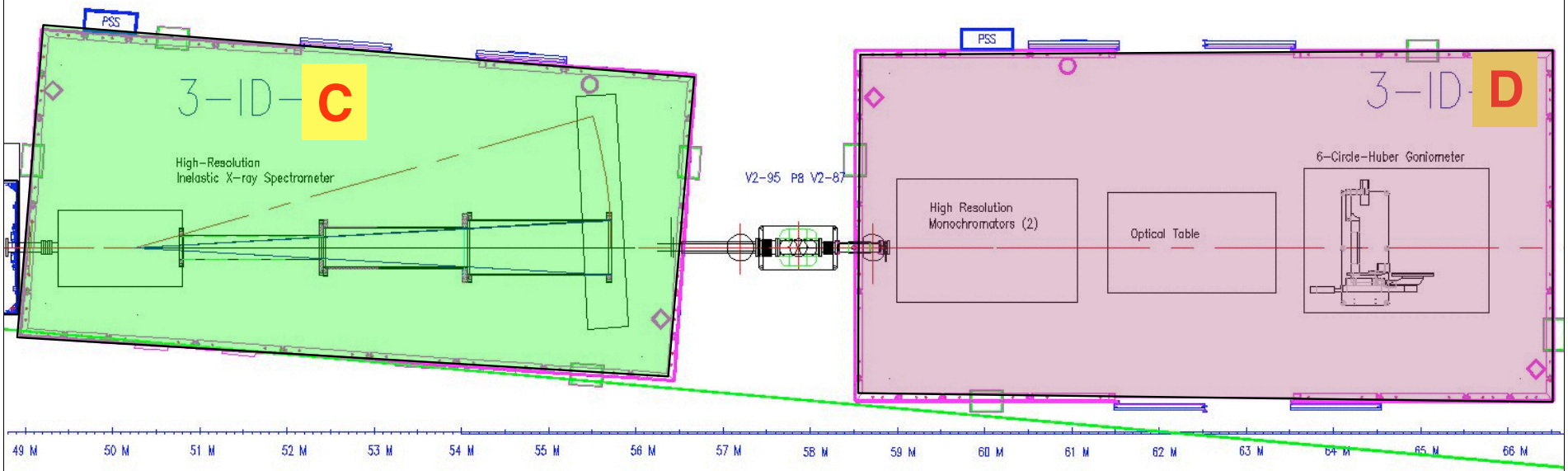
PSS
3-ID-C
High-Resolution
Inelastic X-ray Spectrometer
V2-95 PB V2-87
PSS
3-ID-D
High Resolution
Monochromators (2)
Optical Table
6-Circle-Huber Goniometer
49 M
50 M
51 M
52 M
53 M
54 M
55 M
56 M
57 M
58 M
59 M
60 M
61 M
62 M
63 M
64 M
65 M
66 M

Sapphire
Melting point: 2050°C

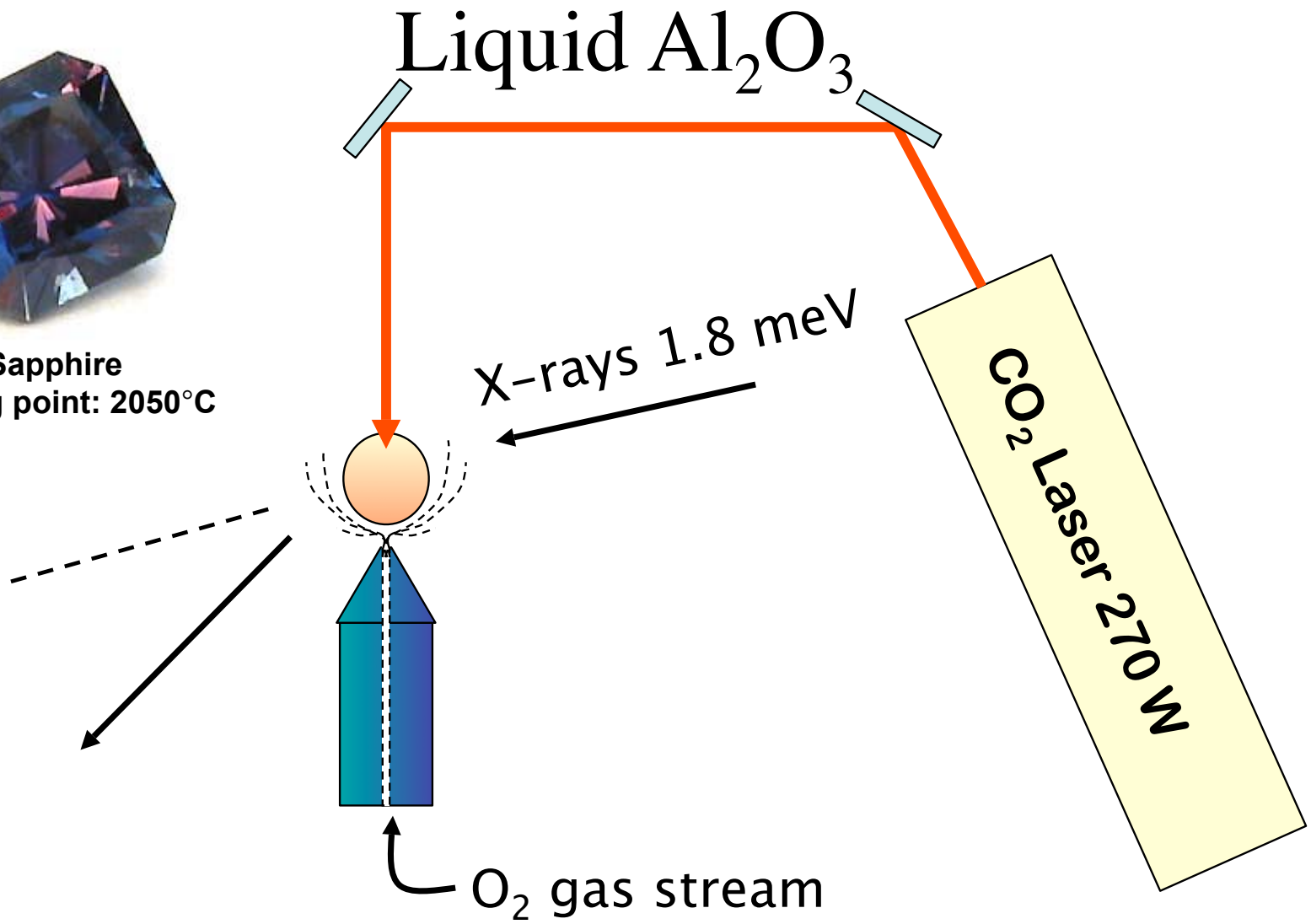

High Melting Point Substances

Lindemann criterion: $mv_{sound}^2 \propto T_{melt}$

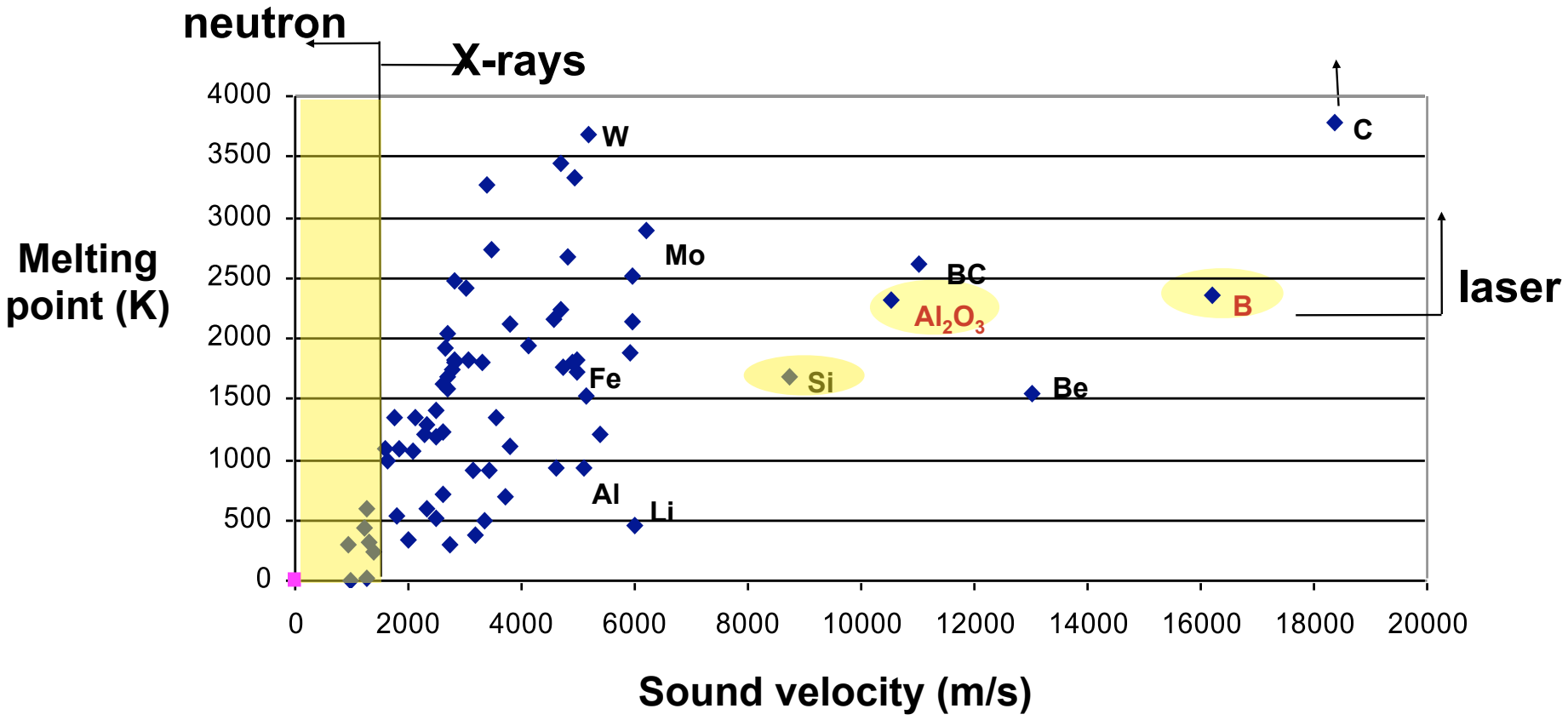

Liquid Al_2O_3 @ 2050°C

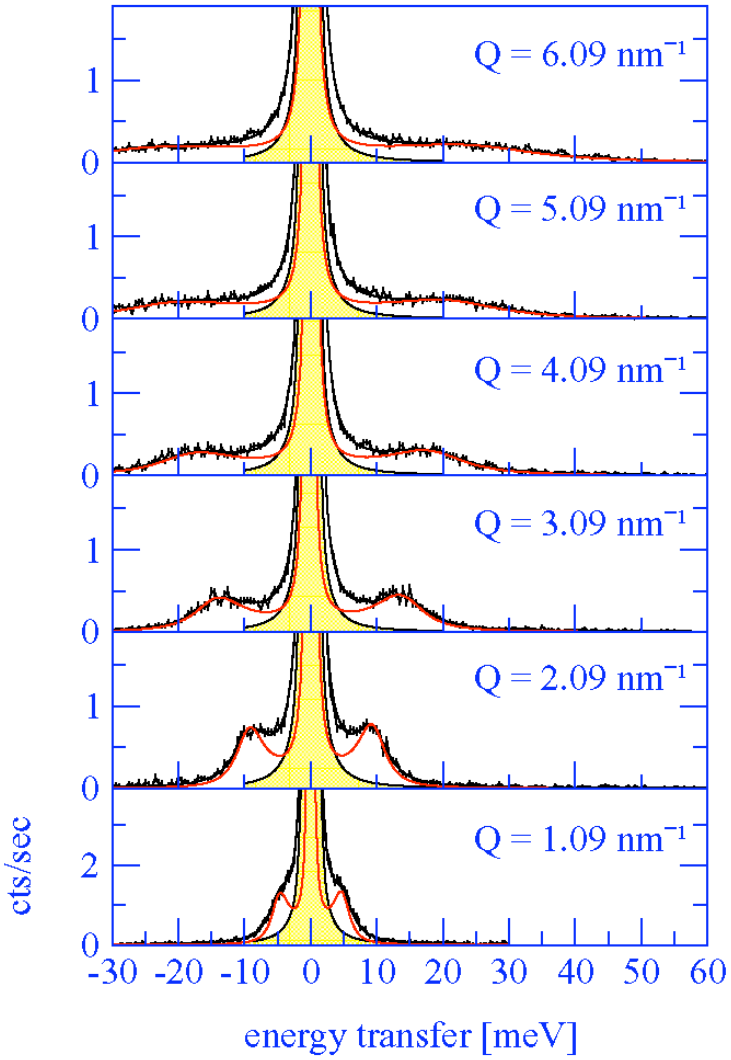

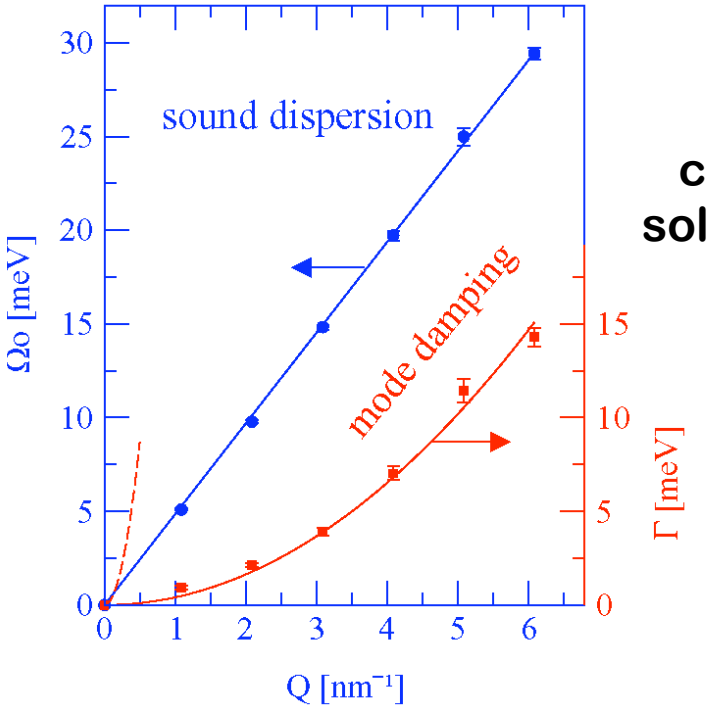

c = 7350 m/s
solid:10500 m/s

Damping is too low by factor 20!

Silicon - IXS spectra

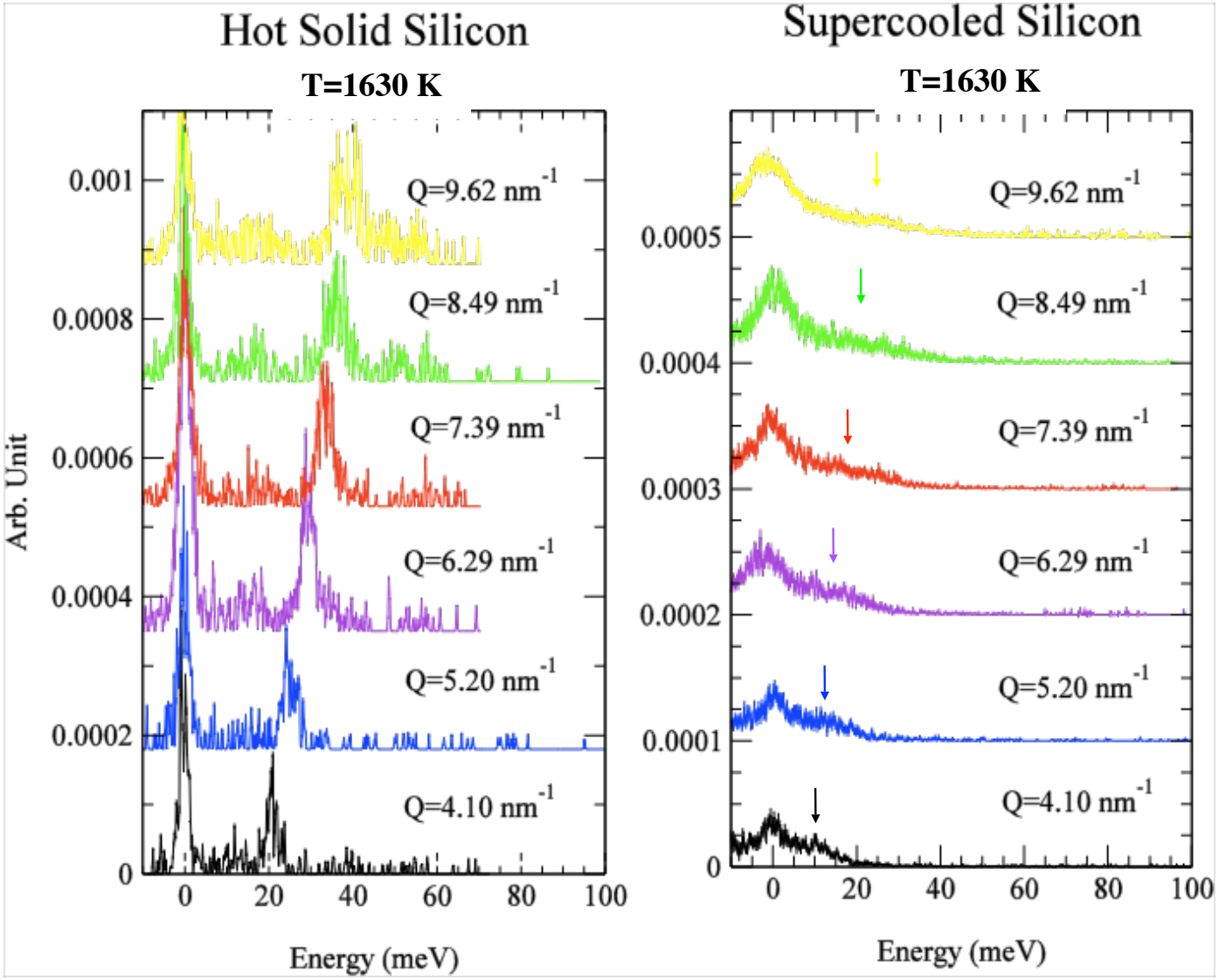

Courtesy: Ahmet Alatas, Ayman Said, &Harald Sinn

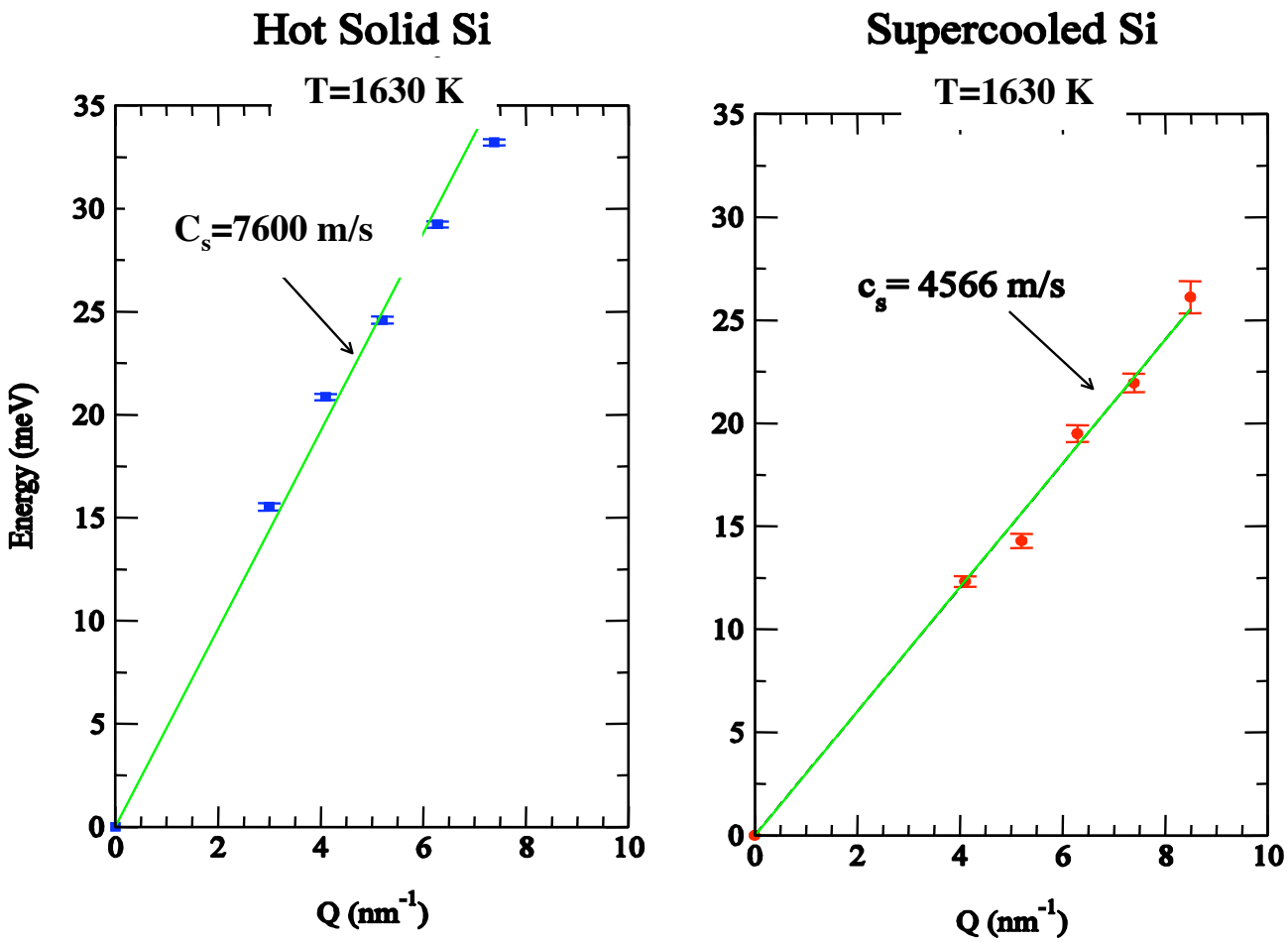
Hot Solid Si
T=1630 K
C_s=7600 m/s
Energy (meV)
Q (nm^-1)
Supercooled Si
T=1630 K
c_s = 4566 m/s
Q (nm^-1)

Sound dispersion in boron

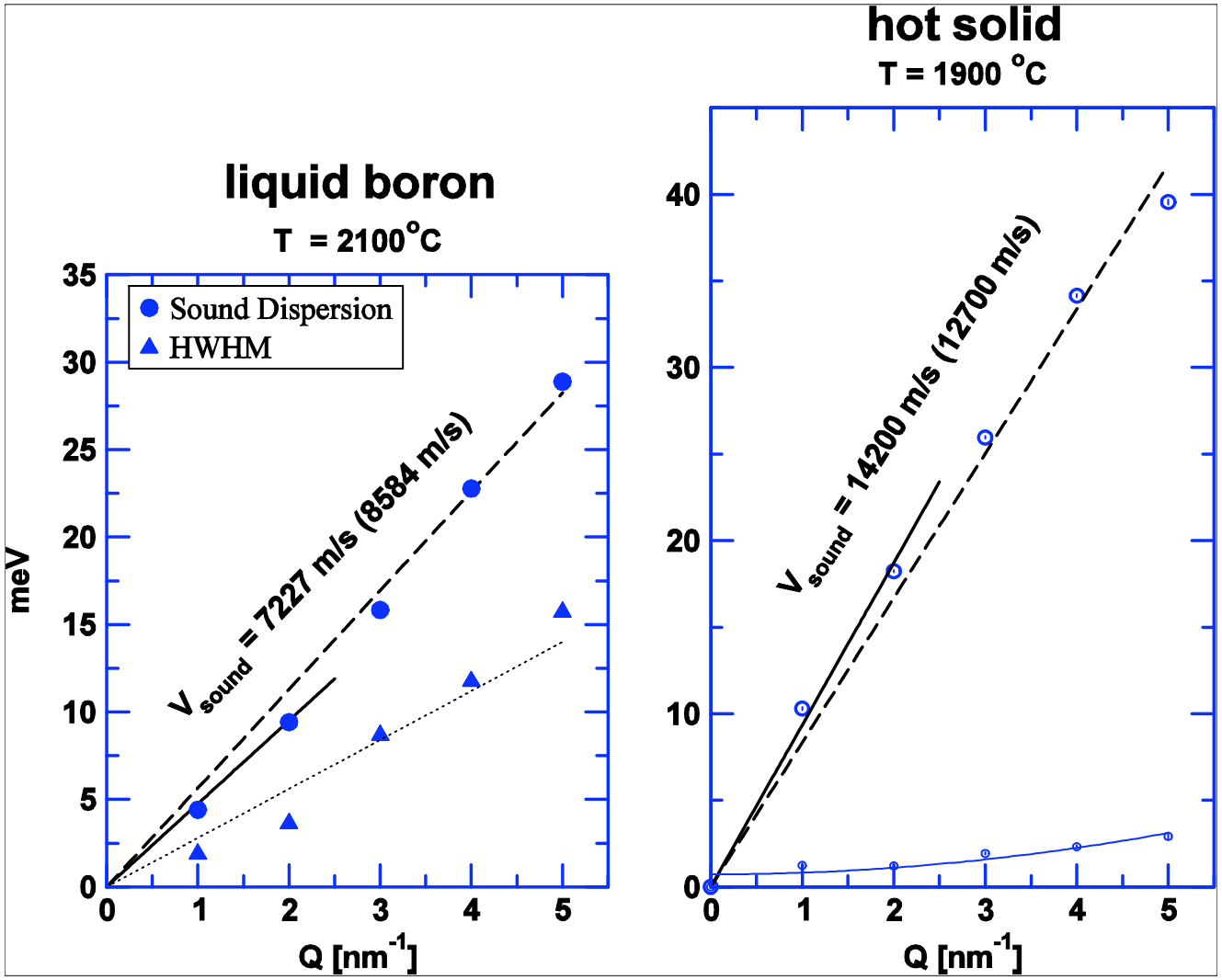

Literature:
14300 -
16000 m/s

49 % reduction in sound velocity upon melting

Si: 47%

Ge: 50 %

η_l (ω=0) = 14 mPas

$\eta_s \approx$ 1.5 mPas (est.)

τ(Q=0) = 0.2 ps

1 meV IXS spectrometer @ 25.7 keV

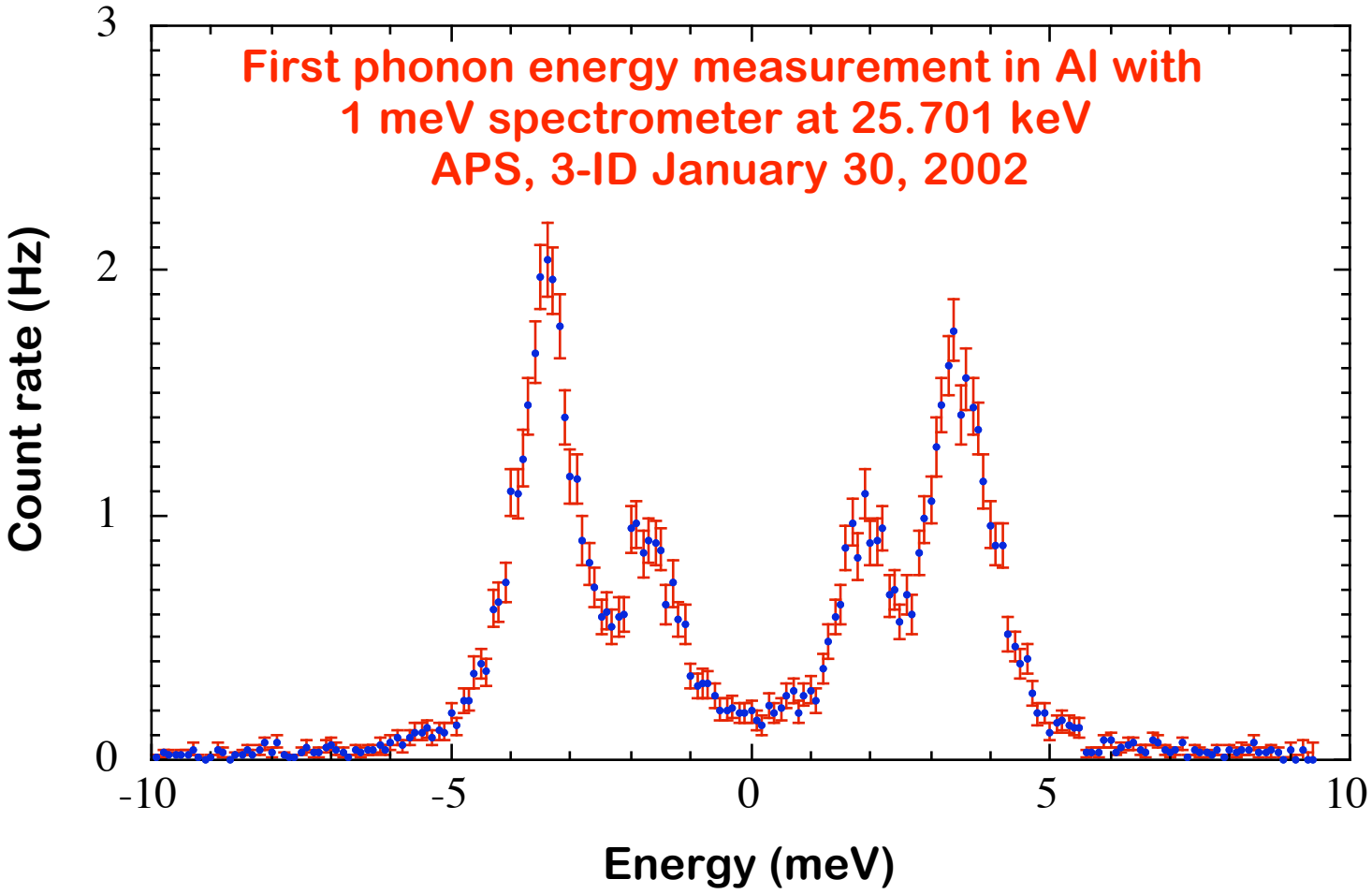

IXS-CDT Beamline: 30-ID

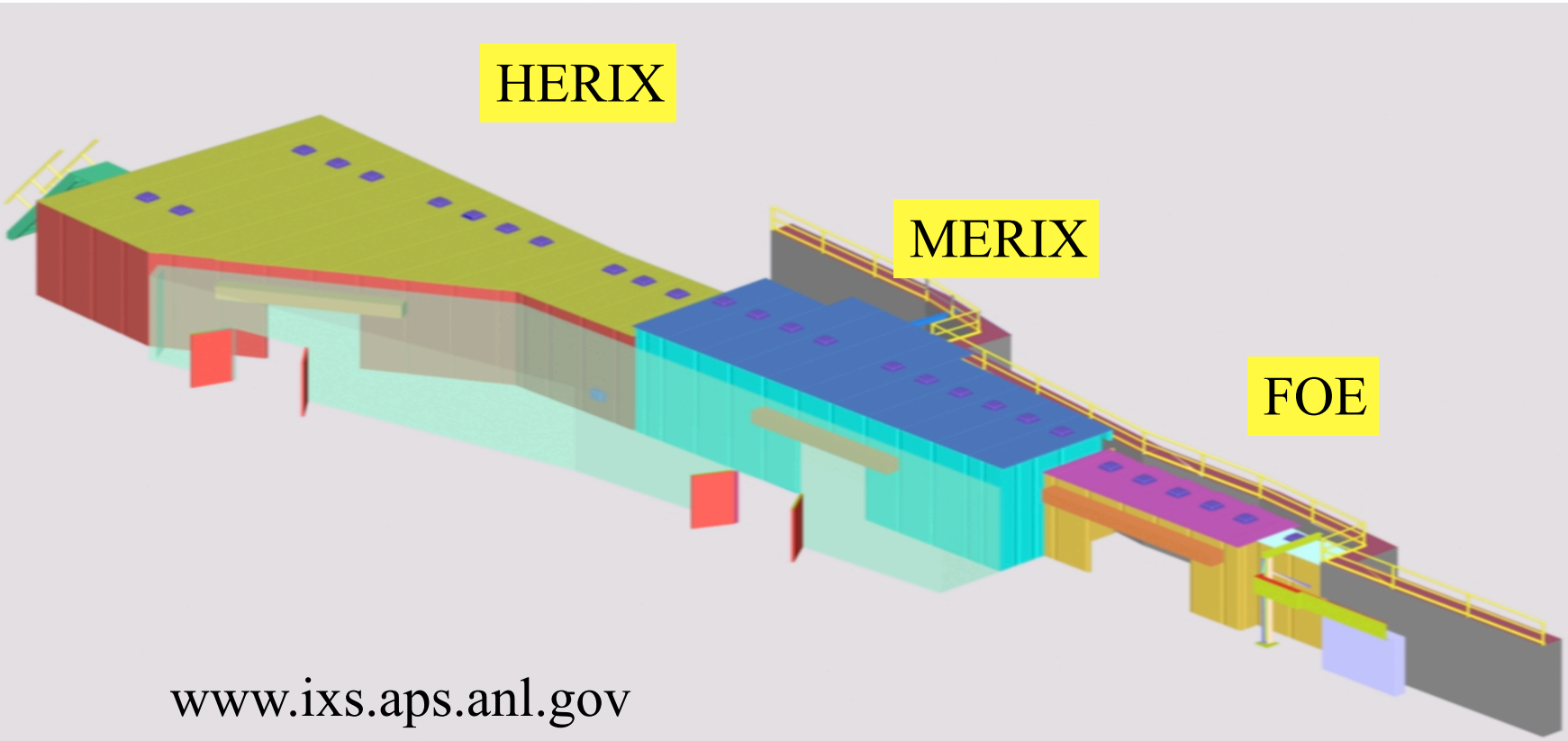

www.ixs.aps.anl.gov

30-ID-C: HERIX Spectrometer

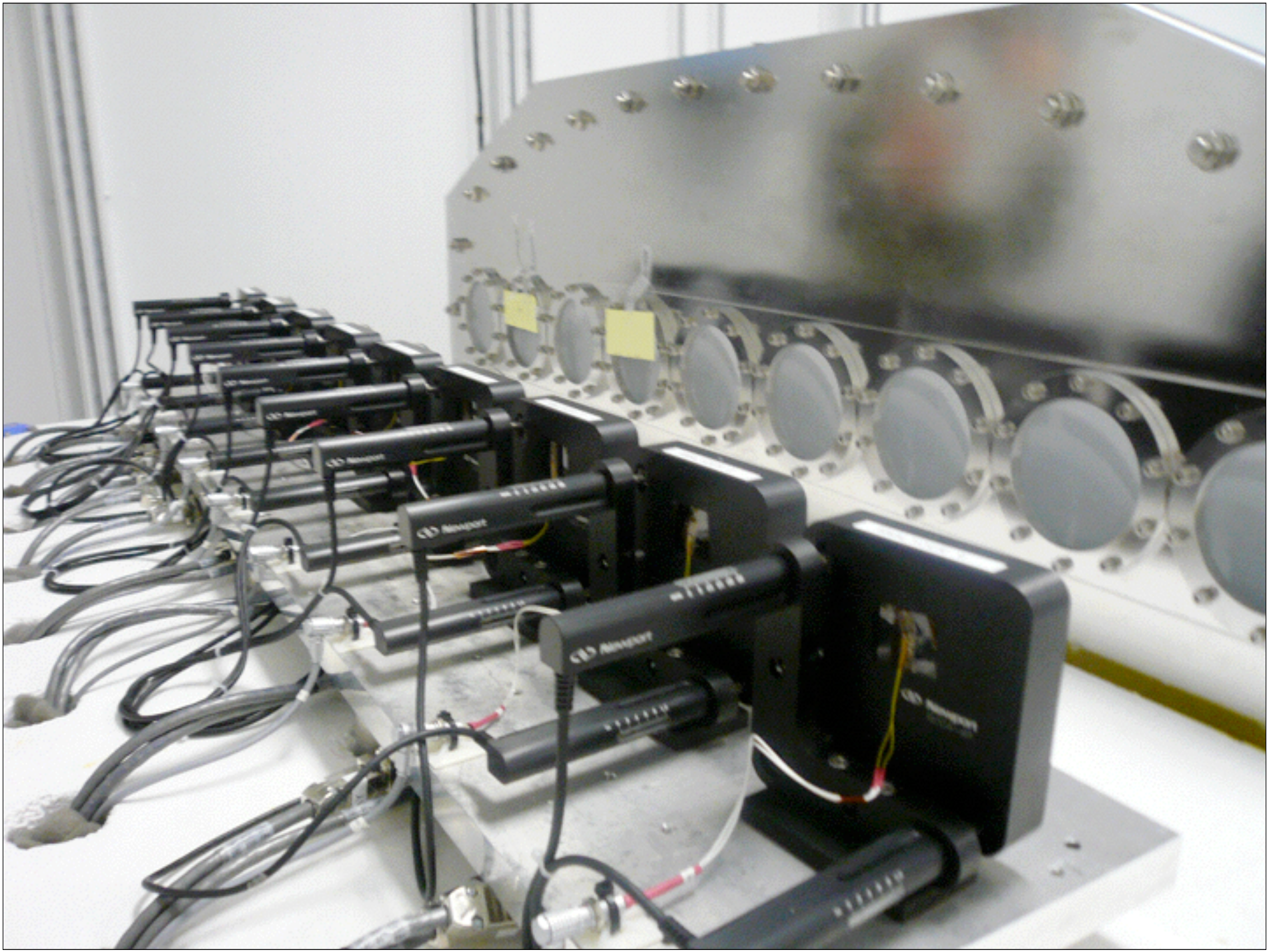

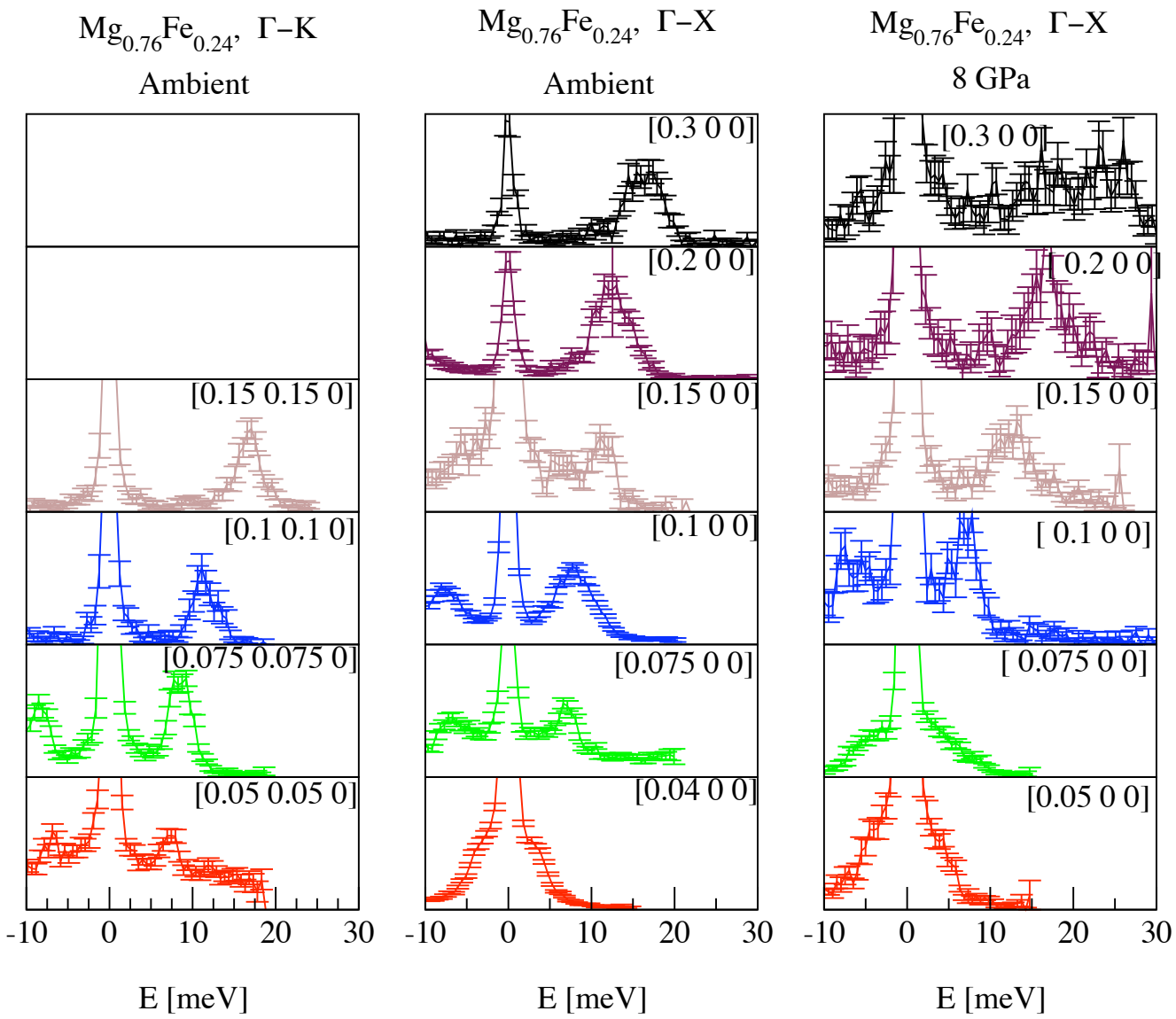

J. Jackson (Caltech), A. Said (APS) 2007

Present Set-up at 9-IDB

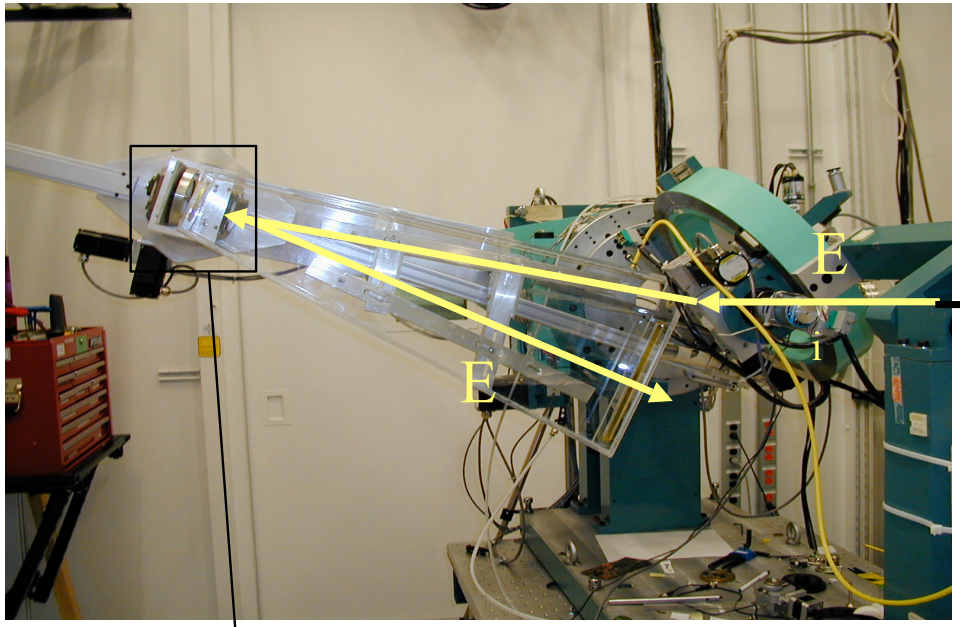

High-Heat Load

Si(111) ΔE~1.5 eV

Si(333) ΔE~0.16 eV

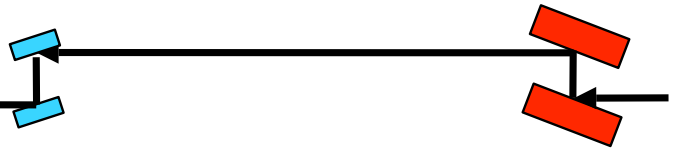

Secondary Mono

Si(444) ΔE~0.09 eV

Si(333) ΔE~0.16 eV

Si(331) ΔE~0.25 eV

R=1m

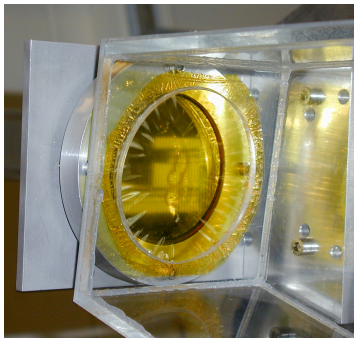

Analyzer

Ge(733) ΔE~0.3 eV

Ge(531) ΔE~0.3 eV

Si(nnn) ΔE~0.3 eV

Instrument gets 30% of time and is available to GUs

X-ray emisson spectroscopy in a diamond anvil cell: Study spin states of Fe in Fe_3C and $(Mg_{0.4},Fe_{0.6})O$

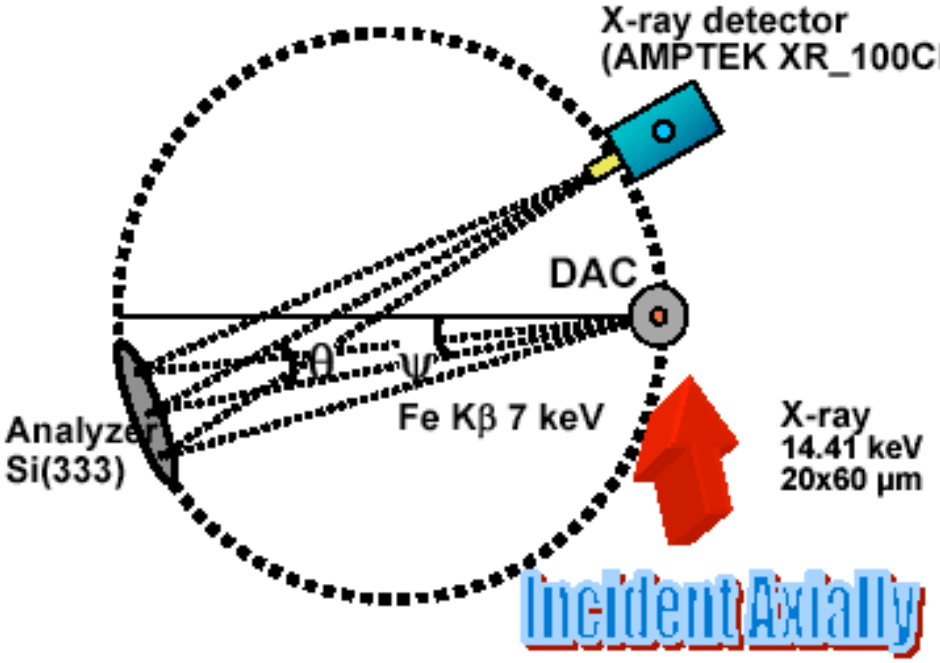

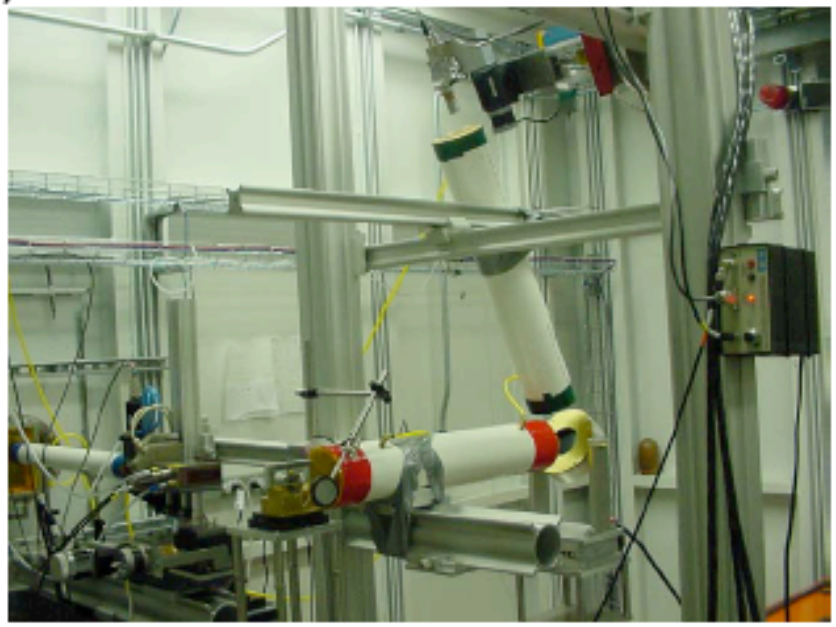

XES system setup at 16 ID-D, HPCAT

- XES of Fe Kβ at 16 ID-D, HPCAT, APS
- Focused X-ray beam (20x60 μm spot)
- High resolution Rowland-circle spectrometer (<1 eV)
- Beryllium+B gasket in a diamond cell

In cooperation with V. Struzhkin, M. Hu, P. Chow, H.K. Mao, and R.J. Hemley

W. Mao, Science 302 (2003) 425

Bonding Changes in Compressed Superhard Graphite

Wendy L. Mao,[1,4]* Ho-kwang Mao,[1,4] Peter J. Eng,[2,3] Thomas P. Trainor,[2,7] Matthew Newville,[2] Chi-chang Kao,[5] Dion L. Heinz,[1,3] Jinfu Shu,[4] Yue Meng,[6] Russell J. Hemley[4]

Compressed under ambient temperature, graphite undergoes a transition at ~17 gigapascals. The near K-edge spectroscopy of carbon using synchrotron x-ray inelastic scattering reveals that half of the π-bonds between graphite layers convert to σ-bonds, whereas the other half remain as π-bonds in the high-pressure form. The x-ray diffraction pattern of the high-pressure form is consistent with a distorted graphite structure in which bridging carbon atoms between graphite layers pair and form σ-bonds, whereas the nonbridging carbon atoms remain unpaired with π-bonds. The high-pressure form is superhard, capable of indenting cubic-diamond single crystals.

Fig. 1. High-pressure IXS spectra for graphite in horizontal and vertical directions plotted as normalized scattered intensity versus energy loss (incident energy – analyzer energy). The scattered intensity is normalized to the incoming intensity. The lower energy peak, labeled π, corresponds to 1s to π* transitions and the higher energy portion, labeled σ, corresponds to 1s to σ* transitions. The bottom spectra, taken in the horizontal direction, probes bonds in the *a* plane and does not show any π-bonding before and after the high-pressure transition. The top seven spectra, taken in the vertical direction, probe the *c* plane. After the transition, the σ bonds increase at the expense of the π bonds.

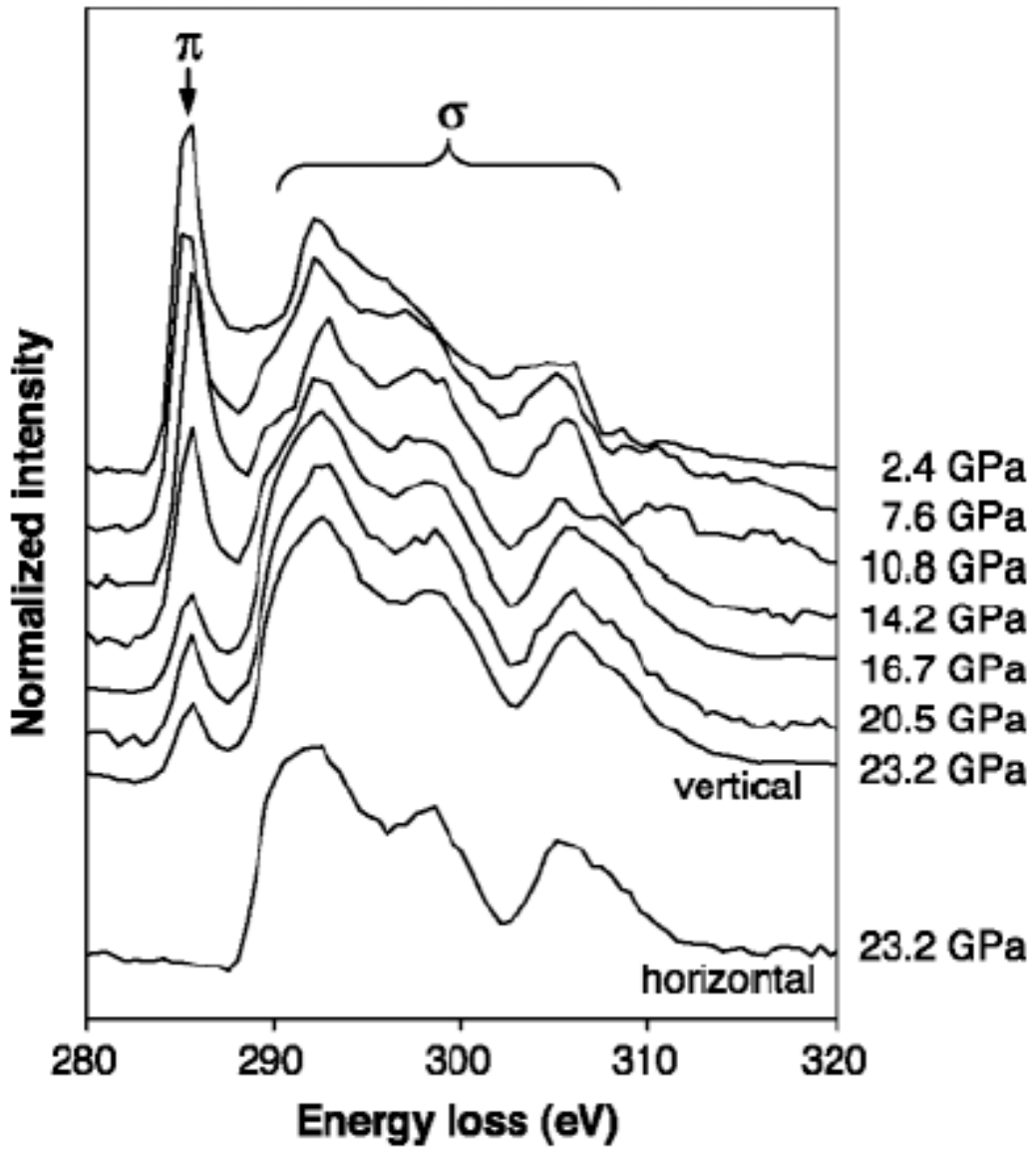

X-Ray Raman: LERIX Spectrometer @ PNC-CAT, Sector 20

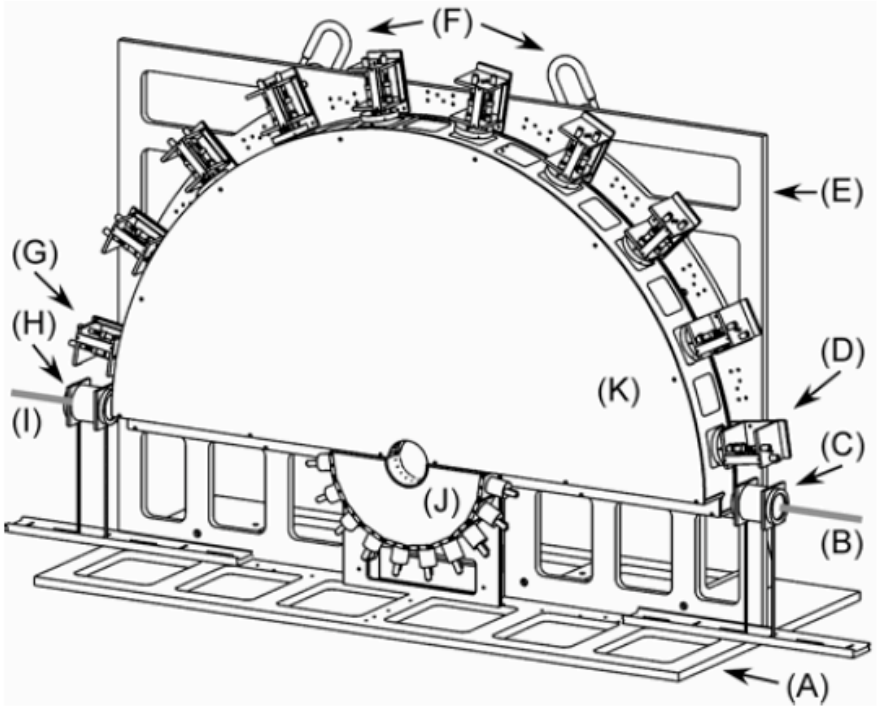

T. T. Fister, G. Seidler, et al,
Rev. Sci. Instr. 77 (2006) 063901

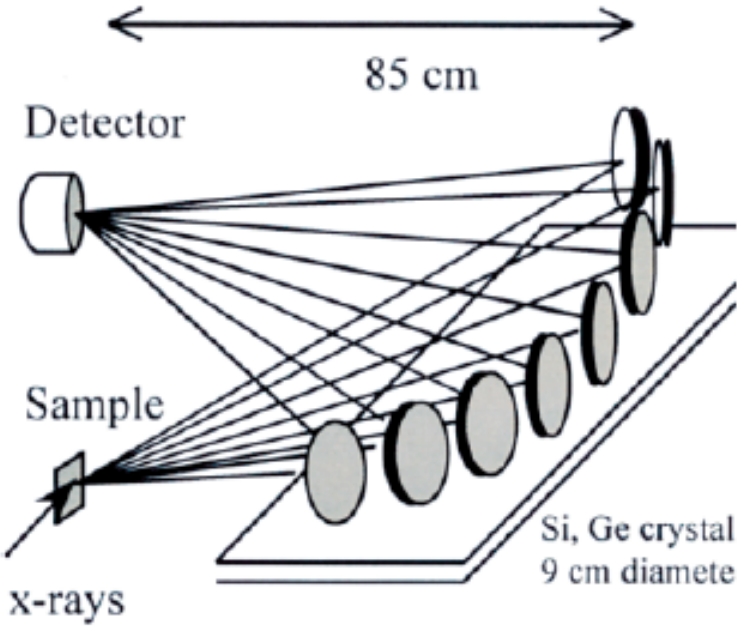

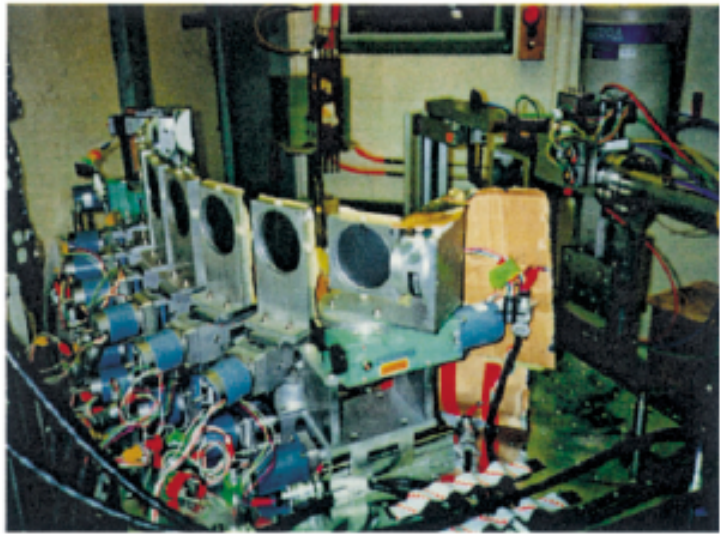

U. Bergmann, et al, Microchemical Journal, 71 (2002) 221

Bulk-sensitive XAS characterization of light elements: from X-ray Raman scattering to X-ray Raman spectroscopy

Uwe Bergmann[a,b,*], Pieter Glatzel[b], Stephen P. Cramer[a,b]

Microchemical Journal 71 (2002) 221–230

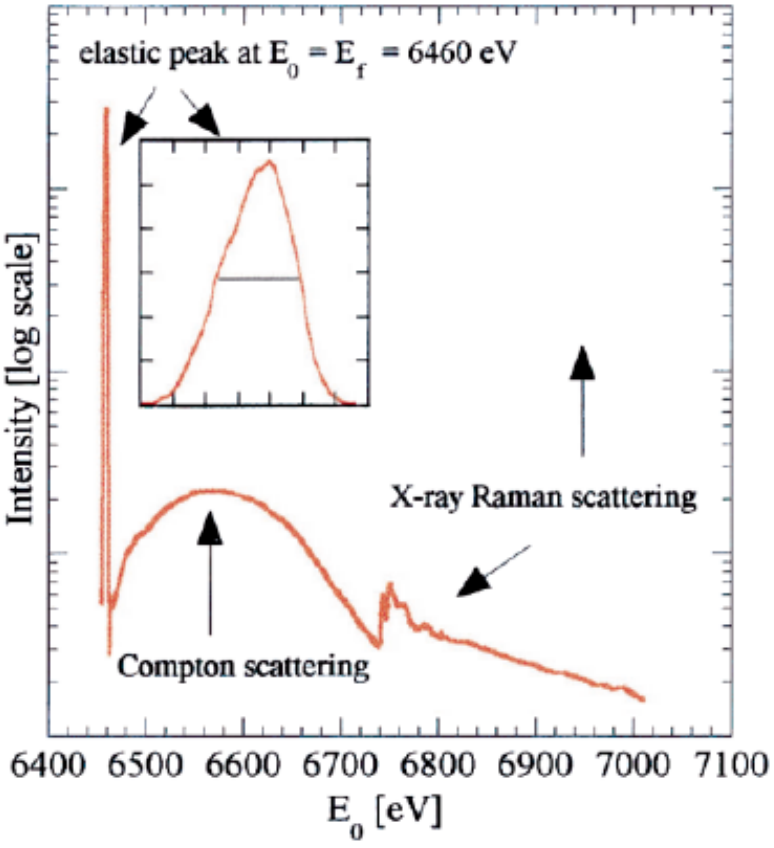

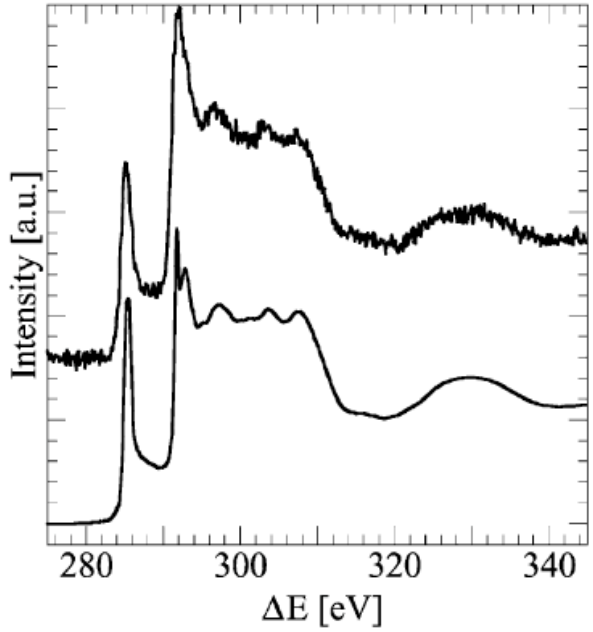

Fig. 2. Comparison of graphite K-edge XANES taken by XRS (top) with 1 eV FWHM resolution and by conventional XAS in electron yield mode (bottom) at 0.15 eV FWHM resolution. The analyzer energy was set to $E_f = 6.46$ keV, at an incident intensity of some 10^{13} photons/s.

Future application of IXS

Pressure, temperature, composition

What we can do now:

1. IXS study of powder samples (Fe, Fe compounds,..) at ESRF
2. Magnetism at high pressures
3. Sound velocities of core materials at high pressure
4. Electronic/magnetic transition at high pressure
5. Bonding changes

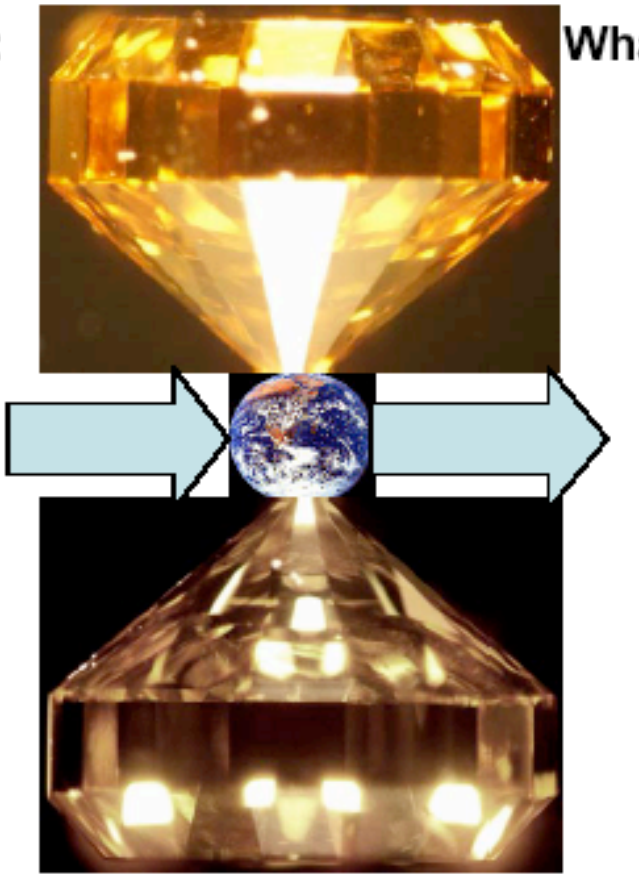

Big CVD diamonds (Yan et al., 2004)

What can we do in the future?:

1. Single crystal IXS study of mw and pv (anisotropy); shear wave
2. Magnetic phase diagram at high PT; Curie temperature
3. Sound velocities of mw and pv at high PT
4. Electronic transition at high PT with EOS and structure information
5. Bonding changes in planetary materials

Time: long-term heating (days)

J.F. Lin, Carnegie Institute of Washington

Inelastic X-Ray Scattering in the Synchrotron Era

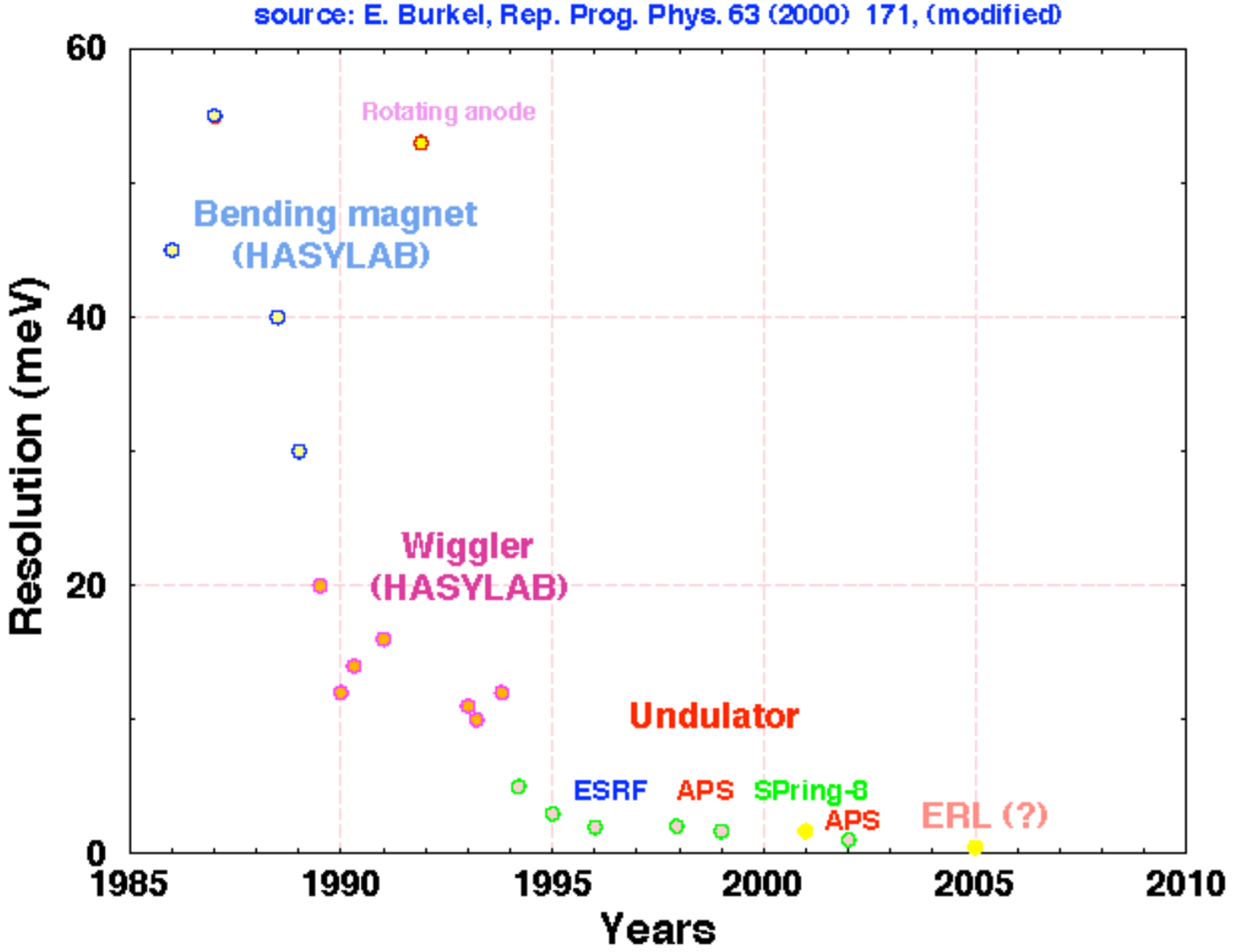

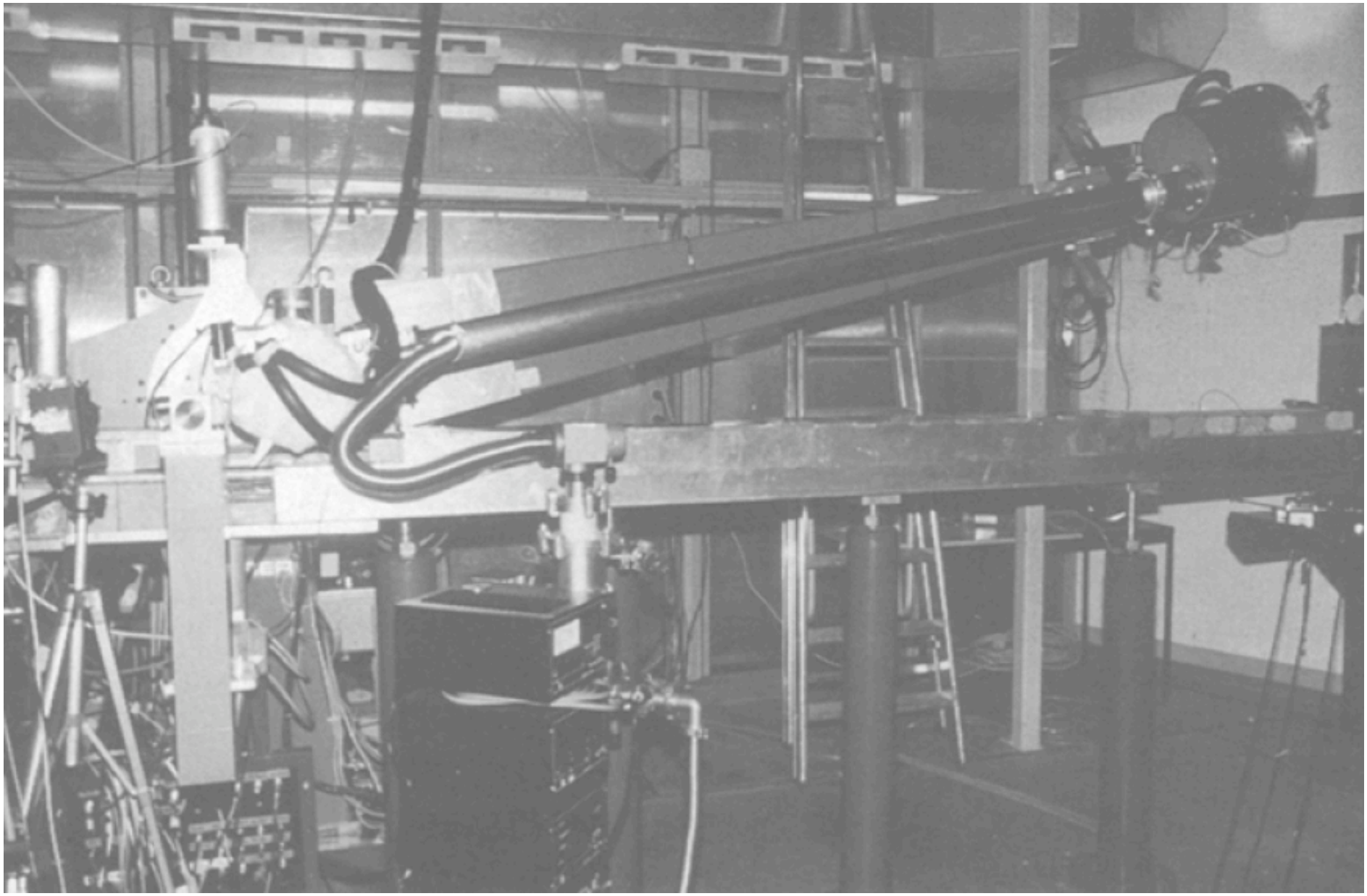

HARWI @ HASYLAB (Burkel, et al)

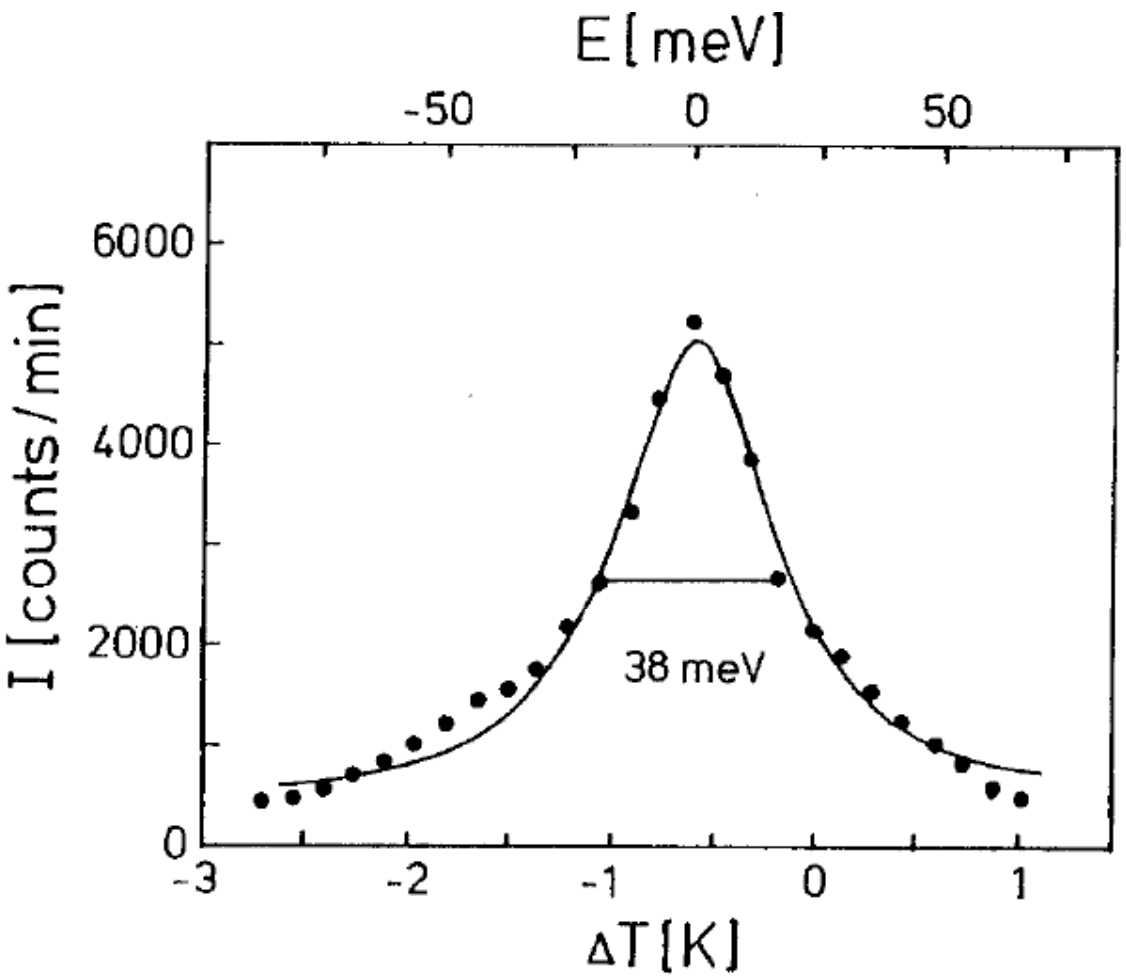

Fig. 4.13. Intensity elastically scattered from fused silica as a function of the temperature difference between monochromator and analyzer and the corresponding energy transfer. Various slits were opened to obtain higher intensity

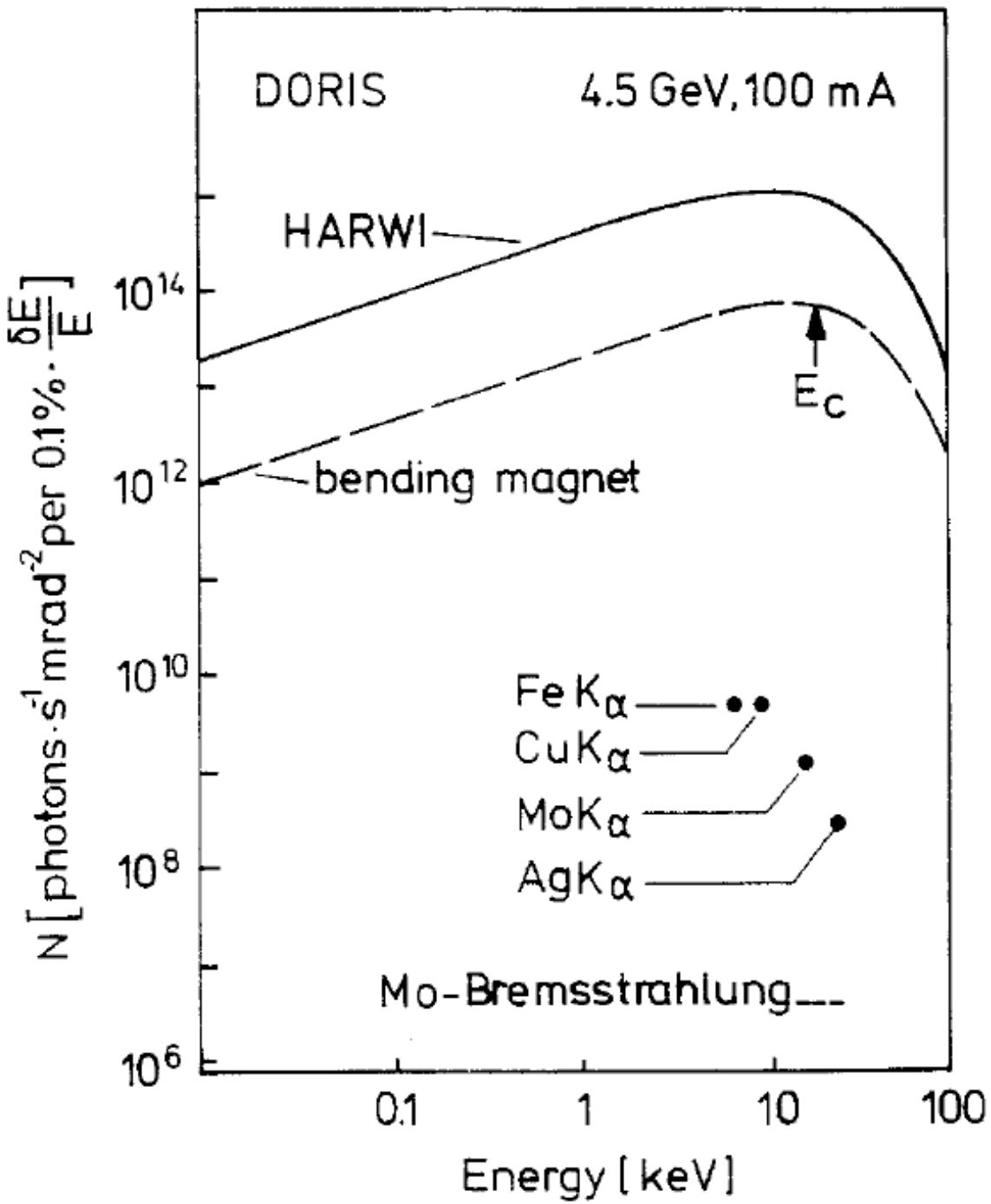

Fig. 3.5. The brightness of a bending magnet and the brightness of the X-ray wiggler HARWI at DORIS II are compared with the brightnesss of an X-ray generator with a rotating anode for the characteristic K_α line of different anode materials and the bremsstrahlung of Mo

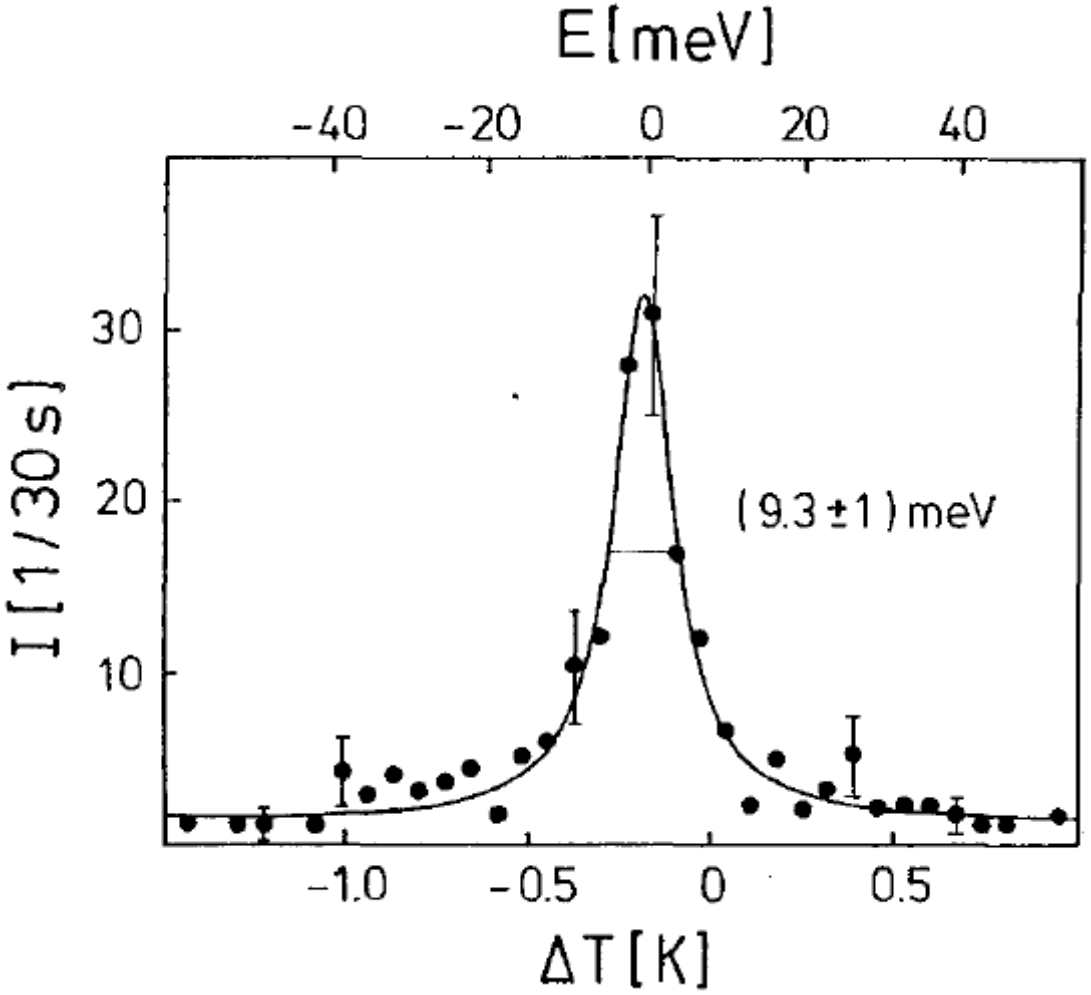

Fig. 4.10. Intensity elastically scattered from fused silica as a function of the temperature difference between the analyzer and the monochromator and the corresponding energy transfer

Momentum Resolved Inelastic X-Ray Scattering

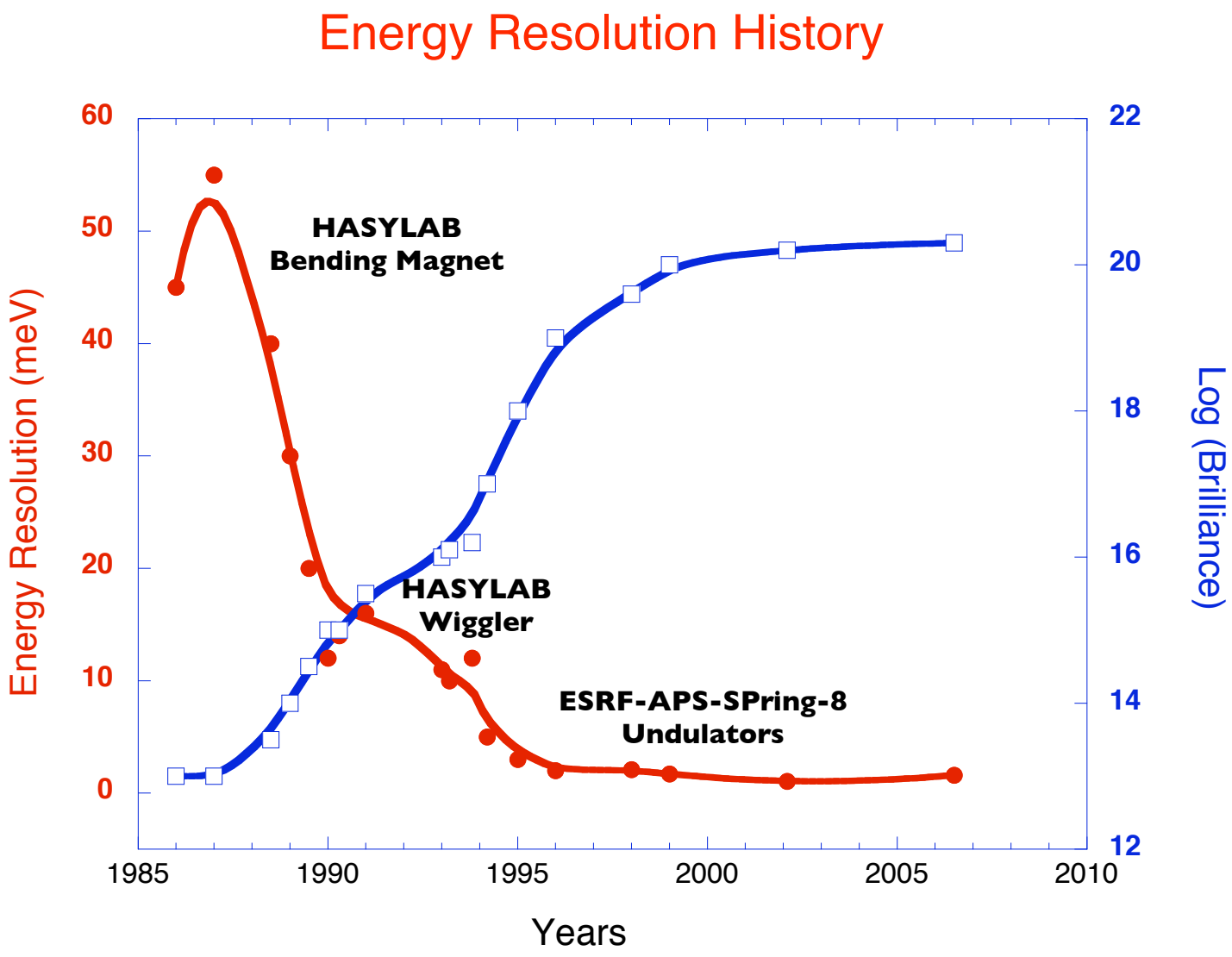

Momentum Integrated Nuclear Resonant Inelastic X-Ray Scattering

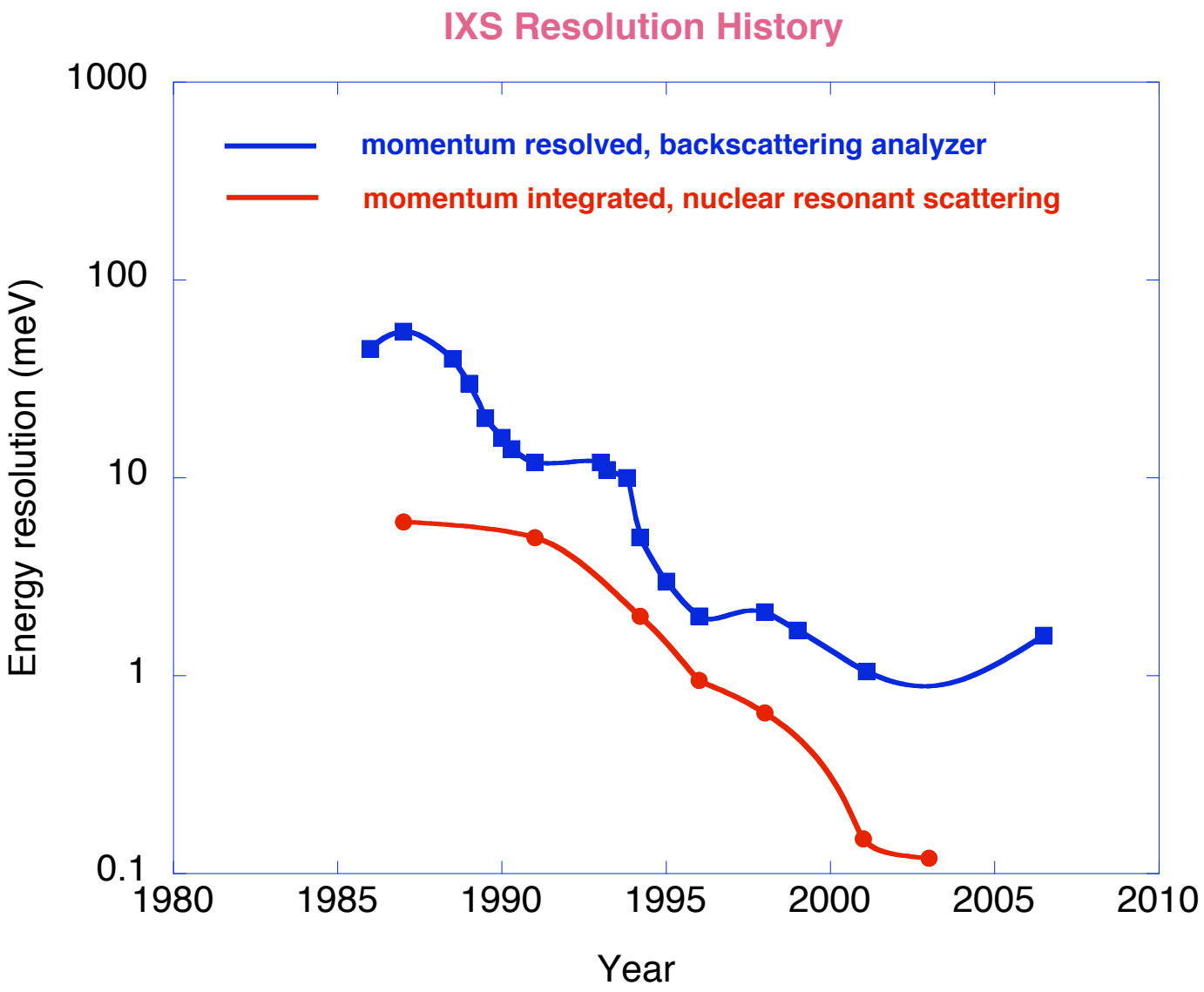

Standard Time structure @ APS

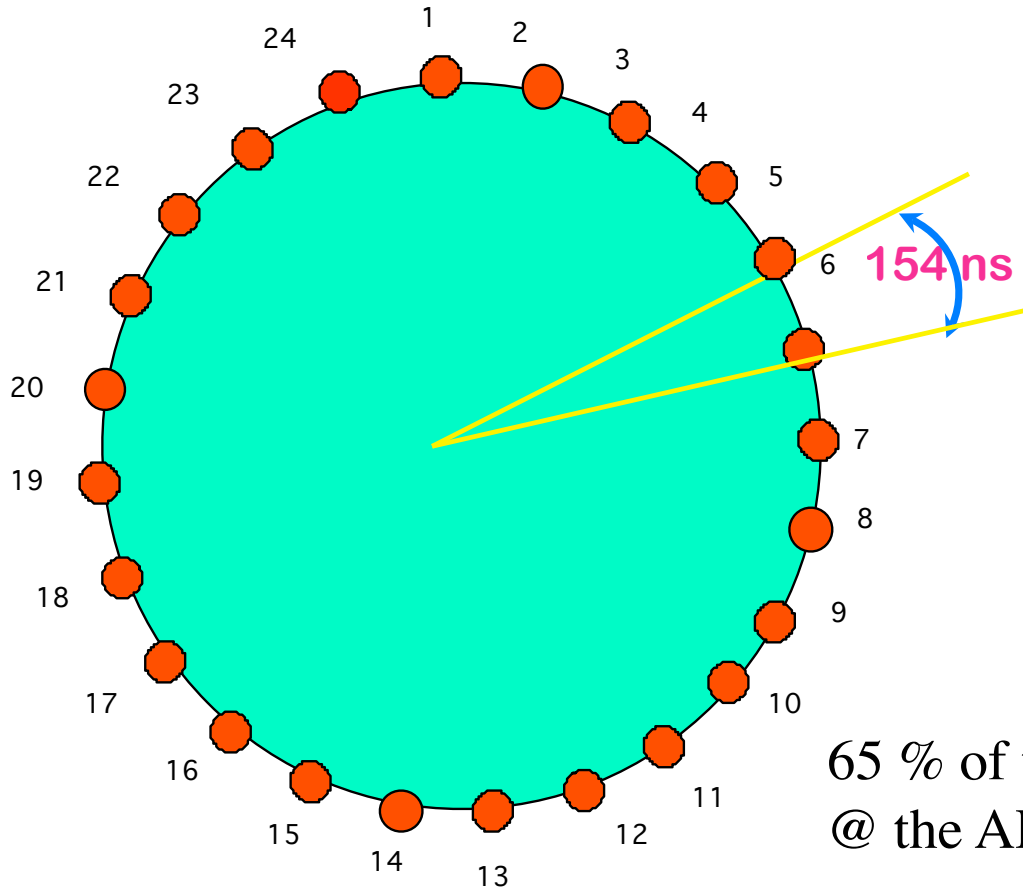

65 % of the time
@ the APS

1 revolution=3.68 μsec =>1296 buckets

Detection of nuclear decay

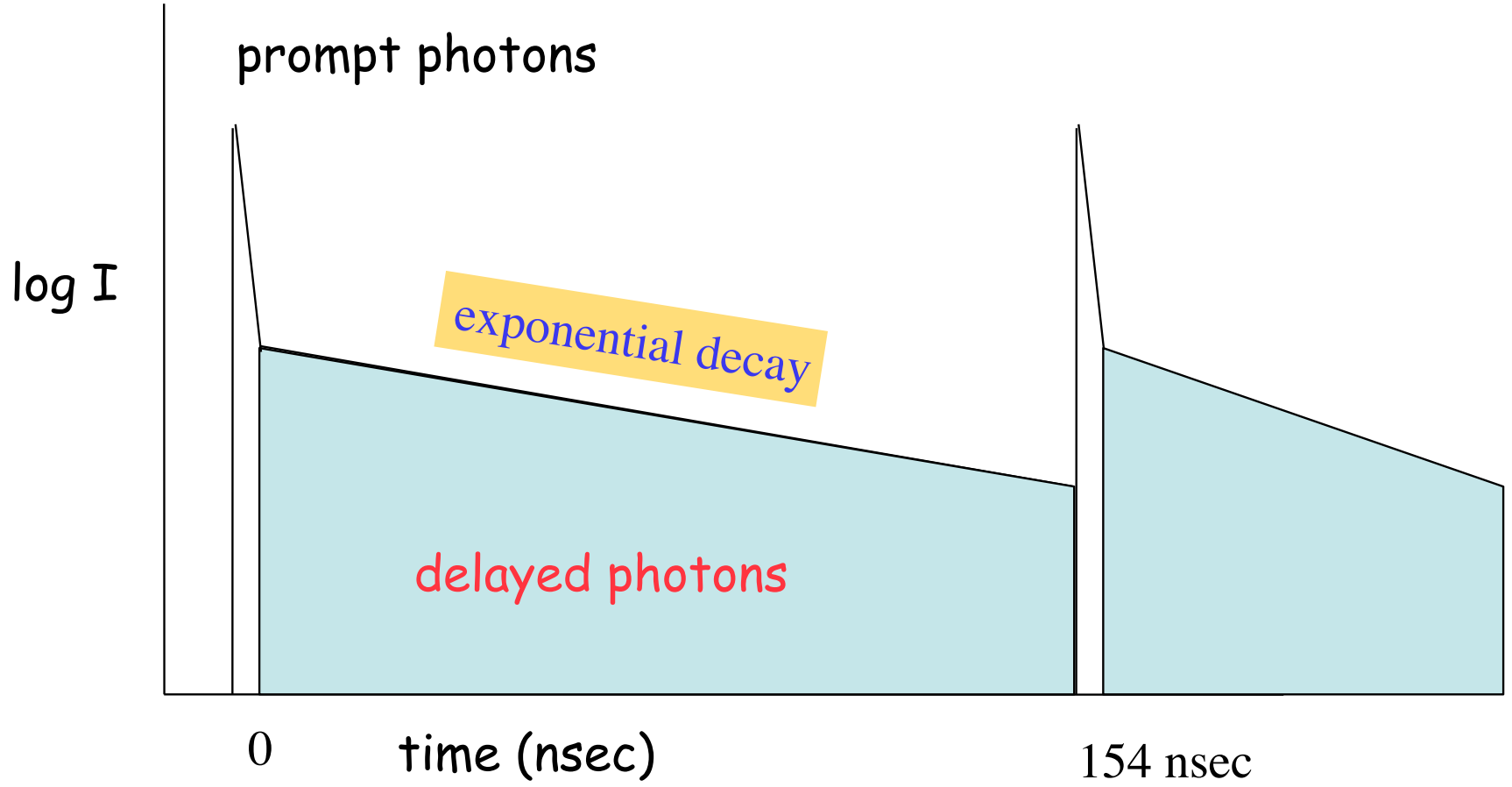

NSLS-II : A suggested filling pattern to enable nuclear resonance

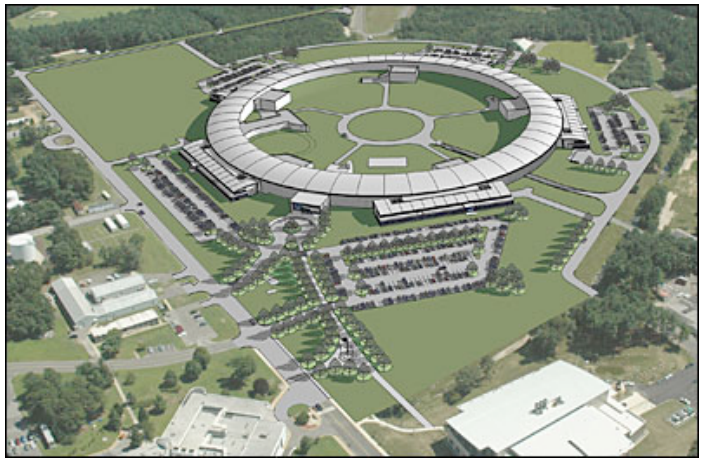

Table 1.1.1 Basic Parameters of the NSLS-II Storage Ring

Energy [GeV]	3
Circumference [m]	792
Number of DBA cells	30
Number of 9.3 m straights	15
Beta-functions in the center of the 9.3 m straights: β_x, β_y [m]	21, 3.0
Number of 6.6 m straights	15
Beta-functions in the center of the 6.6 m straights: β_x, β_y [m]	2.0, 1.0
Number of dipoles	60
Number of quadrupoles	300
Number of sextupoles	300
Circulating current at 3 GeV, multi-bunch [mA]	500
Radio frequency [MHz]	499.68
Harmonic number	1320
Number of bunches at 80% fill	1040

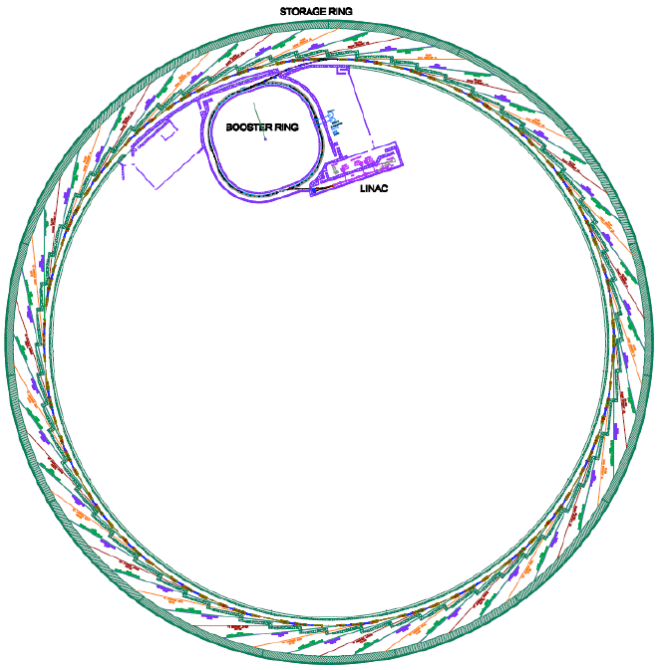

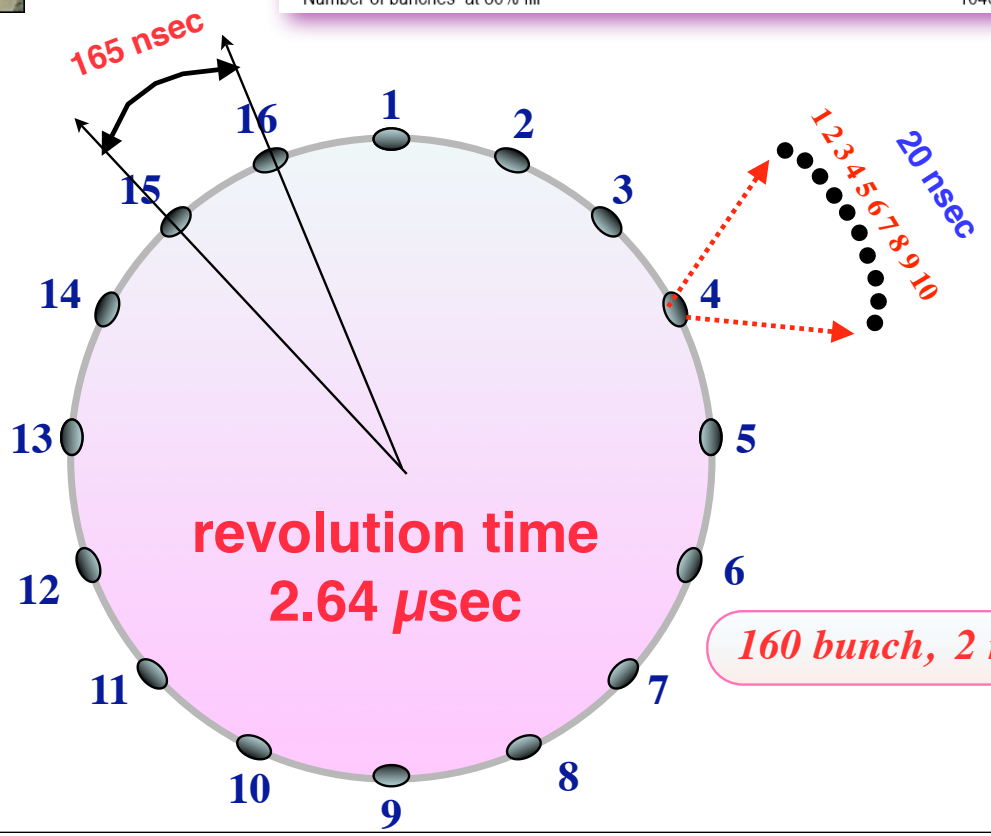

160 bunch, 2 mA each

EVIDENCE FOR QUADRUPOLE INTERACTION OF Fe^{57m}, AND INFLUENCE OF CHEMICAL BINDING ON NUCLEAR GAMMA-RAY ENERGY*

O. C. Kistner and A. W. Sunyar
Brookhaven National Laboratory, Upton, New York
(Received March 30, 19[illegible])

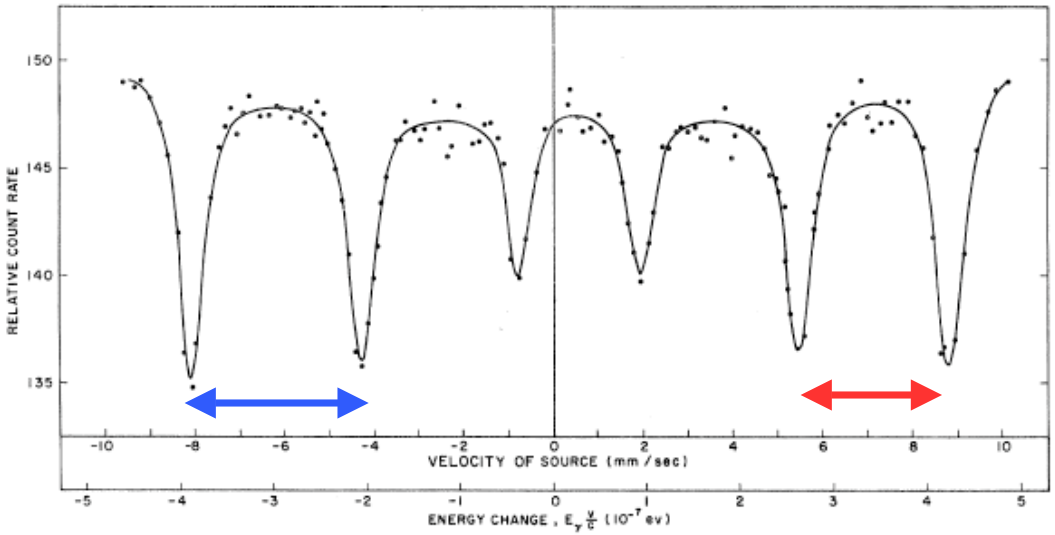

FIG. 1. The absorption by Fe^{57} bound in Fe_2O_3 of the 14.4-kev gamma ray emitted in the decay of Fe^{57m} bound in stainless steel as a function of relative source-absorber velocity. Positive velocity indicates a motion of source toward absorber.

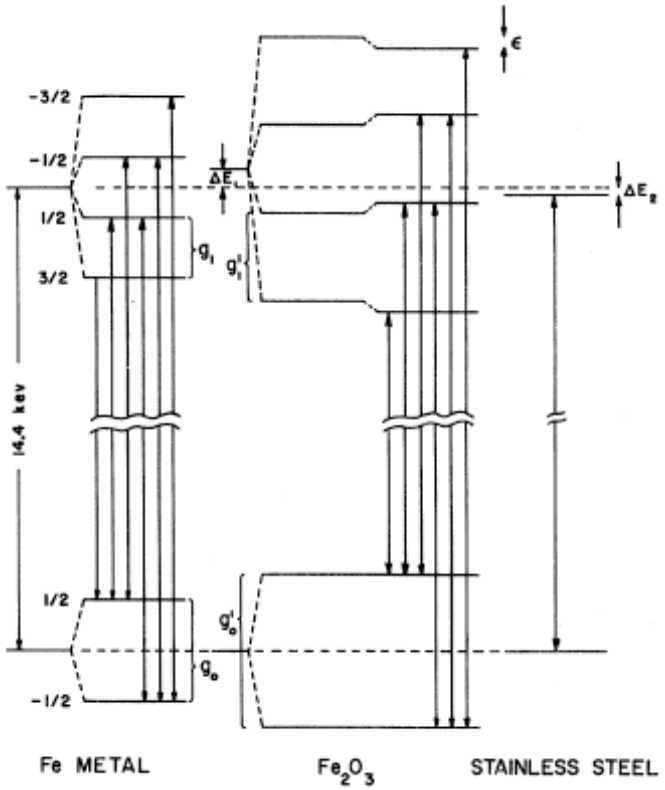

FIG. 2. Schematic representation of the ground and 14.4-kev excited states of Fe^{57} bound in ordinary iron, Fe_2O_3, and stainless steel. This diagram illustrates the details of magnetic hyperfine splitting, quadrupole interaction, and energy shifts due to chemical binding effects.

Hyperfine Structure of the 24-kev Transition in Sn^{119}†

O. C. KISTNER, A. W. SUNYAR,* AND J. B. SWAN‡
Brookhaven National Laboratory, Upton, New York

(Received February 28, 1961)

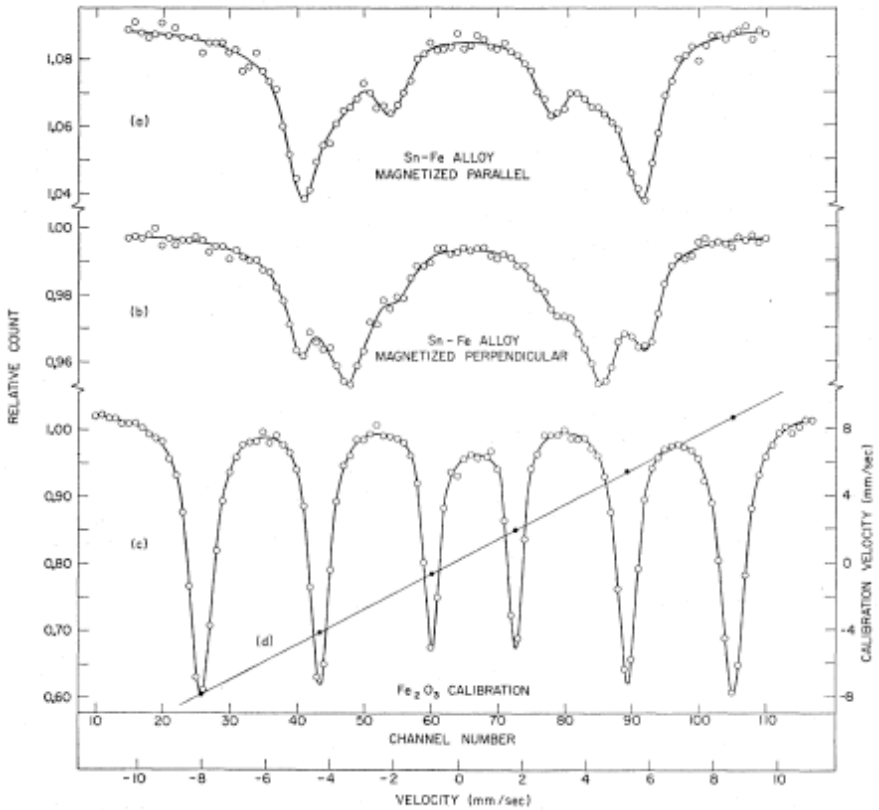

FIG. 3. Experimental absorption spectra obtained by dividing the resonant spectrum by the nonresonant spectrum. Positive velocity indicates the source and absorber approaching each other. (a) and (b) Spectra of magnetized Sn^{119m} in iron source vs grey tin absorber, for γ rays emitted near-parallel and perpendicular to the direction of magnetization, respectively. (c) Calibration spectrum of Co^{57} in stainless steel source vs Fe^{57} enriched Fe_2O_3 absorber. (d) Linear calibration line drawn through the points obtained from the peak positions of curve (c) and the known velocities (right-hand ordinate scale) listed in Table I.

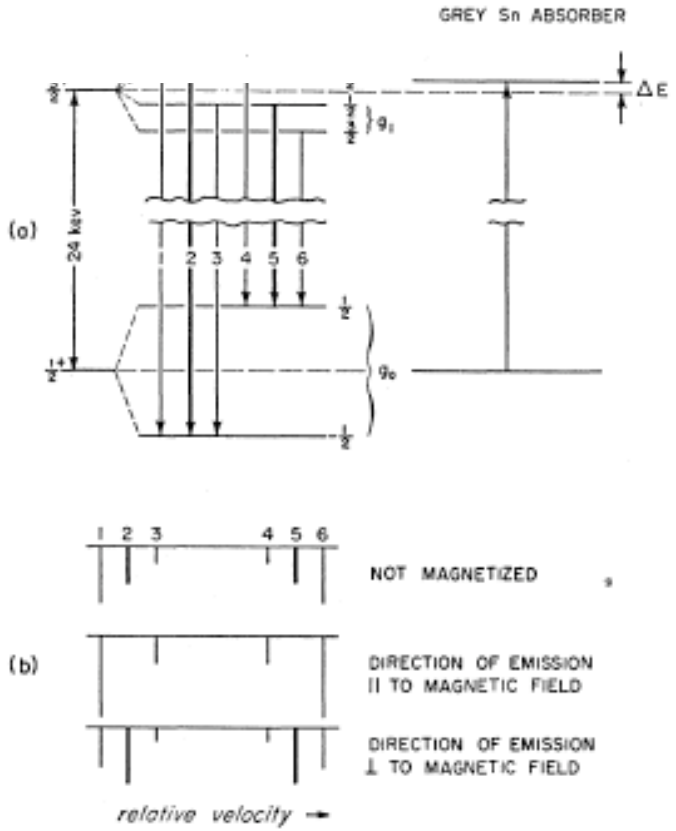

FIG. 4. (a) Zeeman splitting of the 24 kev and ground stat levels in Sn^{119} contained in an iron environment and the chemica shift relative to the unsplit levels in grey tin, as deduced from th absorption spectra. The six components corresponding to M radiation are shown. (b) Theoretical relative intensities of th six absorption lines as they appear in the absorption spectrun for an unmagnetized source and for the two directions of emissio from a magnetized source. The lines are numbered according t the corresponding emission components in (a). The angular de pendence of the radiation, either $\sin^2\theta$ or $1+\cos^2\theta$, is denoted b the use of heavy or light lines, respectively.

Resonant Absorption in the Presence of Faraday Rotation*

M. BLUME AND O. C. KISTNER
Physics Department, Brookhaven National Laboratory, Upton, New York
(Received 15 February 1968)

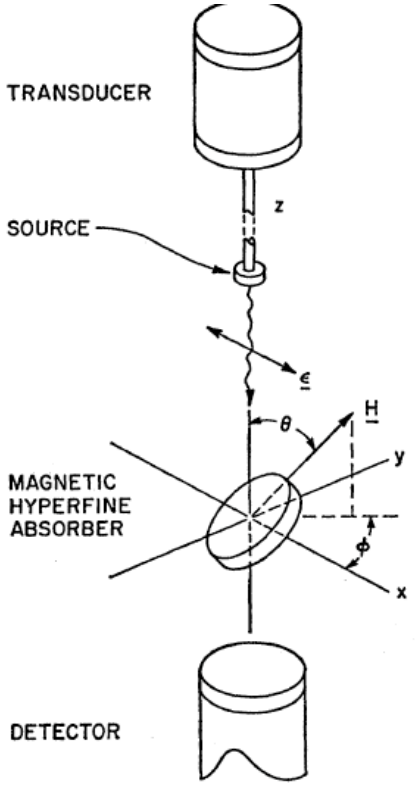

FIG. 1. Schematic of general Mössbauer experiment for observing birefringence and Faraday rotation effects.

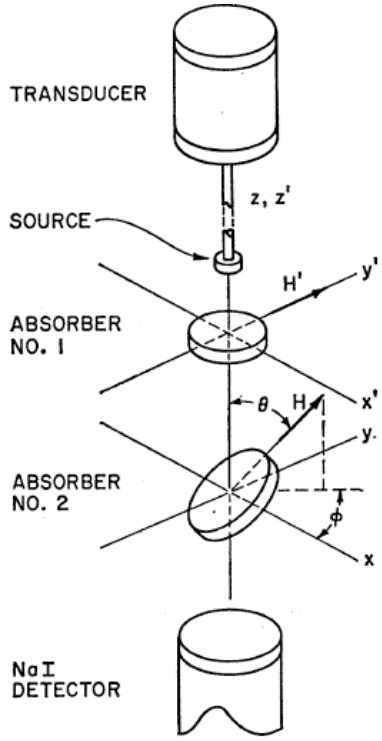

FIG. 2. Schematic of experimental arrangement used in Ref. 4 for testing time-reversal invariance with a single line source and two stationary Ru-Fe hyperfine absorbers. The absorbers are magnetized along the directions indicated by **H** and **H'**.

New Approach to the Study of Nuclear Bragg Scattering of Synchrotron Radiation

G. Faigel,[a] D. P. Siddons, J. B. Hastings, P. E. Haustein, and J. R. Grover
Brookhaven National Laboratory, Upton, New York 11973

and

J. P. Remeika and A. S. Cooper
AT&T Bell Laboratories, Murray Hill, New Jersey 07974
(Received 16 March 1987)

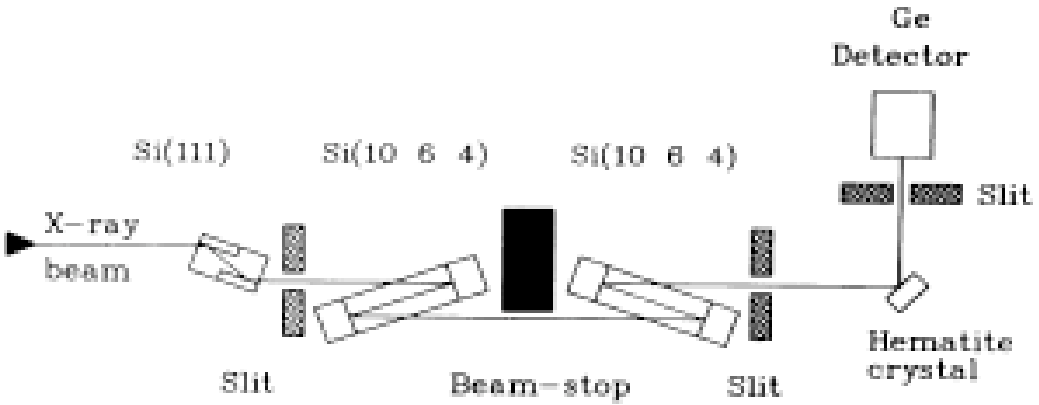

FIG. 1. Schematic view of experimental arrangement.

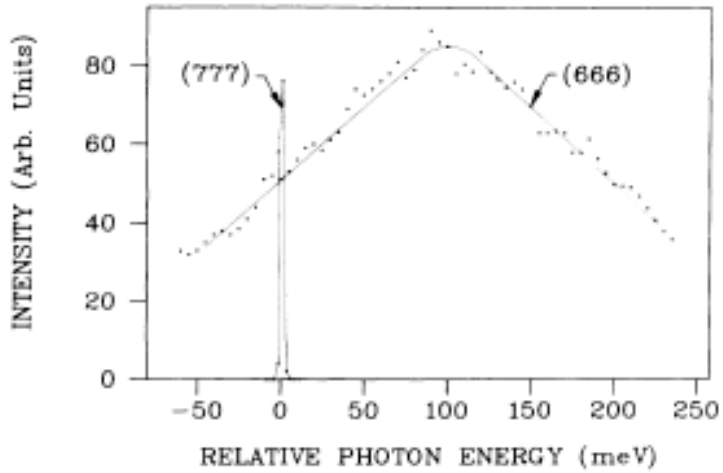

FIG. 3. Energy dependence of the scattered radiation from $^{57}Fe_2O_3$. The broad curve corresponds to the (666) reflection while the sharp curve corresponds to the (777) reflection. The continuous lines are guides for the eye.

Direct Observation of Polarization Mixing in Nuclear Bragg X-Ray Scattering of Synchrotron Radiation

D. P. Siddons, J. B. Hastings, G. Faigel,[a] L. E. Berman, P. E. Haustein, and J. R. Grover

Brookhaven National Laboratory, Upton, New York 119

(Received 3 January 1989)

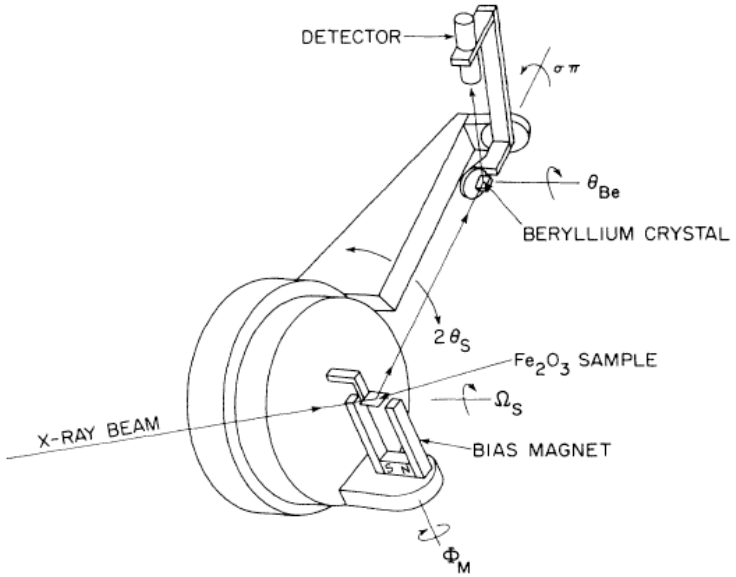

FIG. 1. A schematic view of the diffractometer which carries the sample and its polarizing magnet. The magnetic field direction can be rotated about the sample diffraction vector. Polarization analysis of the diffracted beam is done by the beryllium crystal and its detector. The scattering plane of the beryllium can be rotated about the diffracted beam from the sample.

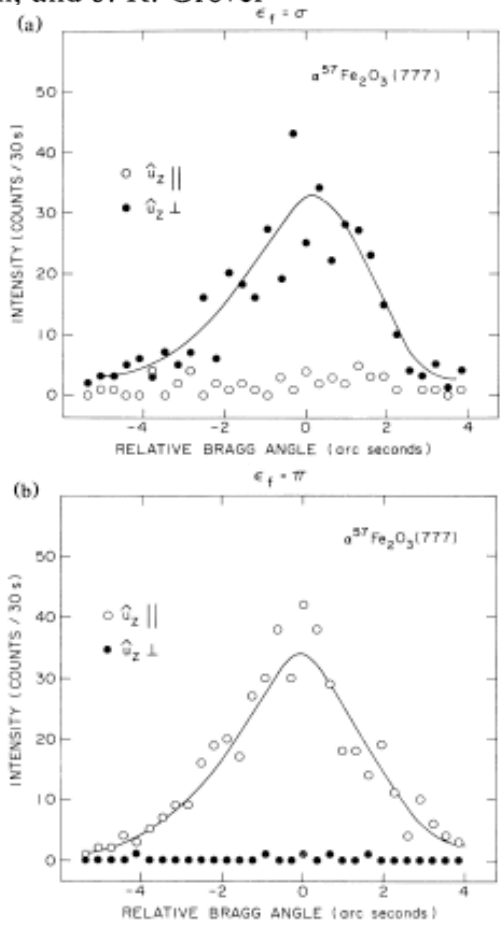

FIG. 2. (a) Rocking curves at resonance for orientations of the magnetic quantization axis parallel and perpendicular to the scattering plane, with the polarization analyzer set to transmit σ-polarized radiation. As predicted, the intensity is greater for $\hat{\mathbf{u}}_z$ perpendicular to the diffraction plane. (b) As in (a), but for the case when the polarization analyzer is set to transmit π-polarized radiation. Note that the signal for $\hat{\mathbf{u}}_z$ perpendicular to the diffraction plane is much less than that for $\hat{\mathbf{u}}_z$ parallel in (a).

Time-Dependent Polarization in Mössbauer Experiments with Synchrotron Radiation: Suppression of Electronic Scattering

D. P. Siddons, U. Bergmann,[a] and J. B. Hastings
National Synchrotron Light Source, Brookhaven National Laboratory, Upton, New York 11973

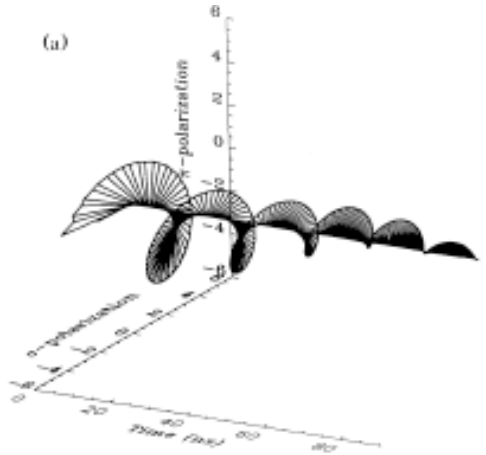

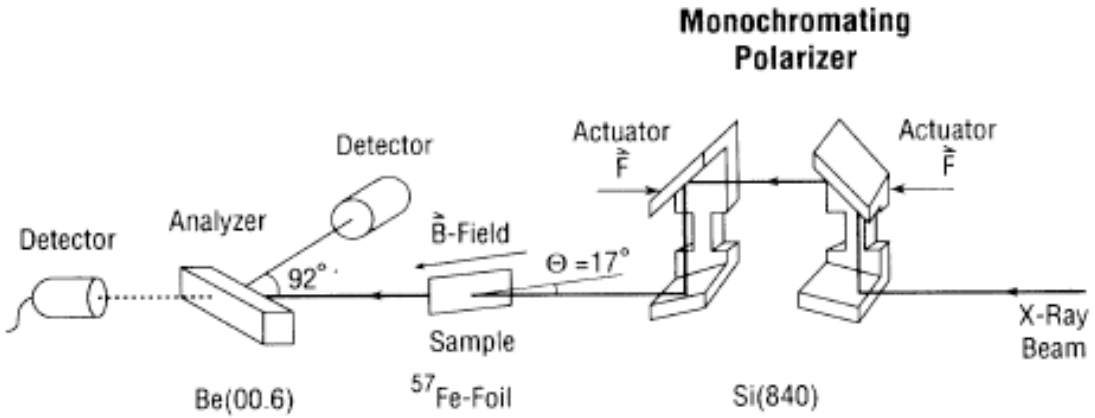

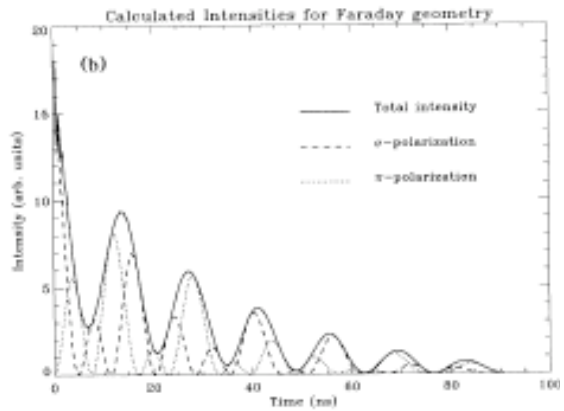

FIG. 2. (a) The calculated amplitude $\mathbf{A}'(t)$, in arbitrary units, of the transmitted wave and its polarization direction during the first 80 nsec after excitation. (b) The intensity components $I_{\sigma\sigma}(t)$ (dashed line), $I_{\pi\sigma}(t)$ (dotted line), and the total intensity $I(t) = I_{\sigma\sigma}(t) + I_{\pi\sigma}(t)$ (solid line), which is the square of the amplitude shown in (a).

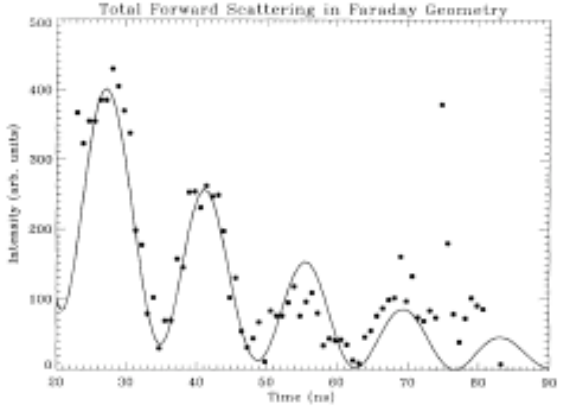

FIG. 3. Comparison between calculated and measured total intensity. No analyzer is used in this geometry.

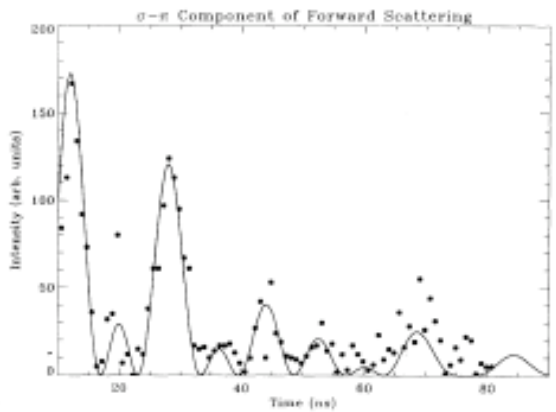

FIG. 4. Comparison between calculated and measured intensity of the rotated component $I_{\pi\sigma}(t)$.

PHYSICAL REVIEW B VOLUME 51, NUMBER 12 15 MARCH 1995-II

Observation of nuclear forward scattering from ^{83}Kr in bulk and monolayer films

D. E. Johnson,* D. P. Siddons, J. Z. Larese, and J. B. Hastings
Brookhaven National Laboratory, P.O. Box 5000, Upton, New York 11973-5000
(Received 7 October 1994)

The coherent nuclear forward scattering of synchrotron radiation from the 9.4-keV level of ^{83}Kr has been observed from bulk films and monolayer Kr adsorbed on exfoliated graphite.

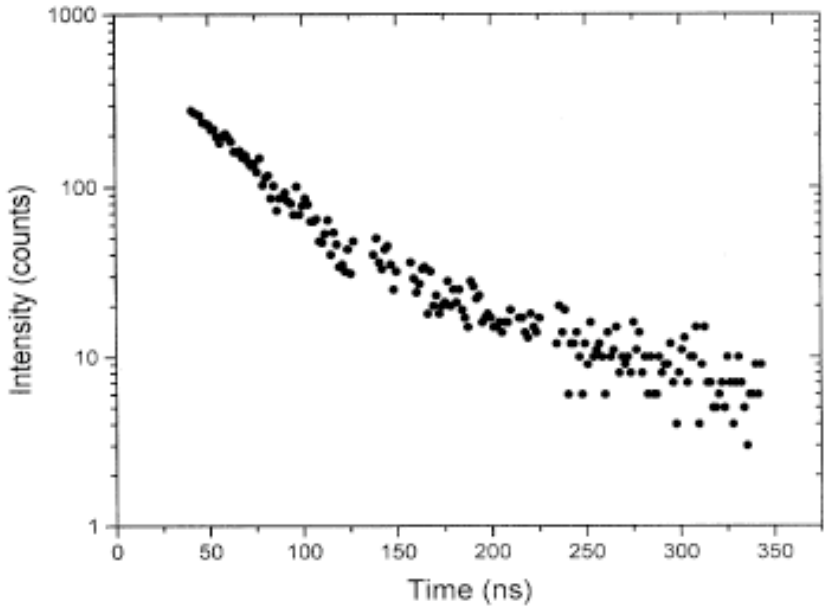

FIG. 1. Typical spectrum observed from Kr condensed on a Be foil at $T=10$ K. The total collection time for this spectrum was 3 h.

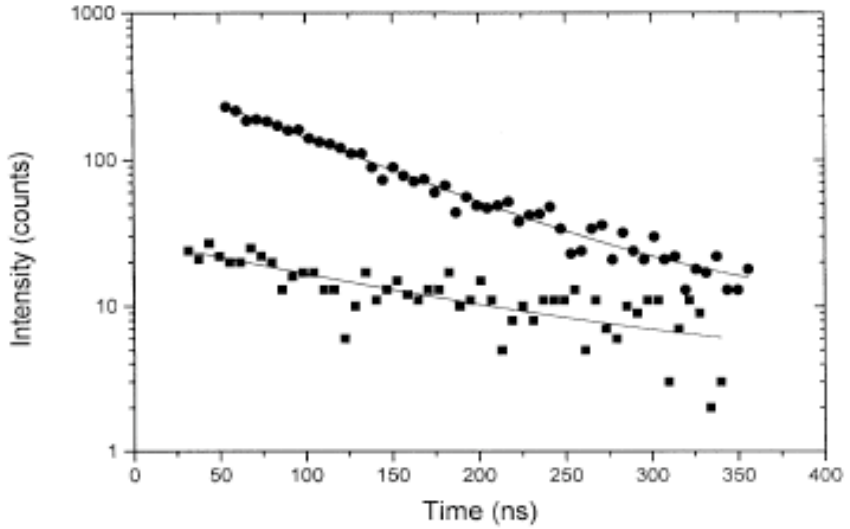

FIG. 2. Time spectra from monolayer Kr adsorbed on graphite at $T=10$ (represented by circles) and 55 K (represented by squares). The solid lines represent fits to the data. Collection time for each spectrum was approximately 3 h. Four-channel summing was used on each data set.

NSLS-II Storage Ring

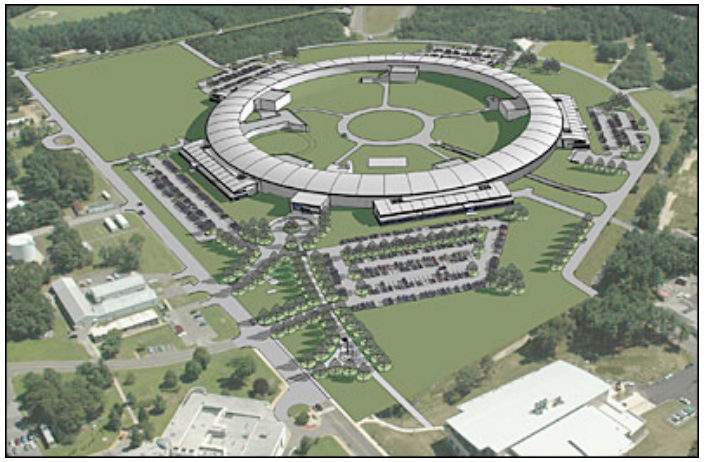

Table 1.1.1 Basic Parameters of the NSLS-II Storage Ring	
Energy [GeV]	3
Circumference [m]	792
Number of DBA cells	30
Number of 9.3 m straights	15
Beta-functions in the center of the 9.3 m straights: β_x, β_y [m]	21, 3.0
Number of 6.6 m straights	15
Beta-functions in the center of the 6.6 m straights: β_x, β_y [m]	2.0, 1.0
Number of dipoles	60
Number of quadrupoles	300
Number of sextupoles	300
Circulating current at 3 GeV, multi-bunch [mA]	500
Radio frequency [MHz]	499.68
Harmonic number	1320
Number of bunches at 80% fill	1040

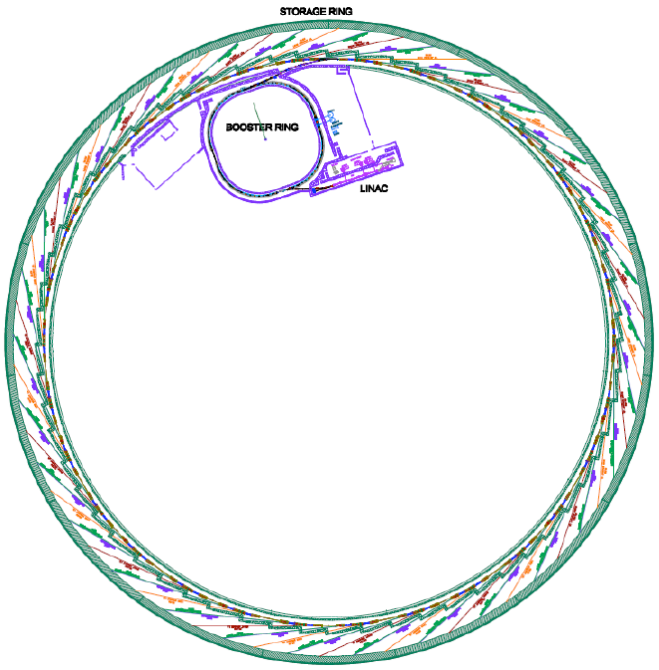

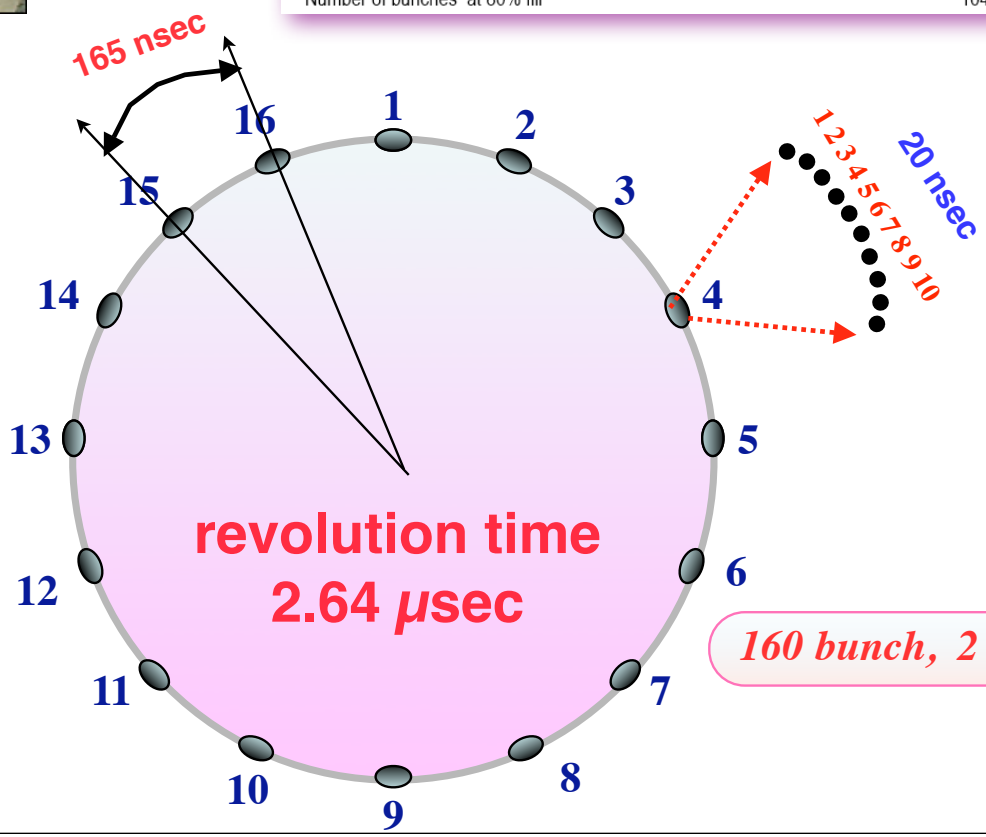

160 bunch, 2 mA each

Momentum Integrated Nuclear Resonant Inelastic X-Ray Scattering

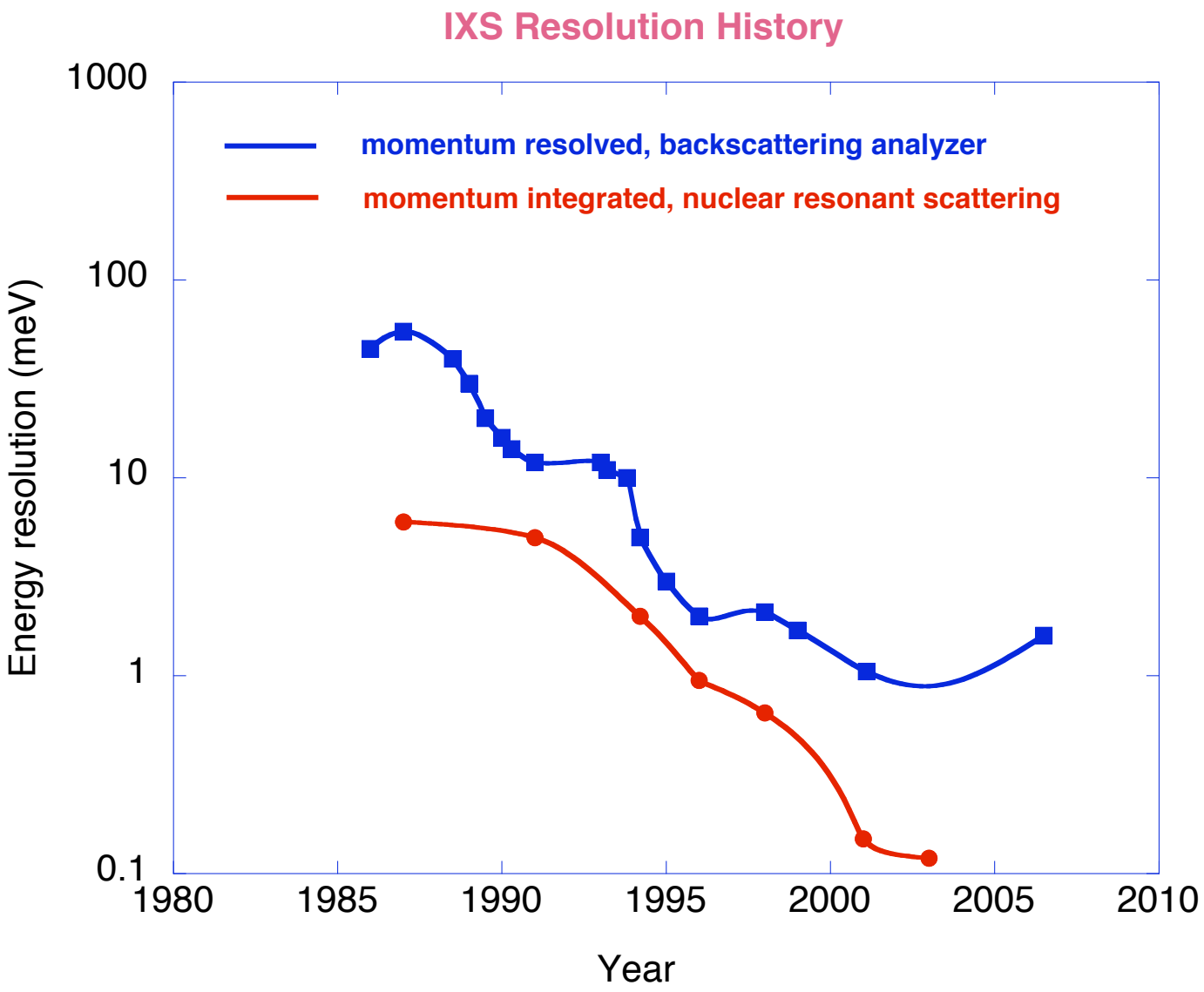

Inelastic Scattering at NSLS-II

Facts:

- NSLS-II with a 3 GeV energy is optimized for 0.1-12 keV.

- NSLS-II with 500 mA stored current and 1 nm-rad emittance requirements has limited bunch structure options, also which also limit the nuclear resonance experiments.

- NSLS-II, with no planned investment in superconducting undulators, and no plans with 20 + m long straight-sections has limited potential in terms of access to 20 keV + energy range to supersede the APS.

- Momentum-resolved IXS with 2 meV or better resolution requires access to 25 keV or higher energies.

- There is no known method to reach 0.1 meV below 10 keV, and perform spectroscopy of any kind.

Inelastic Scattering Options

Available Techniques and their resolution (ca. 2008)

- Medium resolution Resonant IXS (MERIX): dE ~ 50-100 meV @ 5-12 keV
- High-resolution momentum-resolved IXS (HERIX): dE ~ 2 meV @ 20 keV
- Inelastic nuclear resonant scattering: dE ~ 0.1-2 meV @ 9-30 keV
- X-Ray Raman Spectroscopy: dE ~ 0.4-1 eV @ 5-12 keV
- X-Ray Emission Spectroscopy: dE ~ 0.4-1 eV @ 4-12 keV
- Soft-X-Ray IXS : dE ~1-10 meV @ 10-150 eV

Suggestions for IXS @ NSLS-II (2008)

Pursue:

- Medium resolution Resonant IXS (MERIX): dE ~ 50-100 meV
- X-Ray Raman Spectroscopy: dE ~ 0.5-1 eV
- X-Ray Emission Spectroscopy: dE ~ 0.5-1 eV
- Inelastic nuclear resonant scattering: dE ~ 0.1-1 meV
  - include special filling mode in planning NOW

Consider:

- Soft-X-Ray IXS (e.g. MERLIN @ ALS or IUVS @ Elettra)

Challenging:

High-resolution momentum-resolved IXS (HERIX) with dE ~ 0.1 meV

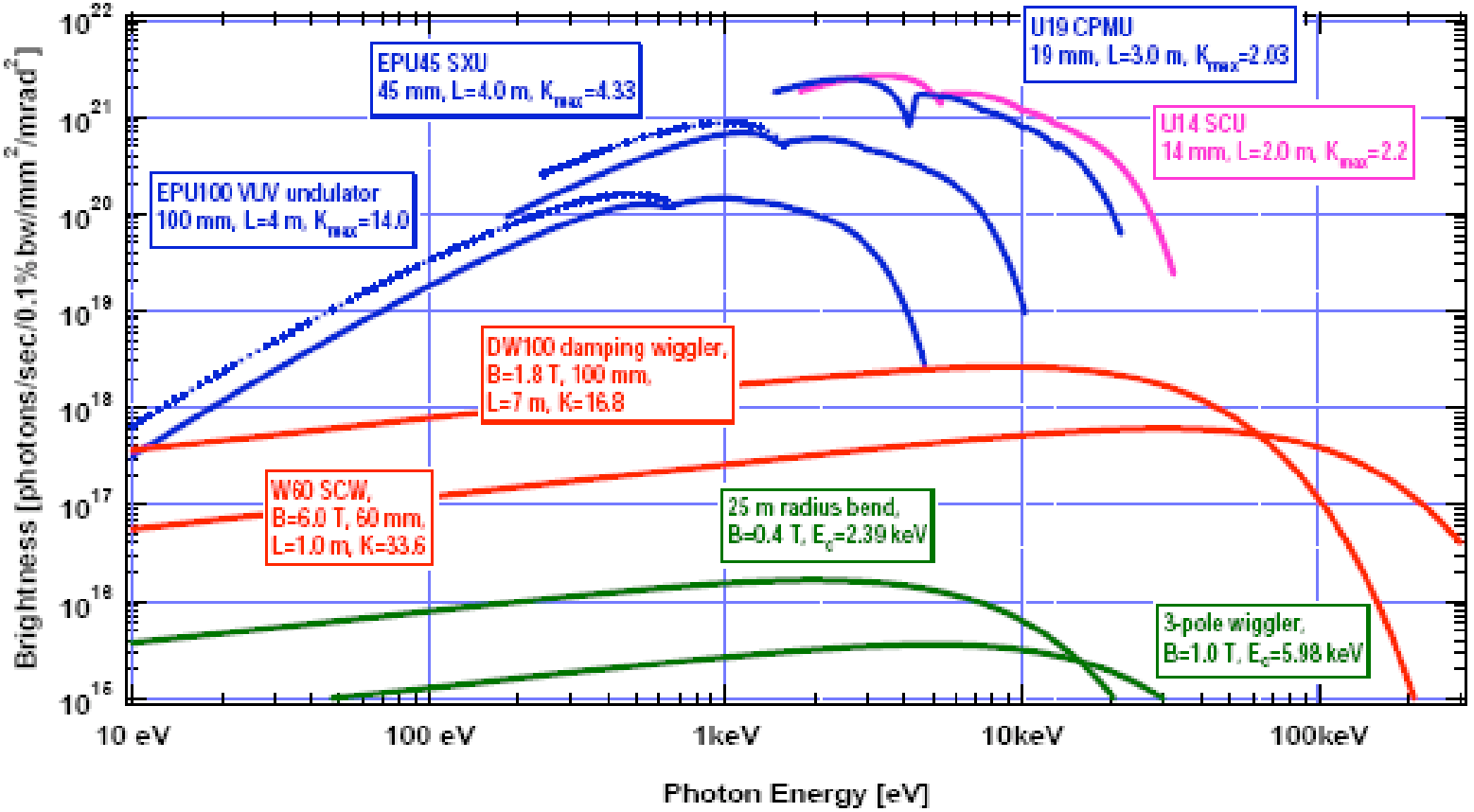

Figure 1. Brightness vs. photon energy for various devices at NSLS-II.

Brilliance in 2003

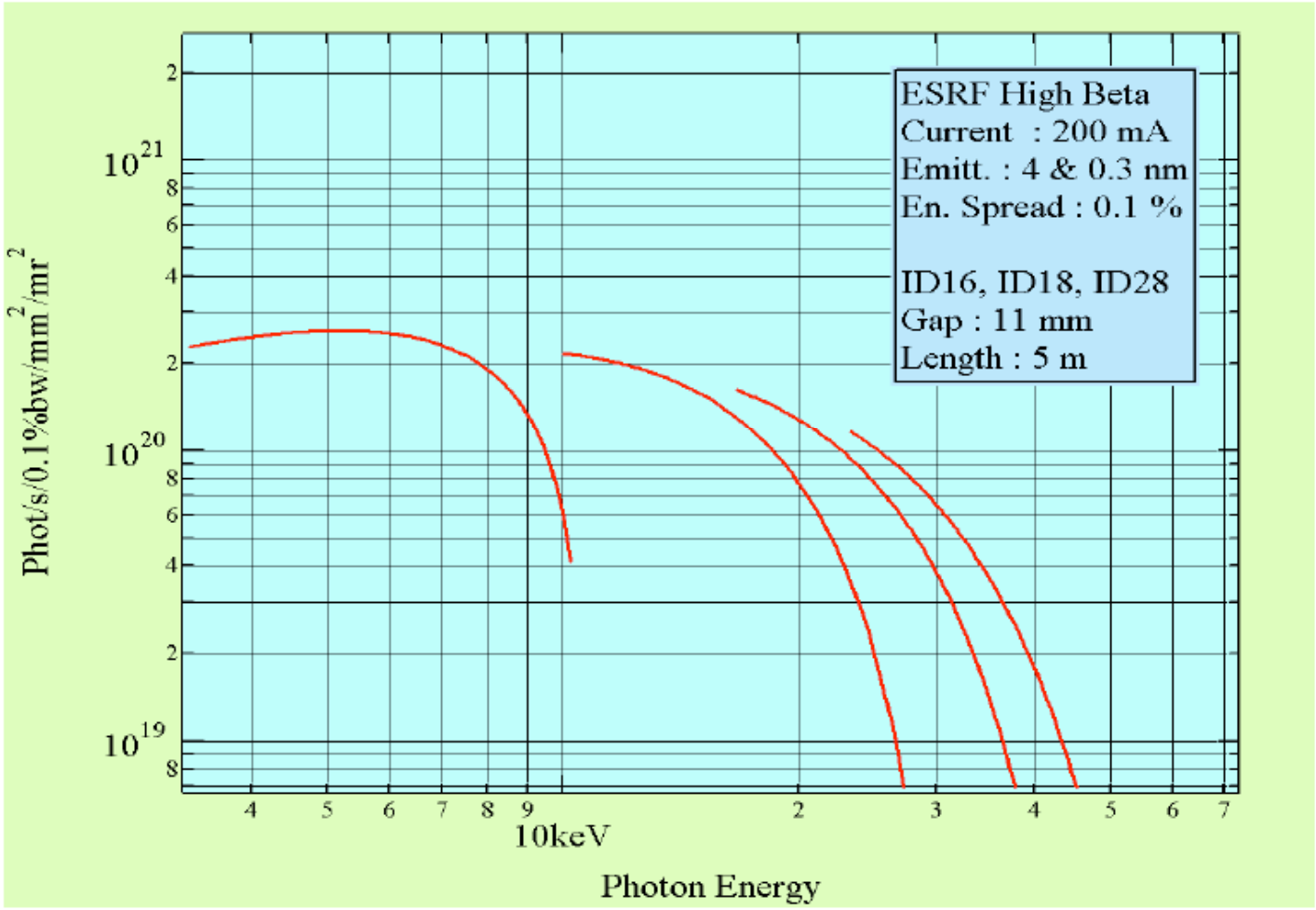

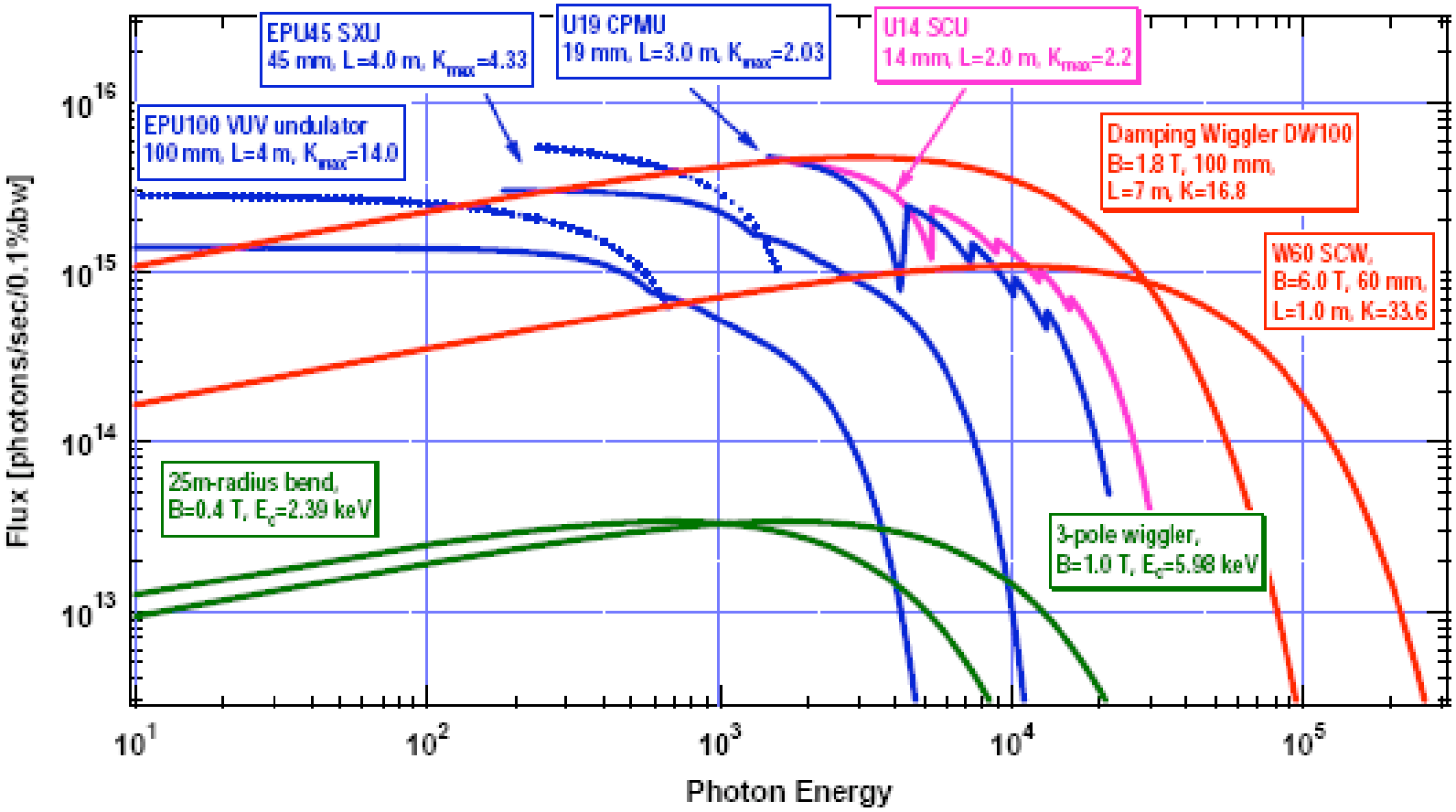

Figure 2. Flux vs. photon energy for various devices at NSLS-II.

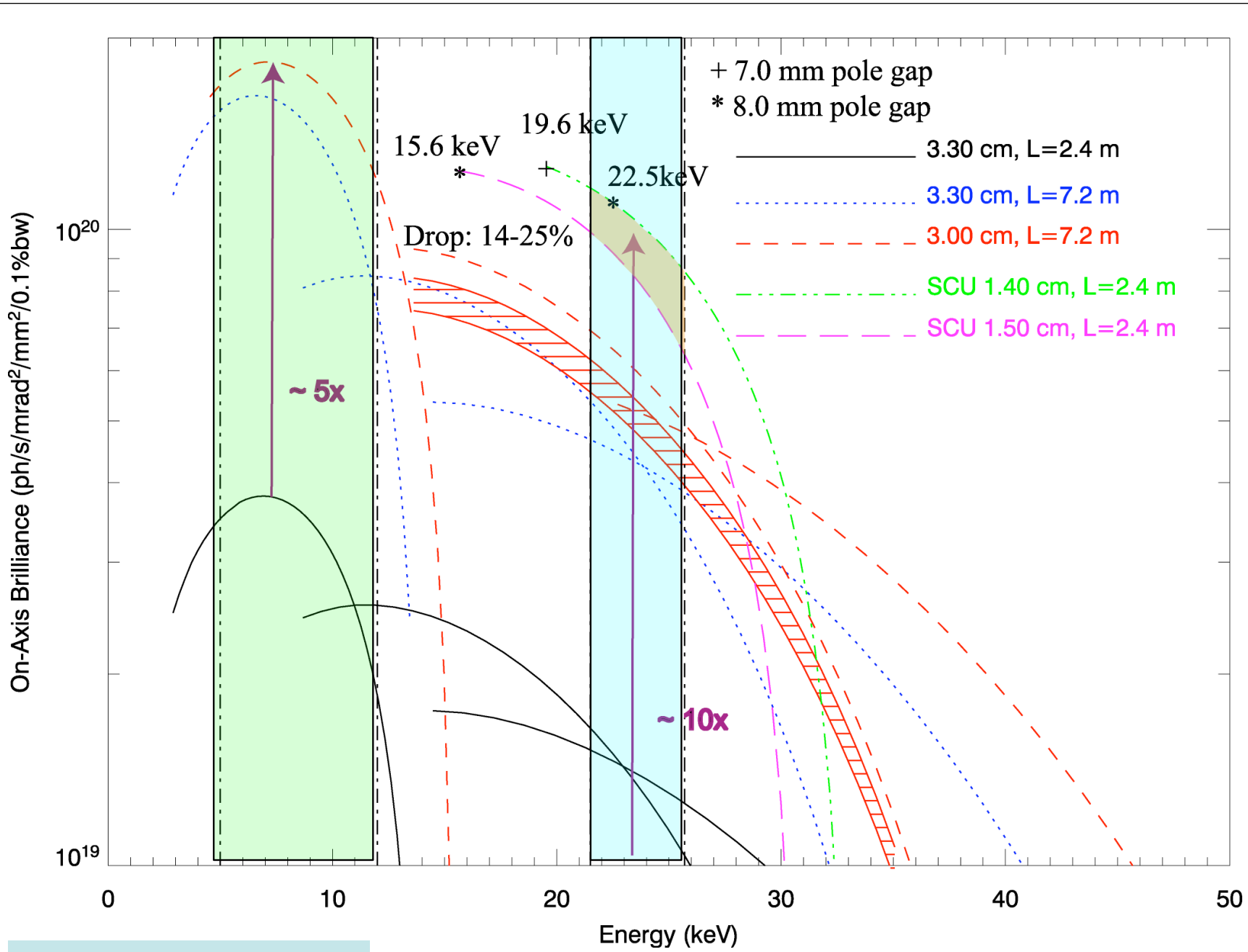

Courtesy: R. Dejus